

QC852
.C6
no.519
ATSL

**OPPOSING MESOSCALE FLOWS IN A
BROKEN MIDLATITUDE SQUALL LINE**

Barbara D. Miner

LIBRARIES
JAN 26 1993
COLORADO STATE UNIVERSITY

**Colorado
State
University**

**DEPARTMENT OF
ATMOSPHERIC SCIENCE**

PAPER NO. 519

**OPPOSING MESOSCALE FLOWS IN A
BROKEN MIDLATITUDE SQUALL LINE**

by

Barbara D. Miner

Department of Atmospheric Science
Colorado State University
Fort Collins, CO 80523

Spring 1993

Atmospheric Science Paper No. 519



or

QC 852
.C6
no. 519
ATSL

ABSTRACT

OPPOSING MESOSCALE FLOWS IN A BROKEN MIDLATITUDE SQUALL LINE

During the period 14-15 June 1985 a broken line of convection with one primary gap (echo-free) region developed along a cold front passing through the Oklahoma-Kansas Preliminary Regional Experiment for STORM-Central (OK PRE-STORM) domain. Radar and satellite data are presented to provide an overview of the life cycle of the line. Observations from the OK PRE-STORM mesonet network and upper air soundings are used to document the occurrence of the gap and an associated surface mesolow.

The convective line initially developed as two mesoscale convective systems (MCSs), one in northeast Kansas, the other in the Texas panhandle, along a weak cold front. As the two MCSs matured, convection developed between the two similar to the broken-line squall line formation described by Bluestein and Jain (1985). Despite strong low-level convergence and strong moisture convergence, an echo-free region remained between the two MCSs throughout the life cycle of the line.

The upper level flow pattern along the line of convection showed strong upper level outflow from the two MCSs converging over the echo-free region and strong subsidence in that region from 250 mb to 650 mb. It is hypothesized that the strong mid- and upper level subsidence was the main factor in the lack of convection in the echo-free region.

During the mature phase of the line, a surface mesolow developed within the echo-free region. Calculations are made using a form of the hypsometric equation to determine if the presence of the surface mesolow could have been produced by the mid and upper level subsidence found in that region. At 0300 UTC the mesolow was 2 mb lower than the surrounding areas. Calculations show that subsidence warming in the column could account for a drop in pressure of .75 mb.

The results of the study show that while strong low-level convergence existed all along the front throughout most of its life cycle, mid- and upper level outflow from the existing MCSs prevented convection in the echo-free region. The resulting subsidence contributed to the formation of the surface mesolow in the echo-free region. This study shows the need for the evaluation of upper-level forcing mechanisms when forecasting the development of thunderstorms along fronts and convergence zones.

ACKNOWLEDGEMENTS

I would like to express my deepest appreciation to my advisor, Dr. Richard Johnson, for his guidance and dedication to the successful, timely completion of this work. I would also like to thank my other committee members, Dr. Thomas McKee and Dr. Bogusz Bienkiewicz.

I would also like to thank Paul Ciesielski, Rick Taft, Bill Gallus, Bob Falvey, Xin Lin, and Scot Loehrer for their willingness to share their programming skills and help with the use of the computer systems at the Atmospheric Science Department.

Thanks are also extended to José Meitín for providing the mesonet network and upper air data, as well as his help acquiring, in conjunction with Robert Hueftle, the radar reflectivity composites.

Finally, thanks to Gail Cordova, who was instrumental in the completion of this manuscript and Judy Sorbie-Dunn, who drafted several of the figures.

This research was supported by the National Science Foundation Grant No. ATM-9013112.

TABLE OF CONTENTS

1 INTRODUCTION	1
2 BACKGROUND	3
2.1 Organization of mesoscale convective systems	3
2.2 Mesoscale circulations	8
2.3 Subsidence warming and the mesolow	12
2.4 Interactions between mesoscale convective systems	13
3 DATA SET AND ANALYSIS PROCEDURES	15
3.1 PRE-STORM	15
3.2 Surface data	15
3.2.1 Pressure adjustments	17
3.3 Upper air data	19
3.3.1 Data network and adjustments to upper air data	19
3.3.2 Calculated fields	19
3.4 Radar Data and Satellite Imagery	21
4 SYNOPTIC OVERVIEW	22
4.1 Synoptic conditions	22
4.2 Satellite and radar overview	30
5 MESOSCALE ANALYSIS	39
5.1 Surface observations	39
5.2 Upper Air Analyses	47
5.2.1 2100 UTC	53
5.2.2 0000 UTC	53
5.2.3 0300 UTC	69
5.2.4 0600 UTC	77
5.3 Surface and Upper Air Synopsis	77
6 MESOSCALE ANALYSIS OF ECHO-FREE REGION AND MESOLOW	82
6.1 Development of the echo-free region	82
6.1.1 2100 UTC	82
6.1.2 0000 UTC	86
6.1.3 0300 UTC	90
6.1.4 0600 UTC	92
6.2 Formation of the surface mesolow in the echo-free region	96
6.3 Schematic	100

7 SUMMARY	105
REFERENCES	107
A INSTRUMENT BIAS CORRECTIONS	114

LIST OF FIGURES

2.1	Schematics depicting (a) symmetric and (b) asymmetric types of precipitation patterns (from Houze et al., 1990).	6
2.2	Schematics depicting (a) symmetric and (b) asymmetric types of precipitation patterns with pressure field overlaid (from Loehrer, 1992).	7
2.3	Schematic showing idealized depiction of squall line formation (from Bluestein and Jain, 1985).	9
2.4	Conceptual model of a squall line with a trailing stratiform region viewed perpendicular to the convective line (from Houze et al., 1989)	10
2.5	Schematic of hypothesized mesoscale circulations for two opposing mesoscale convective systems. (from Stensrud and Maddox, 1988)	14
3.1	The PRE-STORM observational mesonetnetwork (from Meitin and Cuning, 1985).	16
3.2	The PRE-STORM Portable Automated Mesonetnetwork(PAM) and Surface Automated Mesonetnetwork (SAM) surface array.	18
3.3	The PRE-STORM sounding mesonetnetwork.	20
4.1	1200 UTC 14 June 1985 surface and upper air analyses: (a) surface; (b) 850 mb; (c) 700 mb; (d) 500 mb; (e) 300 mb	23
4.1	continued	24
4.1	continued	25
4.2	Same as 4.1 except at 0000 UTC, 15 June 1985.	27
4.2	continued	28
4.2	continued	29
4.3	15 June 1985 infrared (IR) satellite imagery for: (a) 0000 UTC; (b) 0130 UTC; (c) 0200 UTC; (d) 0300 UTC; (e) 0500 UTC; (f) 0600 UTC; (g) 0700 UTC; (h) 0800 UTC; and (i) 0900 UTC.	31
4.3	continued	32
4.3	continued	33
4.4	Radar composites of RADAP-II digitized data for 15 June 1985	35
4.4	continued	36
4.4	continued	37
5.1	Surface analysis of adjusted pressure at 2100 UTC 14 June 1985	40
5.2	Surface analysis of adjusted pressure at 0000 UTC 15 June 1985	41
5.3	Same as Fig. 5.2 except for 0100 UTC 15 June 1985.	43
5.4	Same as Fig. 5.2 except for 0200 UTC 15 June 1985.	44
5.5	Same as Fig. 5.2 except for 0230 UTC 15 June 1985.	45
5.6	Same as Fig. 5.2 except for 0300 UTC 15 June 1985.	46
5.7	Same as Fig. 5.2 except for 0430 UTC 15 June 1985.	48
5.8	Same as Fig. 5.2 except for 0500 UTC 15 June 1985.	49

5.9	Same as Fig. 5.2 except for 0600 UTC 15 June 1985.	50
5.10	Same as Fig. 5.2 except for 0700 UTC 15 June 1985.	51
5.11	Same as Fig. 5.2 except for 0800 UTC 15 June 1985.	52
5.12	Constant pressure plots at 2100 UTC 14 June 1985; (a) 850 mb, (b) 700 mb and (c) 200 mb.	54
5.12	continued	55
5.13	Divergence field at 2100 UTC, 14 June 1985; (a) surface and (b) 850 mb.	56
5.14	Moisture divergence at 2100 UTC, 14 June 1985; (a) surface and (b) 800 mb	57
5.15	Omega field at 2100 UTC, 14 June 1985; (a) 850 mb, (b) 700 mb, (c) 500 mb and (d) 300 mb.	58
5.15	continued	59
5.16	Same as Fig. 5.12 except at 0000 UTC, 15 June 1985.	60
5.16	continued	61
5.17	Divergence field at 0000 UTC, 15 June 1985; (a) surface (b) 850 mb, (c) 700 mb and (d) 200 mb.	63
5.17	continued	64
5.18	Moisture divergence at 0000 UTC, 15 June 1985; (a) surface (b) 950 mb and (c) 800 mb	65
5.18	continued	66
5.19	Omega field at 0000 UTC, 15 June 1985; (a) 850 mb, (b) 700 mb, (c) 500 mb and (d) 200 mb.	67
5.19	continued	68
5.20	Same as Fig. 5.12 except at 0300 UTC, 15 June 1985; (a)850 mb, (b) 700 mb, (c) 500 mb and (d) 200 mb.	70
5.20	continued	71
5.21	Divergence field as in Fig. 5.17 except at 0300 UTC, 15 June 1985: (a) surface, (b) 850 mb and (c) 200 mb.	72
5.21	continued	73
5.22	Moisture divergence field as in Fig. 5.18 except at 0300 UTC, 15 June 1985; (a) surface and (b) 900 mb.	74
5.23	Omega field as in Fig. 5.19 except at 0300 UTC, 15 June 1985; (a) 850 mb, (b) 300 mb and (c) 200 mb.	75
5.23	continued	76
5.24	Divergence field as in Fig. 5.17 except at 0600 UTC, 15 June 1985; (a) surface, (b) 850 mb and (c) 200 mb.	78
5.24	continued	79
5.25	Moisture divergence field as in Fig. 5.18 except at 0600 UTC, 15 June 1985; (a) surface and (b) 900 mb.	80
5.26	Omega field as in Fig. 5.19 except at 0600 UTC, 15 June 1985; (a) 850 mb and (b) 200 mb.	81
6.1	Vertical cross-section area at 2100 UTC, 14 June 1985.	83
6.2	Vertical cross-sections of (a) divergence, (b) wind perturbation, (c) omega, and (d) relative humidity.	84
6.2	continued	85
6.3	Same as Figure 6.1 except for 0000 UTC, 15 June 1985.	87
6.4	Same as figure 6.2 except for 0000 UTC, 15 June 1985.	88

6.4	continued	89
6.5	Upper-air soundings from (a) Pratt, Kansas and (b) Wichita, Kansas at 0000 UTC, 15 June 1985.	91
6.6	Same as figure 6.1 except for 0300 UTC, 15 June 1985.	93
6.7	Same as figure 6.2 except for 0300 UTC, 15 June 1985.	94
6.7	continued	95
6.8	Same as figure 6.1 except for 0600 UTC, 15 June 1985.	97
6.9	Same as figure 6.2 except for 0600 UTC, 15 June 1985.	98
6.9	continued	99
6.10	Vertical cross-section used to calculate omega and temperature deviation at 0300 UTC, 15 June 1985.	101
6.11	Vertical cross-sections of (a) omega and (b) temperature deviation for 0300 UTC, 15 June 1985.	102
6.12	Schematic of upper level flow of 14-15 June 1985 in relation to the positions of the mesoscale convective systems, the echo-free region and the surface mesolow.	103

LIST OF TABLES

2.1 Mesoscale convective complex (MCC) criteria 4
A.1 PAM and SAM pressure corrections for 14-15 June case. 115

Chapter 1

INTRODUCTION

Forecasting the occurrence of, and pinpointing the location of mesoscale convective systems (MCSs) is a problem that continues to plague atmospheric scientists and weather forecasters daily. The OK PRE-STORM (Oklahoma-Kansas Preliminary Regional Experiment for STORM-Central) experiment conducted in May and June of 1985 in the south-central United States provided an opportunity to gather high resolution data and to study various stages in the life cycle of MCSs. Numerous MCSs influenced the PRE-STORM operations area during this time and several have been studied (Augustine and Howard, 1988). While there have been several studies of continuous convection and the organization of single MCSs (Fujita, 1955; Hoxit et al., 1976; Ogura and Liou, 1980; Houze and Rappaport, 1984; Bluestein and Jain, 1985; Johnson and Hamilton, 1988; Houze et al., 1990; Stumpf et al., 1991) there are few studies of broken line convection or the interaction between two MCSs and their effects on the surrounding environment (Bartels and Rockwood, 1983; Stensrud and Maddox, 1988).

During the late afternoon and evening of 14–15 June 1985 a broken line of convection associated with a weak cold front passed through the PRE-STORM network. The line began as two separate MCSs, the first over northeastern Kansas and the second over the Oklahoma and Texas panhandles. Both systems were later classified as mesoscale convective complexes (MCCs) (Augustine and Howard, 1988). As the front progressed southward, smaller cells of convection developed between the two forming a broken line. However a gap (evident both in satellite and radar data) remained despite strong low-level moisture convergence. It is this gap that is of primary interest in this study.

The purpose of this paper is to document the life cycle of the line and to evaluate the processes that contributed to the organization of the broken line as opposed to a solid

line of convection. In addition, the surface and upper air features will be examined to determine the possible mechanisms controlling the development, location and strength of a surface mesolow between the two systems.

Chapter 2 of this paper will provide some research background on the organization of mesoscale convective systems, mesoscale circulations, and subsidence warming and the mesolow. Chapter 3 discusses the data sets used and analysis procedures. Chapter 4 provides a synoptic overview as well as radar and satellite data. Chapter 5 is a detailed mesoscale analysis of surface and upper air features. Chapter 6 provides a hypothesis for the 'gap' and the development of the mesolow. Finally, Chapter 7 summarizes the work.

Chapter 2

BACKGROUND

2.1 Organization of mesoscale convective systems

Mesoscale convective systems have been investigated in several field studies and experiments including SESAME (Severe Environmental Storms and Mesoscale Experiment), PRE-STORM (Preliminary Regional Experiment for STORM-Central), COPT (Convection Profonde Tropicale), and GATE (Global Atmospheric Research Programme's Atlantic Tropical Experiment). Orlanski (1975) classified a mesoscale system as having a horizontal scale from 2 km to 2000 km and a time scale of hours to days. Maddox (1980) included in his definition of mesoscale convective systems squall lines, tropical squall lines, tropical storms, cloud clusters, and mesoscale convective complexes (MCCs). Bartels et al. (1984) used satellite imagery to classify mesoscale convective systems as storm systems having a minimum length of 250 km and persisting at least 3 hours. The definition of a mesoscale convective system used during PRE-STORM was: a precipitation system that has a horizontal scale of 10–500 km and includes significant convection during some part of its lifetime. The MCSs include the MCC described by Maddox (1980), as well as other squall lines and groups of convective storms (Houze et al., 1989).

Like the mesoscale convective system, the mesoscale convective complex (MCC) has been defined by its physical size, shape and longevity, not by its internal structure (Maddox, 1980). A modified definition of the MCC by Augustine and Howard (1988) is given in Table 2.1. Although the appearance of the MCC by satellite is roughly circular, the internal structure of the system has not been well defined. Some systems have squall line characteristics (Leary and Rappaport, 1987) while others do not (Watson et al., 1988). Several systems have been found to develop a mid-level mesovortex (Johnston, 1982; Verlinde and Cotton, 1990; Bartels and Maddox, 1991). Smaller systems often merge to

Table 2.1: Modified mesoscale convective complex (MCC) criteria (from Augustine and Howard, 1988).

Size	Continuous cold cloud shield (IR temperature $\leq -52^{\circ}\text{C}$) must have an area $\geq 50\,000\text{ km}^2$
Initiation	Size definition is first satisfied
Duration	Size definition must be met for a period ≥ 6 hours
Maximum extent	Contiguous cold cloud shield (IR temperature $\leq -52^{\circ}\text{C}$) reaches maximum size
Shape	Minor axis/major axis ≥ 0.7 at time of maximum extent
Termination	Size definition is no longer satisfied

form one system (Maddox, 1980; Rodgers et al., 1985) or a MCC may actually split and become two (Maddox et al., 1982). Houze et al. (1990) identified two 'classifiable' and a third 'unclassifiable' types of precipitation organization in their study of 63 mesoscale convective systems (including both squall lines and MCCs). They found that most systems that produce large amounts of precipitation (minimum of 25 mm of rain in 24 hours over an area exceeding 12,500 km²) had both a convective echo region and a stratiform echo region.

Fig. 2.1a represents a schematic of the precipitation pattern in the symmetric case (Houze et al., 1990). Note the leading line of convective cells with the trailing stratiform region centered behind it. The most intense cells may be found at any location in the convective line. Fig. 2.1b represents the schematic for the asymmetric case (Houze et al., 1990). In this case new cell growth and the most intense cells are located on the southwestern end of the convective line and the stratiform region is behind the northeastern edge of the convective line. While many of the cases Houze et al. (1990) studied fit either the symmetric or asymmetric schematics, nearly one third of the cases fit neither and were termed 'unclassifiable'. These systems had both convective and stratiform regions but no pattern or relationship was discernable. The 14 - 15 June case studied in this paper with its leading stratiform region fits into this category.

A number of case studies support the findings of Houze et al. (1990). The symmetric pattern is similar to systems studied by Newton (1950), Fujita (1955), Ogura and Liou (1980), and Johnson and Hamilton (1988). The asymmetric pattern was found in studies by Smull and Houze (1987a) and Houze et al. (1989). A recent study by Loehrer (1992) looked at the precipitation structure of 16 PRE-STORM MCSs. He found that 12 of the 16 systems developed into the asymmetric pattern during the mature-to-dissipating stage of their lifecycles. He also found the stratiform region to be north of the main convective line with the strongest pressure gradient at the back edge of the stratiform region (Fig. 2.2).

Bluestein and Jain (1985) and Bluestein et al. (1987) looked at the formation of mesoscale lines of precipitation both in severe and non-severe squall line cases. The two

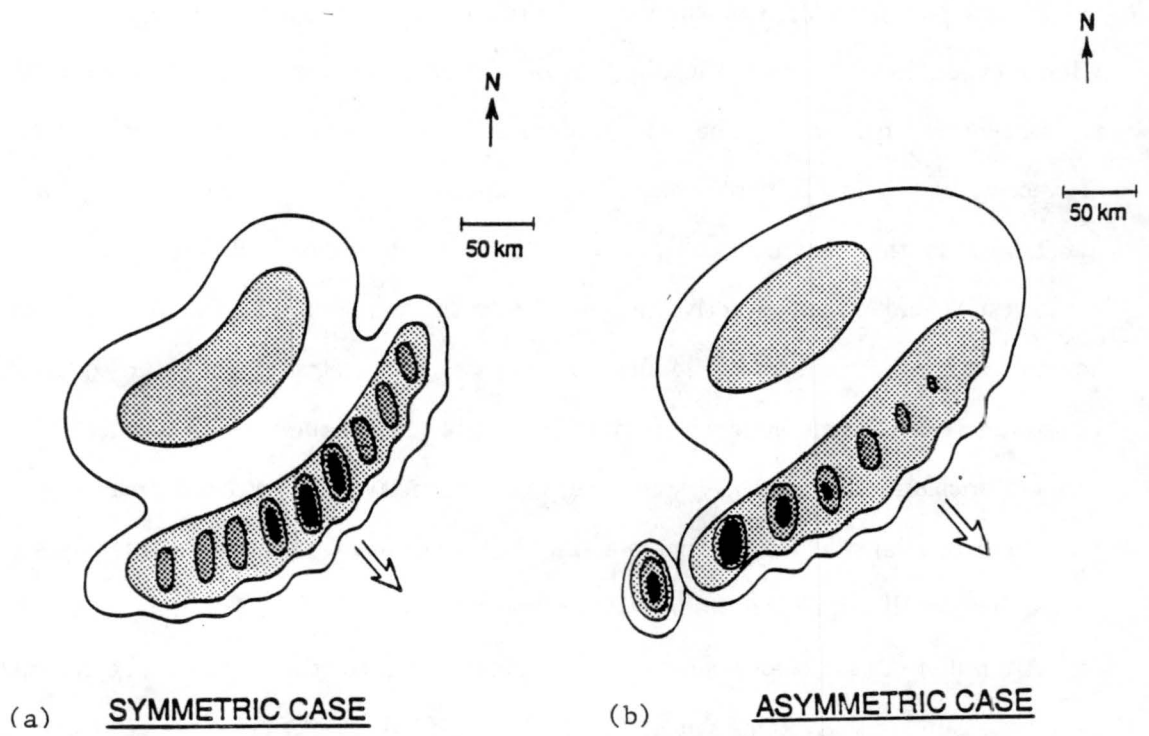


Figure 2.1: Schematics depicting (a) symmetric and (b) asymmetric types of precipitation patterns (from Houze et al., 1990).

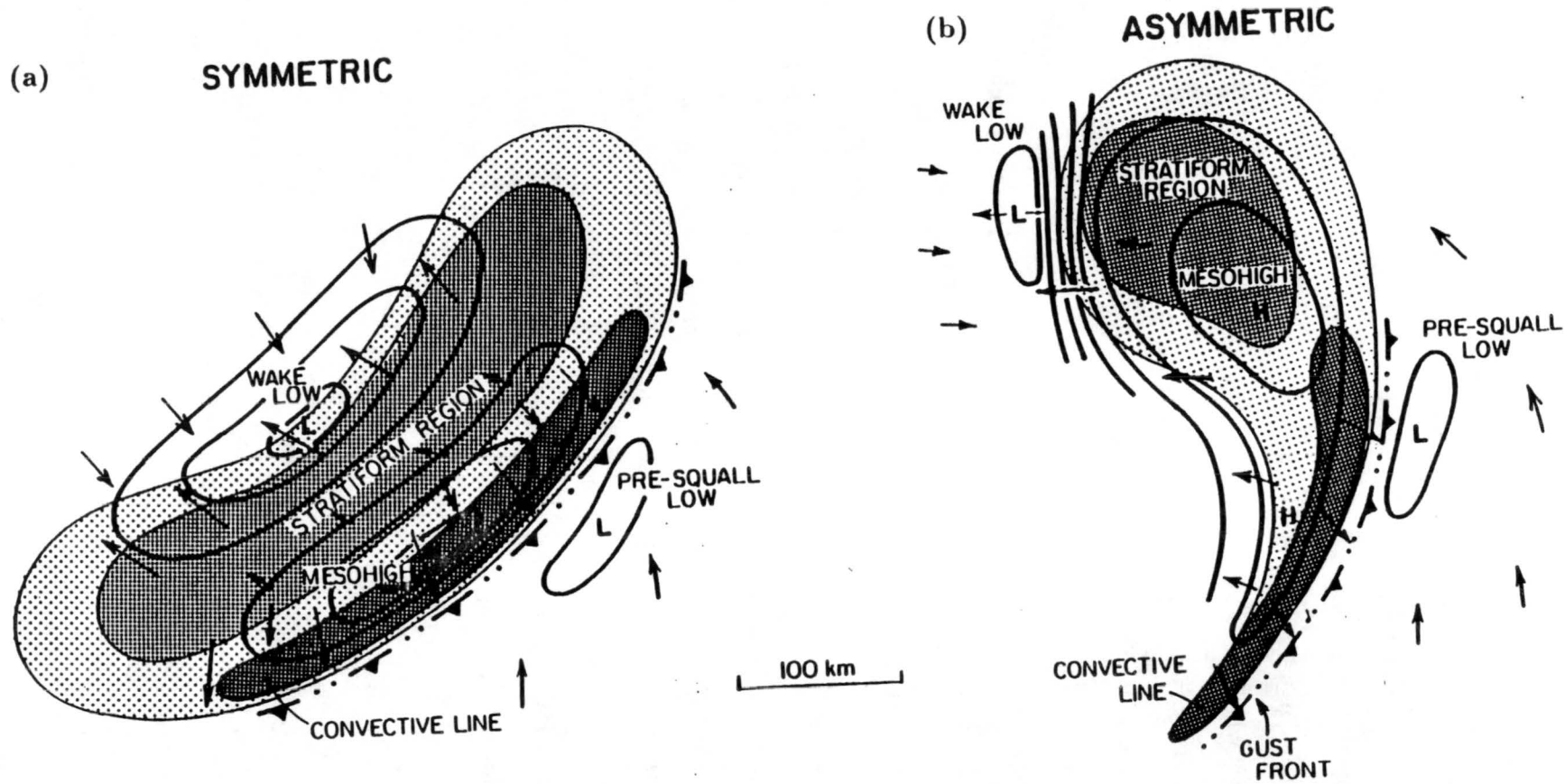


Figure 2.2: Schematics depicting (a) symmetric and (b) asymmetric types of precipitation patterns with pressure field overlaid (from Loehrer, 1992).

studies examined 150 cases over an 11-year period and formulated four classifications of squall line development. Fig. 2.3 represents a schematic of the four types of squall line formation (Bluestein and Jain, 1985). Note the different ways the lines develop. The broken-line squall line develops as a discrete number of cells grow and new cells develop between them. This type of growth is most often associated with a cold front. Back-building occurs when a new cell appears upstream (relative to cell motion) of the older cells and eventually forms a line. Back-building occurs near fronts and dry lines. When an area of initially disorganized, moderate-to-intense cells develop into a solid line of convection, the squall line is termed a broken areal. Embedded areal formation occurs when a convective line develops within a larger area of stratiform precipitation. The development of the 14 - 15 June case resembles the broken-line formation.

2.2 Mesoscale circulations

An understanding of the airflow patterns in and around the mesoscale convective system has provided information regarding the formation of these systems, their internal structure, associated pressure fields, and their influence on the surrounding environment.

Circulations within the mesoscale convective system have been studied by Fujita (1955), Newton (1966), Ogura and Liou (1980), Gamache and Houze (1985), Maddox (1983), Houze and Rappaport (1984), Smull and Houze (1985), Srivastava et al. (1986), Rutledge and Houze (1987), and Houze et al. (1989) among others. A schematic of flow through a squall line with a trailing stratiform region by Houze et al. (1989) is shown in Fig. 2.4.

The convective region is dominated by a system-relative, ascending, front-to-rear flow. This flow begins in the low levels ahead of the gust front and slopes upward through the convective region into the stratiform area, transporting hydrometeors rearward which contribute to the precipitation in that region (Smull and Houze, 1985; Rutledge and Houze, 1987; Houze et al., 1989). A system-relative, rear-to-front flow (often referred to as a rear inflow jet) enters the stratiform region just below the trailing stratiform cloud and descends toward the convective line (Srivastava et al., 1986; Smull and Houze, 1987b;

**CLASSIFICATION OF SQUALL-LINE
DEVELOPMENT**

BROKEN LINE (14 Cases)			
BACK BUILDING (13 Cases)			
BROKEN AREAL (8 Cases)			
EMBEDDED AREAL (5 Cases)			
	$t=0$	$t=\Delta t$	$t=2\Delta t$

Figure 2.3: Schematic showing idealized depiction of squall line formation (from Bluestein and Jain, 1985).

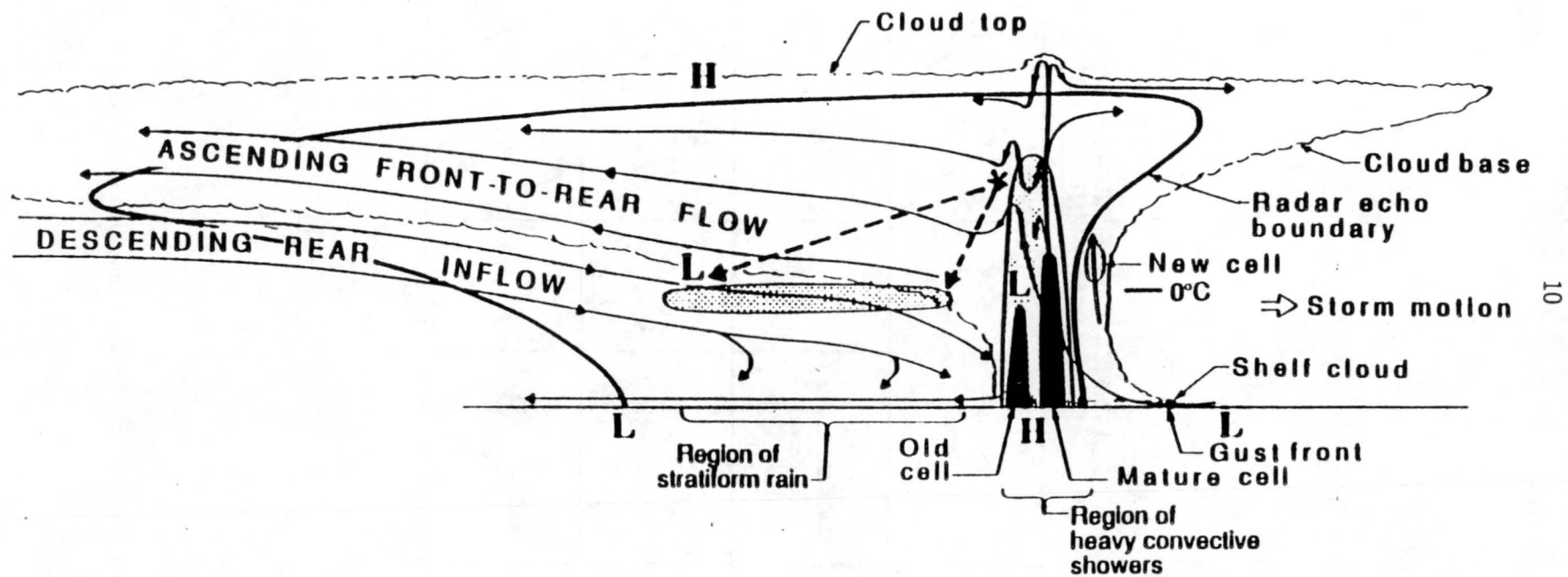


Figure 2.4: Conceptual model of a squall line with a trailing stratiform region viewed perpendicular to the convective line (from Houze et al., 1989)

Houze et al., 1989). In the case of a leading stratiform region, Houze and Rappaport (1984) found a strong system-relative, rear-to-front flow from 400 mb to 200 mb in place of the ascending, front-to-rear flow found in systems with trailing stratiform regions.

Motions within a squall-line type MCS with a leading convective region and a trailing stratiform region are generally characterized by low-level convergence near the leading edge, low-level divergence in the stratiform region and divergence at upper levels (Ogura and Liou, 1980). A second region of convergence is found in the mid-levels of the stratiform region. Studies by Gamache and Houze (1982), Houze and Rappaport (1984), and Johnson and Hamilton (1988) show similar results. In his study of MCCs, Maddox (1983) found strong convergence from the surface to 450 mb with a peak near 700 mb and divergence above with a peak near 200 mb. Wetzel et al. (1983) also documented strong divergence in upper levels of an MCC.

The squall-line type MCS has strong upward vertical motion in the convective region with downward motion in the low-to-mid levels of the stratiform region and upward motion in the mid-to-high levels of the stratiform region (Ogura and Liou, 1980; Gamache and Houze, 1982; and Houze and Rappaport, 1984). The MCC is dominated by upward motion in the system and compensating subsidence in the clear air regions around it (Maddox, 1983). In addition to divergence in the upper levels of an MCC, Wetzel et al. (1983) also detected strong convergence beyond the storm at upper levels. This implies subsidence in the clear region surrounding the MCC. Evidence of subsidence in the mid-levels of the clear air region was also found by Wetzel et al. (1983) by examining sounding stations in the vicinity of the MCC.

Compensating subsidence has been measured in the clear air regions adjacent to and between clouds both in low- and mid-latitudes. These areas are often drier and warmer than their surroundings. Aircraft observations have measured anomalous warming in these areas suggesting that the air is forced to warm by adiabatic compression (Fritsch, 1975) and humidity observations show areas of anomalously dry air. An experiment by Cunningham (1959) showed a rise in air temperature of 2 to 3° C and a drop in relative humidity to one fourth the environmental humidity. According to Fritsch (1975), the

speed of the subsidence is 25 to 50 percent of the updraft speed in the convection and the area affected by the subsidence is double the area of moist ascent. If the subsidence is sufficiently strong, it can suppress convection in the area.

2.3 Subsidence warming and the mesolow

The formation of mesohighs and mesolows within MCSs has been studied extensively by a number of authors (e.g. Byers and Braham, 1949; Fujita, 1955, 1959, 1963; Williams, 1963; Hoxit et al., 1976; Fritsch and Chappell, 1980; Ogura and Liou, 1980; Cunning and DeMaria, 1986; and Johnson and Hamilton, 1988). Mesohighs are usually found following the leading edge of convection (Williams, 1948; Brunk, 1949; Fujita, 1955; Johnson and Nicholls, 1983; and Johnson and Hamilton, 1988). The causes of the mesohigh may be attributed to evaporational cooling by precipitation (Fujita, 1959) and precipitation loading (Sanders and Emanuel, 1977). The wake low (mesolow behind the MCS) is usually found along the back edge of the stratiform region of the MCS (Williams, 1953; Fujita, 1955; Johnson and Nicholls, 1983; Johnson and Hamilton, 1988). The probable mechanism for the formation of the wake low is a hydrostatic pressure fall due to subsidence beneath and to the rear of the anvil cloud (Williams, 1963) which can be related to the rear-inflow jet (Johnson and Hamilton, 1988). In addition, a collapsing cold pool may contribute to wake lows (Johnson et al., 1989). While the surface pressure field is not a main focus of this study (see Loehrer, 1992) the development of a mesolow between the two MCSs is investigated.

Hoxit et al. (1976) studied the formation of a mesolow in advance of a squall line. Subsidence in the mid- and upper troposphere was found above the region where the mesolow developed. They calculated that sinking motion on the order of tens of centimeters per second in the upper troposphere (100 – 500 mb) would result in adiabatic warming of the layer by roughly $0.4^{\circ}\text{C h}^{-1}$ and hydrostatic surface pressure falls of $2 - 4 \text{ mb h}^{-1}$. Fankhauser (1974) also found subsidence associated with the development of the mesolow.

A modeling study by Fritsch and Chappell (1980) strongly supports the subsidence warming hypothesis for the formation of surface mesolows. As mentioned in the previous

section, subsidence has been measured in the clear air regions adjacent to and between clouds. Fritsch and Chappell (1980) found that the subsidence in fact occurs all around the convective system. The timing, location, and intensity of the surface mesolow induced by subsidence warming depends on many factors (shown in Table 1 of Fritsch and Chappell (1980)). The formation of the mesolow also depends on where the individual systems are located and how they interact with each other. If the subsidence regions of two convective systems overlap they will produce a more concentrated area of subsidence warming and increase the possibility of a surface mesolow. This hypothesis will be applied to the mesolow that develops between mesoscale convective systems in the 14–15 June case.

2.4 Interactions between mesoscale convective systems

It is well known that new convection often develops along intersecting thunderstorm outflows, convergence lines and fronts (Purdom and Marcus, 1982; Weaver and Nelson, 1982; Wilson and Schreiber, 1986). An outflow boundary or convergence line may also strengthen an existing system (Bartels and Rockwood, 1983; Leary and Rappaport, 1987). A case study by Stensrud and Maddox (1988) examined the interaction between two mesoscale circulations that occurred on 23–24 June 1985. Both mesoscale systems produced cold outflows that collided over central Kansas. Although the collision of the outflows produced strong low-level convergence ($1.2 \times 10^{-4} \text{ s}^{-1}$) and forced upward motion in the low levels, no new thunderstorms developed in this region. In a post analysis of the data an area of strong convergence and subsidence in the mid and upper levels was found between the two mesoscale systems. Stensrud and Maddox (1988) hypothesized that the upper-level anvil outflows from the two mesoscale convective systems had collided and forced strong subsidence in the mid-levels, helping to suppress the development of new thunderstorms. A schematic of the hypothesized mesoscale circulations in this case is shown in Fig. 2.5.

The 14–15 June case has very similar characteristics to the one studied by Stensrud and Maddox (1988). Since documentation of such events is very limited and the potential difficulties they present for forecasting are significant, a detailed analysis of the 14–15 June case is conducted using PRE-STORM sounding, surface and radar data.

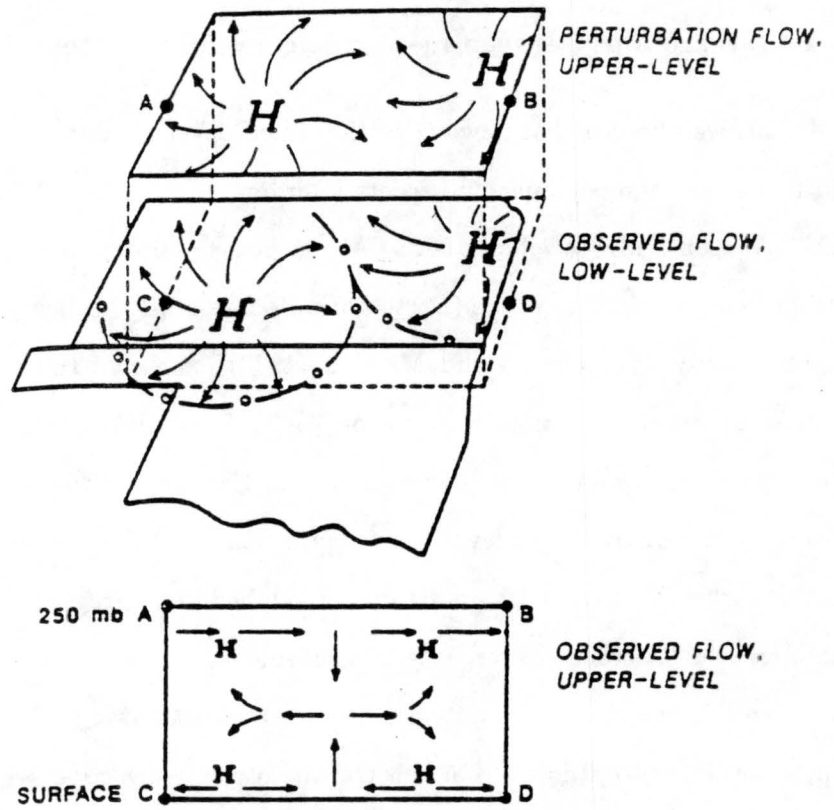


Figure 2.5: Schematic of hypothesized mesoscale circulations for two opposing mesoscale convective systems. (from Stensrud and Maddox, 1988)

Chapter 3

DATA SET AND ANALYSIS PROCEDURES

3.1 PRE-STORM

The Oklahoma-Kansas Preliminary Regional Experiment for STORM-Central (OK PRE-STORM or PRE-STORM) was conducted over the south central United States from 1 May to 27 June 1985 with the primary purpose of studying the structure and dynamics of mesoscale convective systems. Several MCSs passed through the network during the May – June timeframe. In fact, more MCCs (a subset of MCSs) occurred in 1985 than in any year since the recording of them began in 1978 (Augustine and Howard, 1988). The systems that influenced the PRE-STORM network are documented in a daily operations summary by Meitin and Cuning (1985).

The experiment made use of several observing systems including a dense network of surface observation sites, Doppler radar, NWS radar, NWS and supplemental rawinsondes, wind profilers, lightning location sensors, satellite data and aircraft. Fig. 3.1 shows the mesonet network while a full explanation of the operating systems is presented by Cuning (1986). Data used in this study includes surface observations, upper air data, radar and satellite data.

3.2 Surface data

Surface observations were recorded using a mesonet network of 84 automated observing systems deployed for the PRE-STORM project. Forty NCAR/FOF¹ Portable Automated

¹NCAR/FOF: National Center for Atmospheric Research/ Field Observing Facility

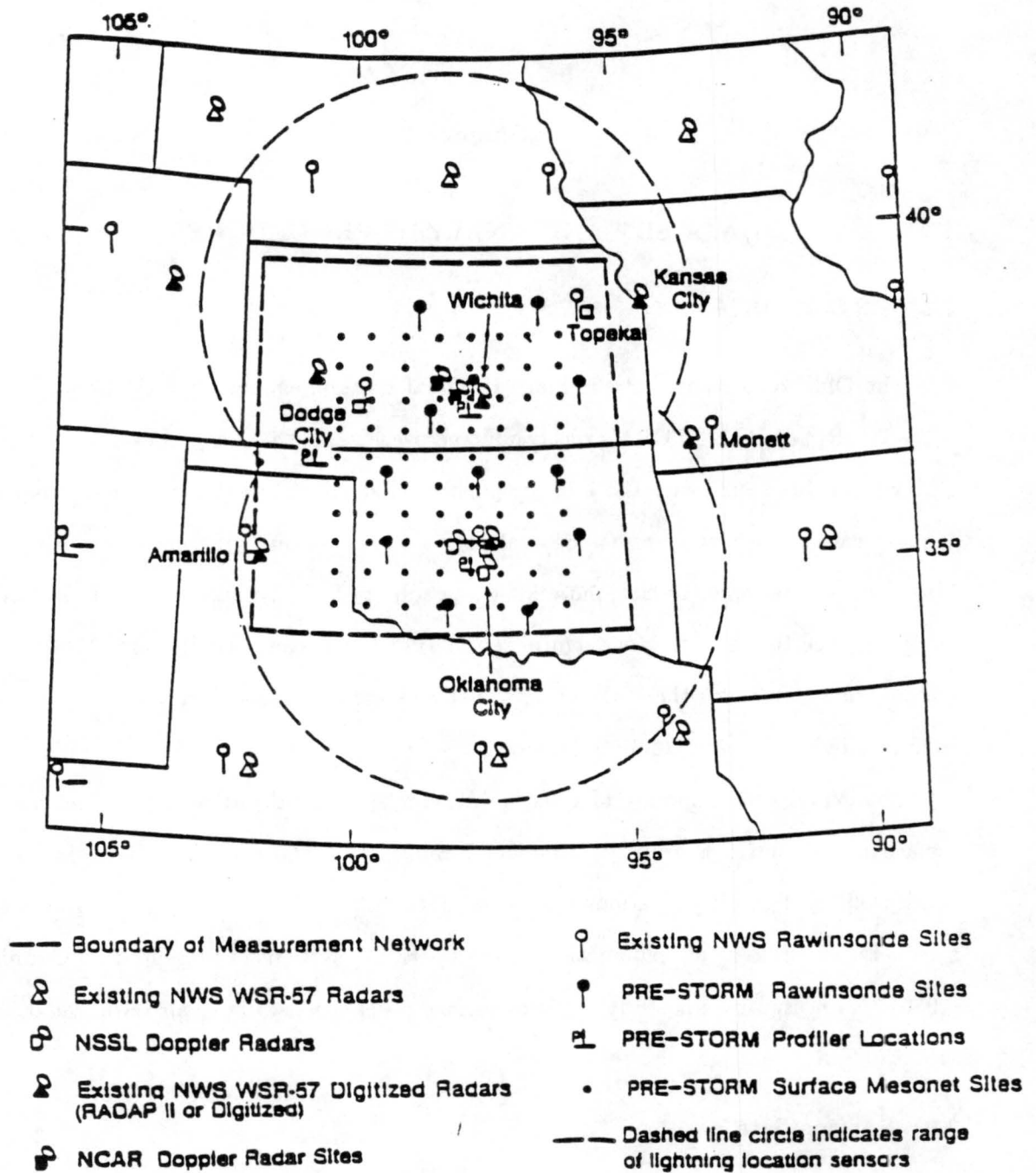


Figure 3.1: The PRE-STORM observational mesonet (from Meitin and Cuning, 1985).

Mesonetwork-II (PAM) stations and 42 NSSL² Surface Automated Mesonetwork (SAM) stations were placed in a rectangular grid with approximately 50-km spacing between stations (Fig. 3.2). In addition, two PAM stations were colocated with the other SAM stations for comparison purposes. The PAM and SAM stations measured station pressure, dry-bulb temperature, wet-bulb temperature, u- and v-wind components, and rainfall. Data were reported as 5-minute averages for wind, temperature, wet-bulb temperature and pressure; 5-minute maxima for wind gusts; and 5-minute accumulated amounts for rainfall.

3.2.1 Pressure adjustments

To obtain meaningful pressure analyses, the pressure data from the 84 stations had to be adjusted to a common level; diurnal and semi-diurnal effects had to be removed; and pressure biases due to individual instrument errors also had to be removed. All pressure data were first adjusted to 480 m (the mean elevation of the stations) using the following equation:

$$p_{480} = p_s \exp \left[\frac{g(480 - z_s)}{R_d \bar{T}_v} \right] \quad (3.1)$$

where p_{480} is the pressure adjusted to 480 m, p_s is the station pressure in millibars and z_s is the station elevation in meters. Gravity $g = 9.8 \text{ m s}^{-2}$ and the gas constant for dry air $R_d = 287 \text{ J kg}^{-1} \text{ K}^{-1}$. The mean virtual temperature of the air, \bar{T}_v , is approximated by the surface virtual temperature.

After the pressures were adjusted to 480 m, a correction was applied to remove the effects of the diurnal and semi-diurnal pressure tides (Stumpf, 1988). Pressure instrumentation errors were found during calibration checks. Furthermore, these errors sometimes drifted in time. Loehrer (1992) performed an extensive data quality check of the data and developed correction tables for the sites. These corrections were applied to the pressure at 480 m to obtain a final adjusted pressure used in the surface analyses.

²National Severe Storms Laboratory

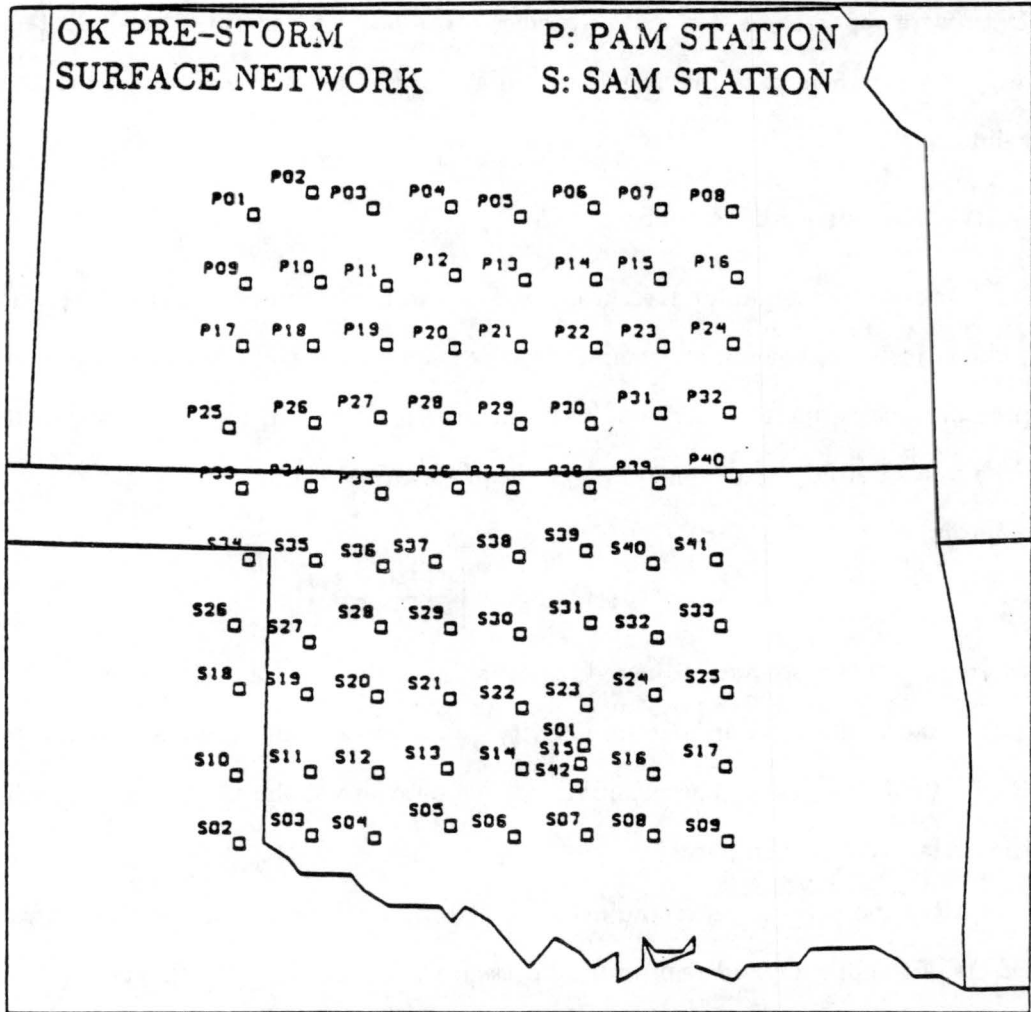


Figure 3.2: The PRE-STORM Portable Automated Mesonetwork(PAM) and Surface Automated Mesonetwork (SAM) surface array.

3.3 Upper air data

3.3.1 Data network and adjustments to upper air data

The upper air network consisted of NWS sites and eleven supplemental sounding stations. Soundings were taken approximately every three hours from the supplemental sites and every 12 hours from the NWS sites. Sounding stations were approximately 150 km apart (Fig. 3.3). Data collected included temperature, moisture, wind, pressure, height, and balloon displacement.

The sounding data were interpolated to 25 mb levels and checked for unrealistic features. If an unrealistic feature occurred over a small vertical layer, it was replaced by data interpolated from outside the layer. If it occurred over a much deeper layer the sounding was removed. The 15/0300 UTC sounding from Woodward (WWR) in northeast Oklahoma was removed from the data set.

The observation locations at each level were calculated taking into account balloon displacement and the time of the observation. The sounding data were then gridded onto a $1/2^\circ$ by $1/2^\circ$ grid using a Barnes objective analysis scheme (Barnes, 1964).

3.3.2 Calculated fields

The gridded upper air data were used to create constant pressure maps as well as vertical cross-sections of divergence, vertical velocity, moisture divergence, relative humidity, wind, and temperature fields. All vertical cross-sections were made along the line of convection to compare the calculated fields within the convective regions to the fields in the region between the convection. In order to condense the three-dimensional system into a two-dimensional representation, the data were averaged over a band 50 to 100 km wide, normal to the line, depending on the width of the line at the time of the observation.

The vertical velocity fields were adjusted following O'Brien (1970). O'Brien's method requires that the vertical velocity be zero at the top and bottom of the atmosphere. The PRE-STORM region slopes significantly (undisturbed surface pressures fall from 980 mb to 930 mb, east to west). In calculations of the vertical velocity, Gallus (1989) showed that using a no-slope surface of 975 mb did not produce significant differences compared

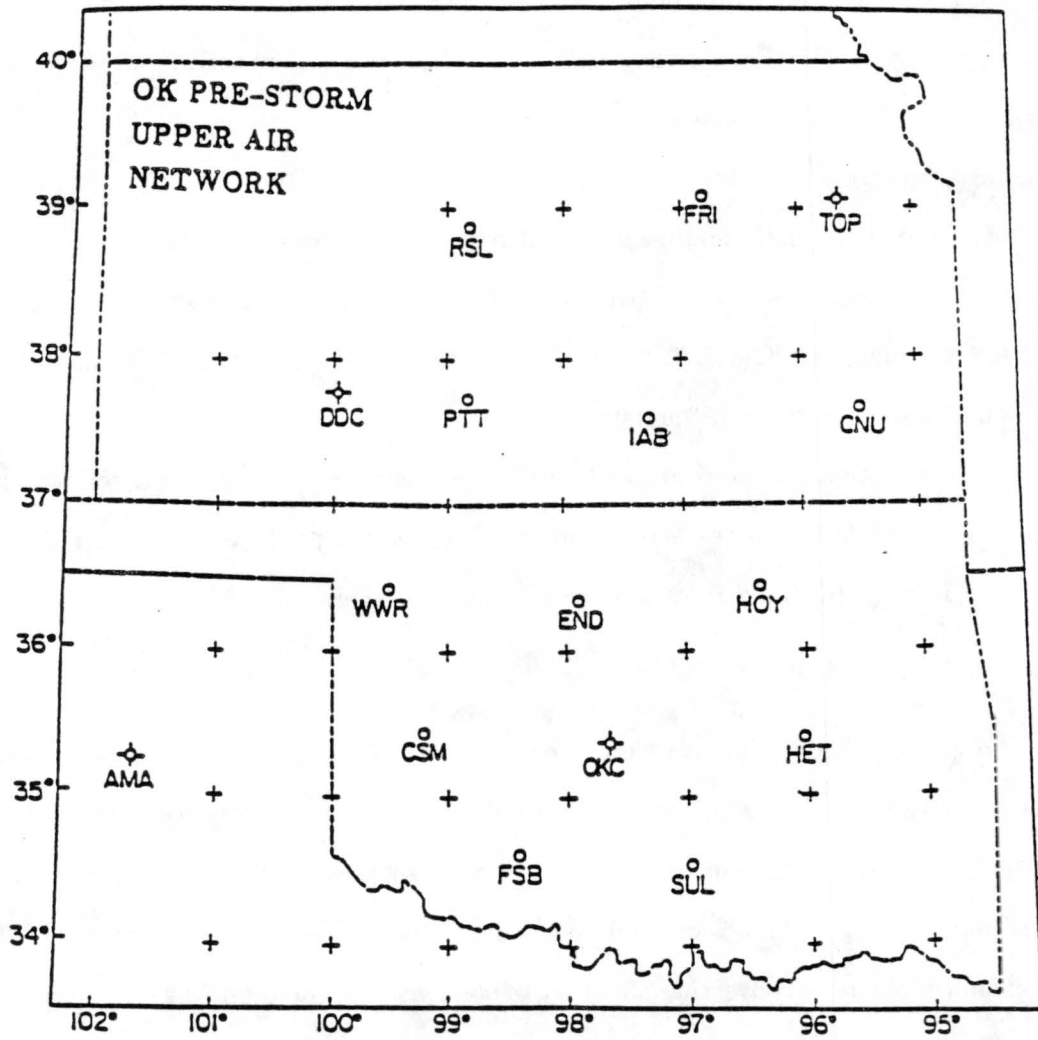


Figure 3.3: The PRE-STORM sounding mesonet network.

to a sloped surface. Therefore, the 975 mb level was set as the zero-vertical velocity level. The 125 mb level, which is just above the level of the tropopause, was chosen as the upper limit with zero vertical velocity.

3.4 Radar Data and Satellite Imagery

Radar data from the NWS WSR-57 radars located at Amarillo TX, Oklahoma City OK, Garden City KS, and Wichita KS were used in this study. After 0600 UTC the WSR-57 at the National Severe Storms Laboratory (NSSL), Norman OK replaced the Oklahoma City radar. NWS's second generation Radar Data Processor (RADAP-II) digitized the volume-scan radar data from the NWS WSR-57 radars. Low-level reflectivity (0.5 elevation angle) scans were used for the analyses. Radar image composites were made using the digitized data from the five radar sites. These data were processed using the analysis system located at the National Severe Storms Laboratory/Mesoscale Research Department (NSSL/MRD) laboratories in Boulder, Colorado.

The satellite data used were from the GOES-West, which was situated at 105°W during the experiment.

Chapter 4

SYNOPTIC OVERVIEW

The period 14 - 15 June 1985 provided an interesting study of the interactions between two mesoscale convective systems (MCSs). The two systems developed at roughly the same time, both ahead of a weak cold front in Kansas and Oklahoma, and traveled toward the south-southeast. While they traveled side-by-side, skirting the edges of the PRE-STORM network, the two never joined as anticipated by forecasters in the PRE-STORM region (R. H. Johnson, personal communication). A mesolow developed between the two during their mature stages. Another interesting feature was the leading stratiform region as opposed to the more common trailing stratiform region. In order to study these features more closely, an overview is needed.

4.1 Synoptic conditions

The surface analysis for 14 June at 1200 UTC (0600 local time) (Fig. 4.1a) showed a closed low of 1005 mb over the Nebraska-South Dakota border. A second closed low near the Colorado-Kansas border had a pressure of 1004 mb. Stationary frontogenesis was analyzed, extending west-east from northeast Colorado through southern Nebraska. Flow was from the south-southeast through much of Kansas and Oklahoma, and from the northwest in Nebraska (north of the frontogenesis region). Showers and a weak outflow boundary from the previous evening's thunderstorms persisted in northeast Nebraska and Iowa.

The 850 mb analysis (Fig. 4.1b) showed a trough axis from central North Dakota, through central South Dakota, western Nebraska, into northeast Colorado and northwest New Mexico. A reanalysis of temperature at every two degrees showed a thermal ridge just ahead of the height trough from southeast Colorado through northeast Nebraska. The

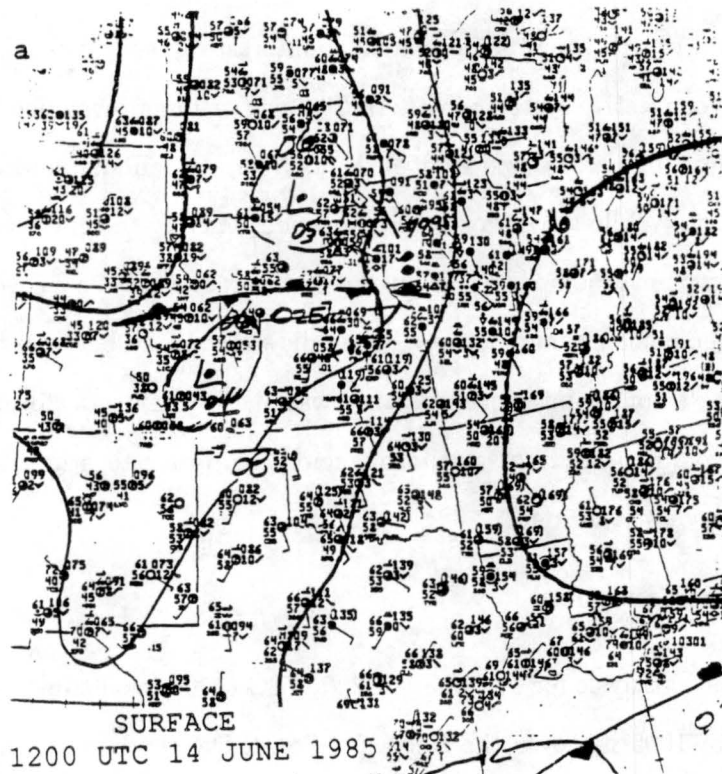


Figure 4.1: 1200 UTC 14 June 1985 surface and upper air analyses: (a) surface analysis; (b) 850 mb; (c) 700 mb; (d) 500 mb; (e) 300 mb. Solid lines on (a) are sea level pressure in millibars. Solid contours in (b) - (e) represent geopotential height in meters. Dashed contours represent temperature in °C.

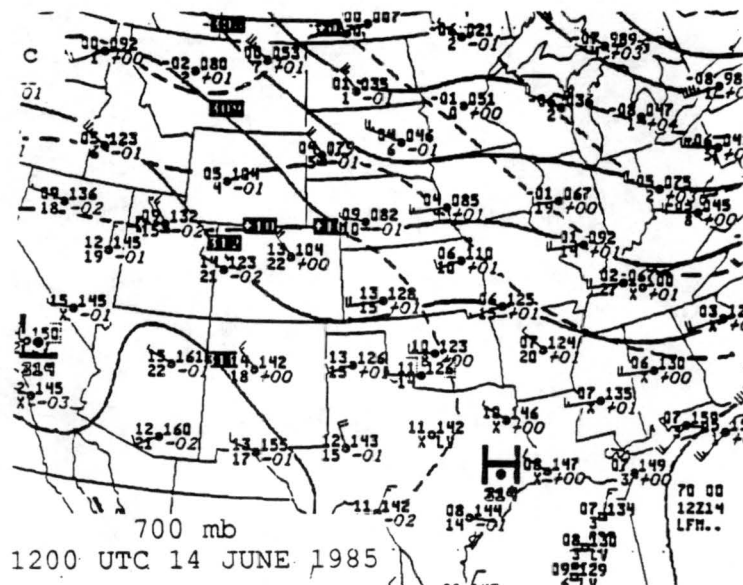
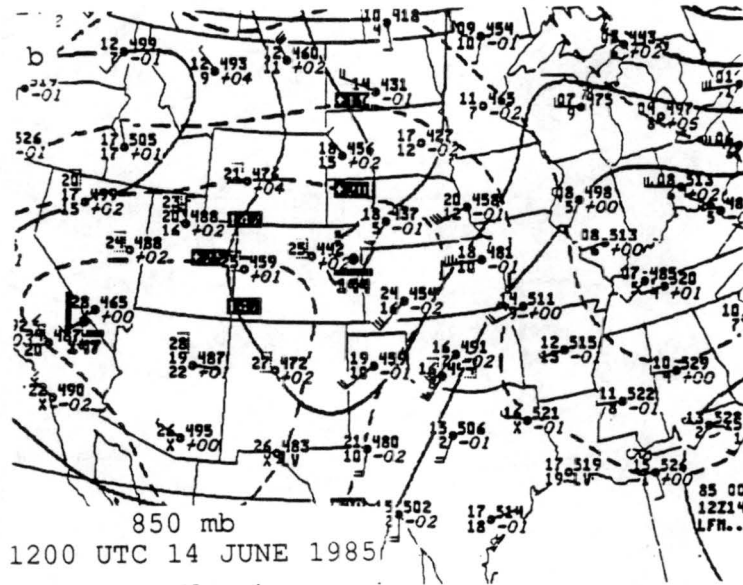


Figure 4.1: continued

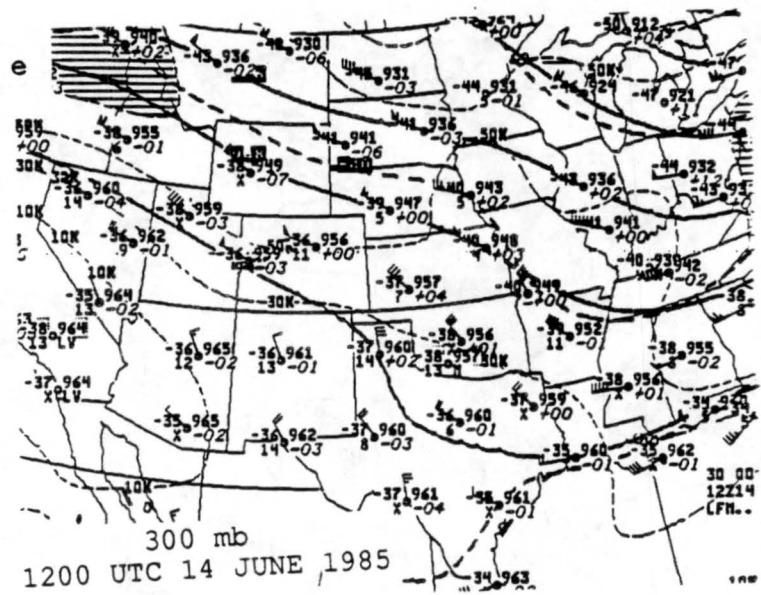
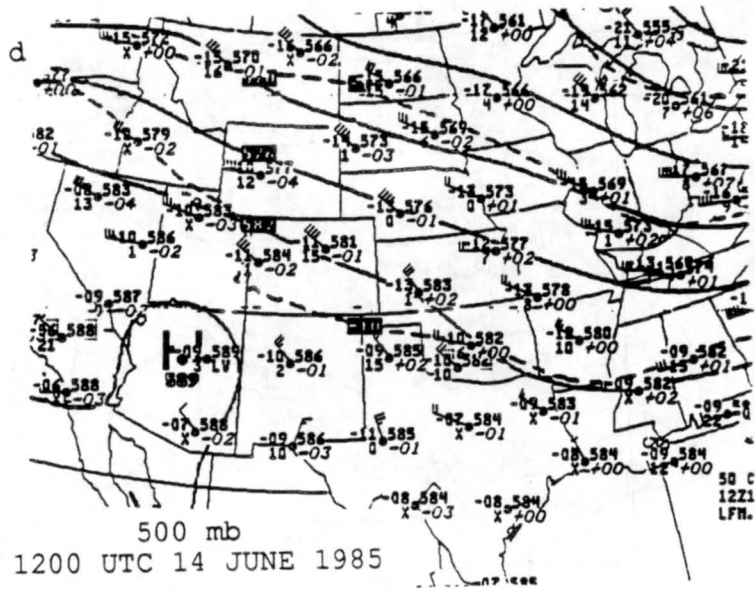


Figure 4.1: continued

flow was from the southwest at $10 - 15 \text{ m s}^{-1}$ with some anticyclonic curvature in the wind field. The Oklahoma-Kansas region was very dry.

The 700 mb trough (Fig. 4.1c) was nearly coincident with the 850 mb trough. A thermal ridge was evident with the trough. There was warm advection ahead of the trough and cold advection behind. A dry flow was from the west-southwest in the Oklahoma-Kansas region. Some moisture associated with the convection in Iowa was seen.

The flow at 500 mb (Fig. 4.1d) had veered to the northwest at $10 - 15 \text{ m s}^{-1}$ in Oklahoma and Kansas and 20 m s^{-1} in Nebraska and Colorado. Western Kansas and Nebraska were nearly saturated while eastern Kansas and Oklahoma remained dry. A 25 m s^{-1} jet extended from Wyoming through central Nebraska and into northeast Kansas at 300 mb (Fig. 4.1e). The convection over Nebraska and Iowa was situated in the left exit region of the 300 mb jet.

By 1800 UTC (not shown) the low near the Colorado - Kansas border moved south-eastward into southwest Kansas and filled to 1005 mb. The front was detectable only as a windshift line. Between 1800 and 0000 UTC showers began to develop in the northeast corner of Kansas. Likewise, thunderstorms had developed over the southern Colorado mountains and had begun to move into the plains (Toth, 1987).

The 15 June 1985 0000 UTC surface chart (Fig. 4.2a) depicted a 1005 mb low in southwest Minnesota with a cold front extending from the low, through northeast Nebraska, central Kansas and into southern Colorado. The second low had moved into the Texas Panhandle and had a central pressure of 1003 mb. South of the front, temperatures were $26 - 35^\circ\text{C}$ with dewpoints $13 - 18^\circ\text{C}$ and a southeast flow. To the north of the front temperatures were cooler ($22 - 25^\circ\text{C}$), and the dewpoints lower ($7 - 15^\circ\text{C}$) with flow from the north.

At 850 mb (Fig. 4.2b) there was a closed low over northeastern New Mexico with a trough extending from western Minnesota through Kansas and the far west corner of the Oklahoma panhandle. A 10 m s^{-1} southerly flow was over Texas and Oklahoma. A very moist tongue of air was found in this same region (dewpoints up to 15°C). The flow

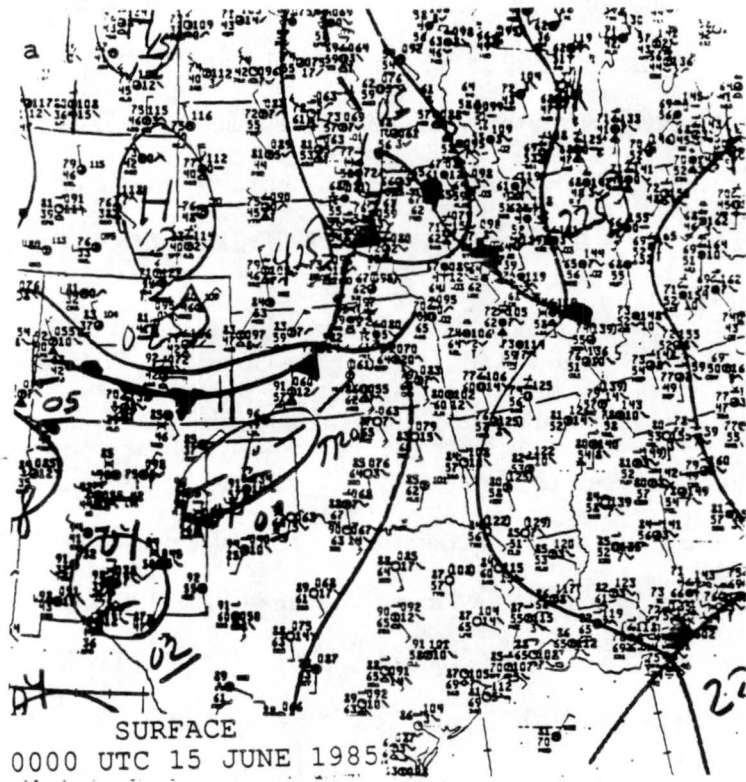


Figure 4.2: Same as 4.1 except at 0000 UTC, 15 June 1985.

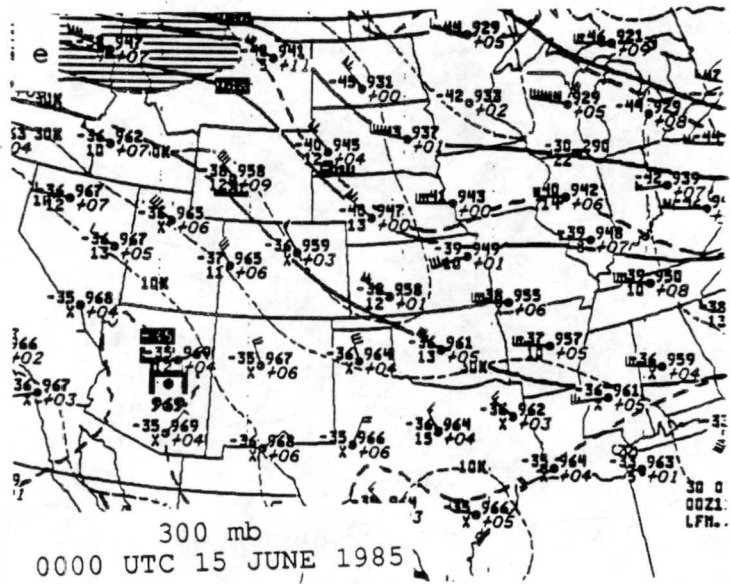
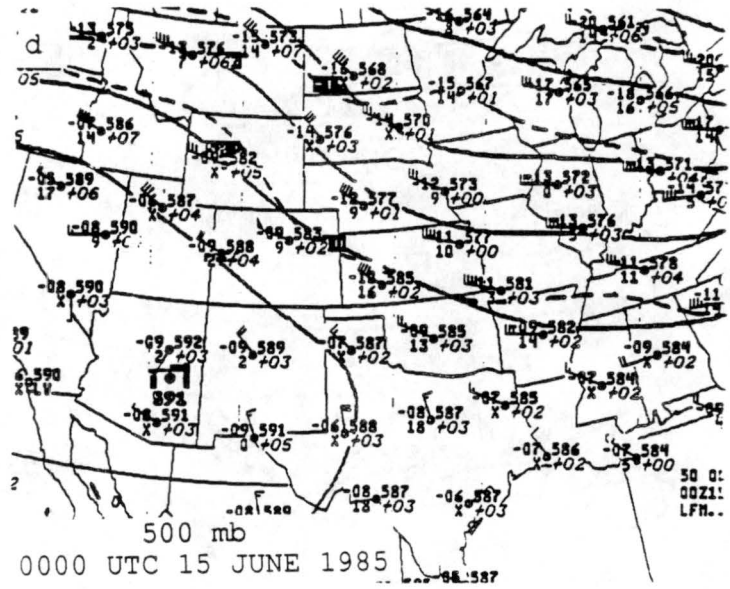


Figure 4.2: continued

in Kansas was from the north-northeast while in Nebraska the flow was from the north-northwest. Similar to 14/1200 UTC, a thermal ridge lay just south of the height trough with strong cold advection in western Kansas.

The trough was also evident at 700 mb (Fig. 4.2c). The flow was from the northwest through much of the region and from the southwest in northeast Kansas. Oklahoma and western Kansas were very dry while eastern Kansas shows moisture from the thunderstorms. A 20 m s^{-1} northwest flow was found at 500 mb (Fig. 4.2d). At 300 mb (Fig. 4.2e) the jet had moved southeastward into central Kansas. The left front exit region of the jet was over the northeast corner of Kansas favoring the continued growth of convection in that region.

4.2 Satellite and radar overview

This section presents sequences of satellite and radar imagery in order to illustrate the larger scale lifecycles and interactions between the two mesoscale convective systems.

The satellite sequence (Figs. 4.3a-i) shows the development and movement of the cloud shields associated with the MCSs. The system that developed in northeast Kansas will be referred to as MCS1 and the system that developed in the Oklahoma panhandle as MCS2. MCS1 moved to the south-southeast at 12 m s^{-1} while MCS2 moved toward the southeast at roughly 9 m s^{-1} .

Convection developed in both areas around 2200 UTC on the 14th (not shown) (Augustine and Howard, 1988). At 0000 UTC (Fig. 4.3a), MCS1 was just moving into the northeast corner of the mesonet, while MCS2 was in the Oklahoma panhandle. The area between the two showed a few enhanced clouds near MCS2. By 0130 UTC (Fig. 4.3b), new convection had developed near MCS2 forming a broken line with MCS1. MCS1 had reached MCC size by this time (Augustine and Howard, 1988). Note the echo-free or clear region between the two systems at this time. This gap was very prominent through much of the lifecycle of the two systems, closing at 0500 UTC (Fig. 4.3e) and opening again by 0600 UTC (Fig. 4.3f) as the systems began to dissipate.

The cloud shields associated with MCS2 and the new area of convection combined into one system by 0200 UTC (Fig. 4.3c) and reached MCC proportions by 0300 UTC

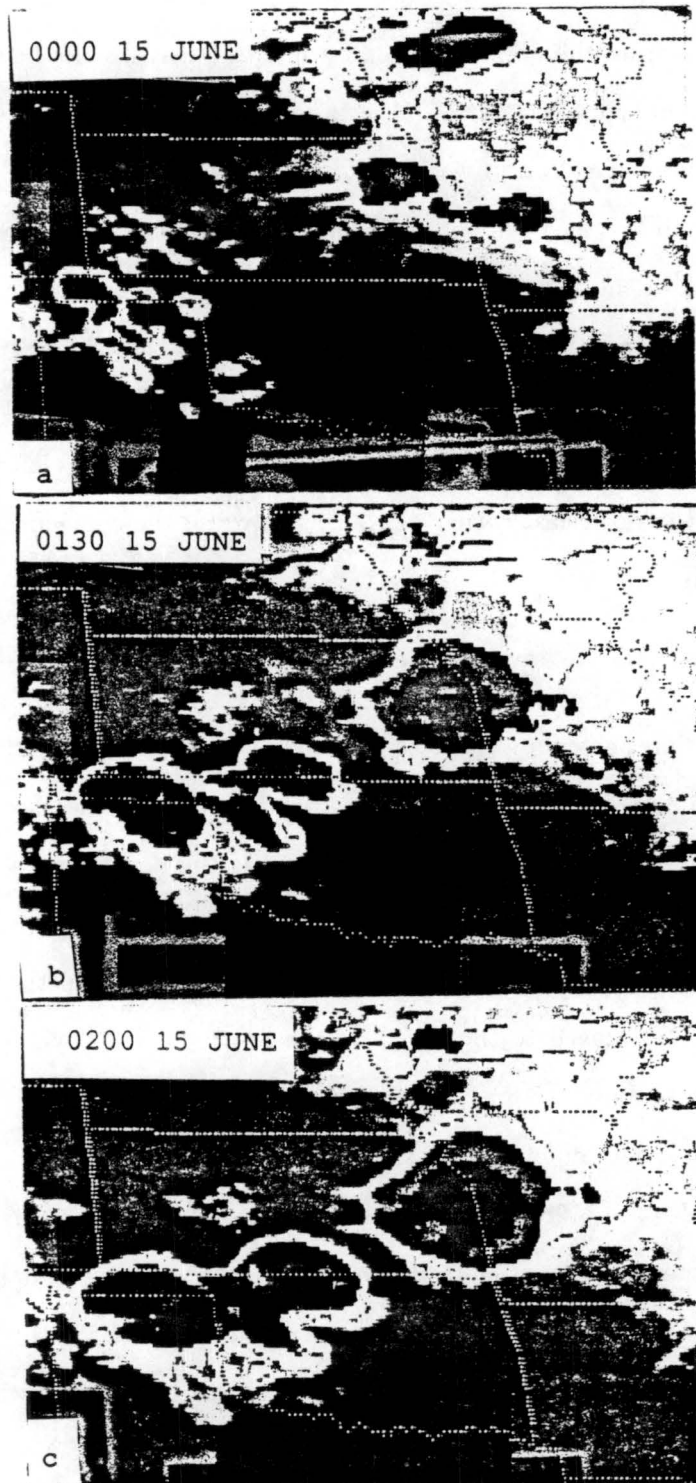


Figure 4.3: 15 June 1985 infrared (IR) satellite imagery for: (a) 0000 UTC; (b) 0130 UTC; (c) 0200 UTC; (d) 0300 UTC; (e) 0500 UTC; (f) 0600 UTC; (g) 0700 UTC; (h) 0800 UTC; and (i) 0900 UTC.

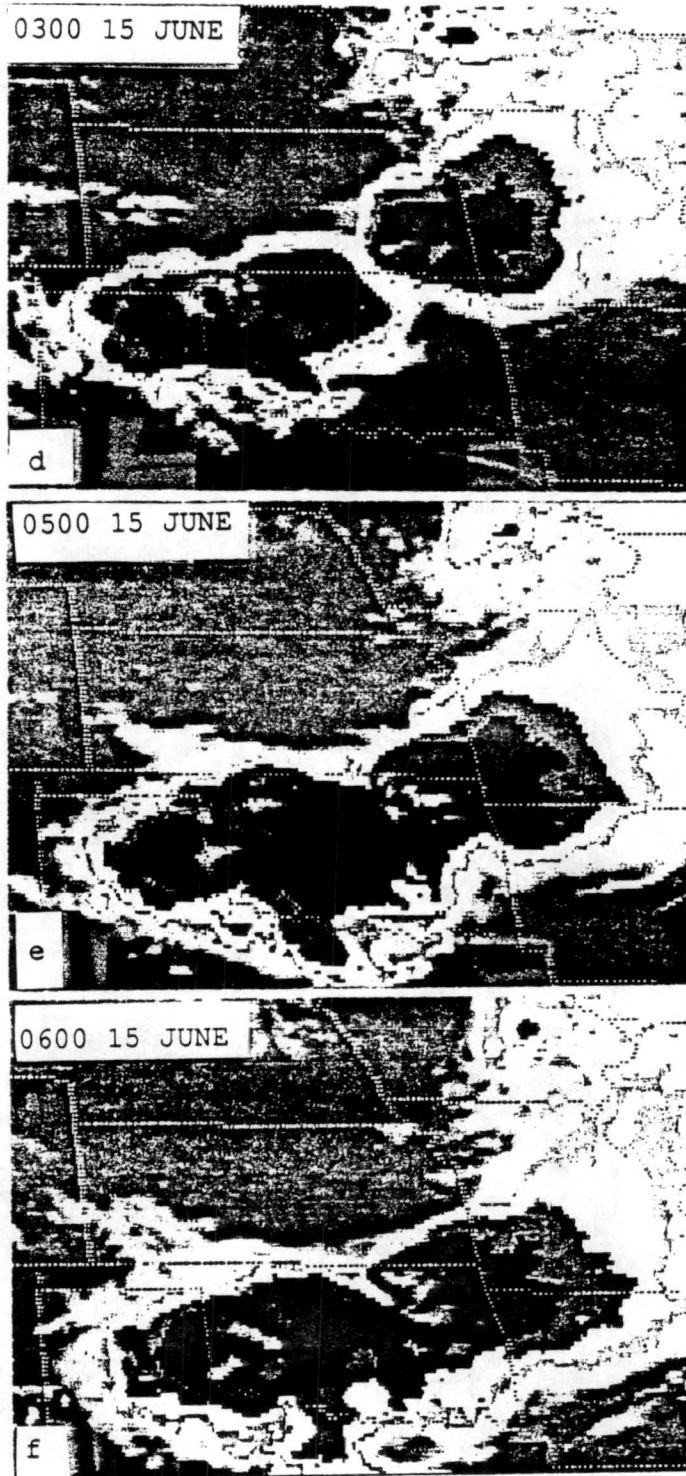


Figure 4.3: continued

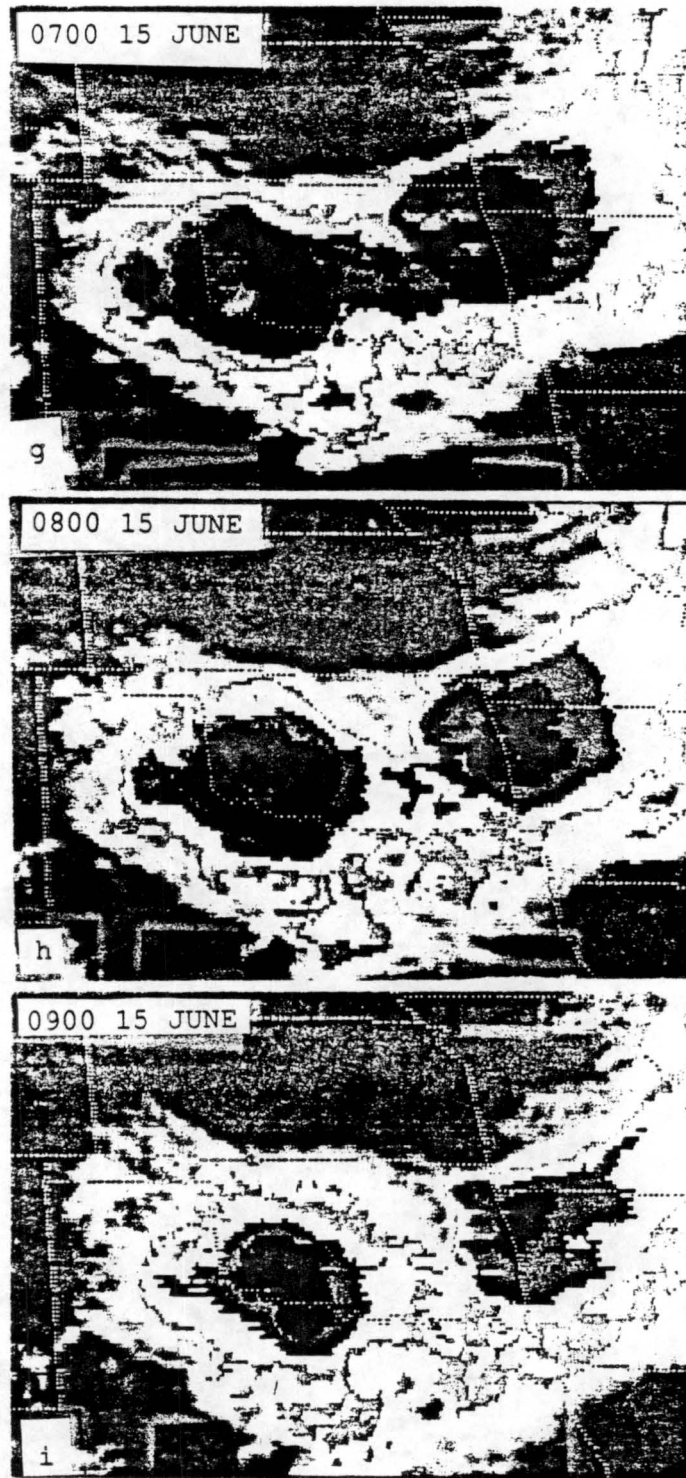


Figure 4.3: continued

(Fig. 4.3d), (Augustine and Howard, 1988). Figs. 4.3f-i show the sequence as the two systems began to dissipate. Augustine and Howard (1988) reported hail, one tornado, damaging winds and two injuries associated with MCS1, and damaging hail with MCS2.

The radar sequence shown in Figs. 4.4a-i depicts the low-level reflectivity field associated with the cloud features. At 0000 UTC (Fig. 4.4a) the precipitation pattern associated with MCS1 was just within range of the Wichita radar. Three bands of convection were apparent with the center band being the strongest. The lead band (which was also visible in the satellite imagery (Fig. 4.3a)) moved to the east and out of the mesonet and radar range by 0030 UTC (not shown). The central band became the dominant line of convection in MCS1. Precipitation associated with MCS2 was moving into radar range at 0000 UTC and could be seen in the Oklahoma panhandle as scattered cells.

Figs. 4.4b-c show the new convection as it developed between MCS1 and MCS2 at 0130 UTC and 0200 UTC. While the 0200 UTC satellite imagery (Fig. 4.3c) appeared to show MCS2 and this new convection as one at this time, the radar imagery showed three distinct areas of precipitation. MCS1 developed a stratiform region to the east with the strongest convection on the southern end and weaker convection to the north and northeast during this period. The convection in MCS2 had a more random pattern with some stratiform precipitation developing to the south. The new convection in northern Oklahoma developed into a northeast - southwest line by 0200 UTC.

Fig. 4.4d shows a large area of stratiform precipitation ahead of the convective line of MCS2 at 0300 UTC. By 0330 UTC (not shown) MCS2 and the line of convection in Oklahoma had become one. The stratiform region of MCS1 was well to the east of the convective region by this time. Note the area between MCS1 and MCS2 that coincides with the clear air region in Figs. 4.3c-d.

Fig. 4.4e shows the two MCSs at 0500 UTC. The convective line of MCS1 was still visible but the stratiform region was by this time out of radar range. MCS2 had lost most of its leading stratiform region and had taken on a very random pattern. MCS2 began to develop a trailing stratiform region around 0600 UTC (Fig. 4.4f). As the two systems

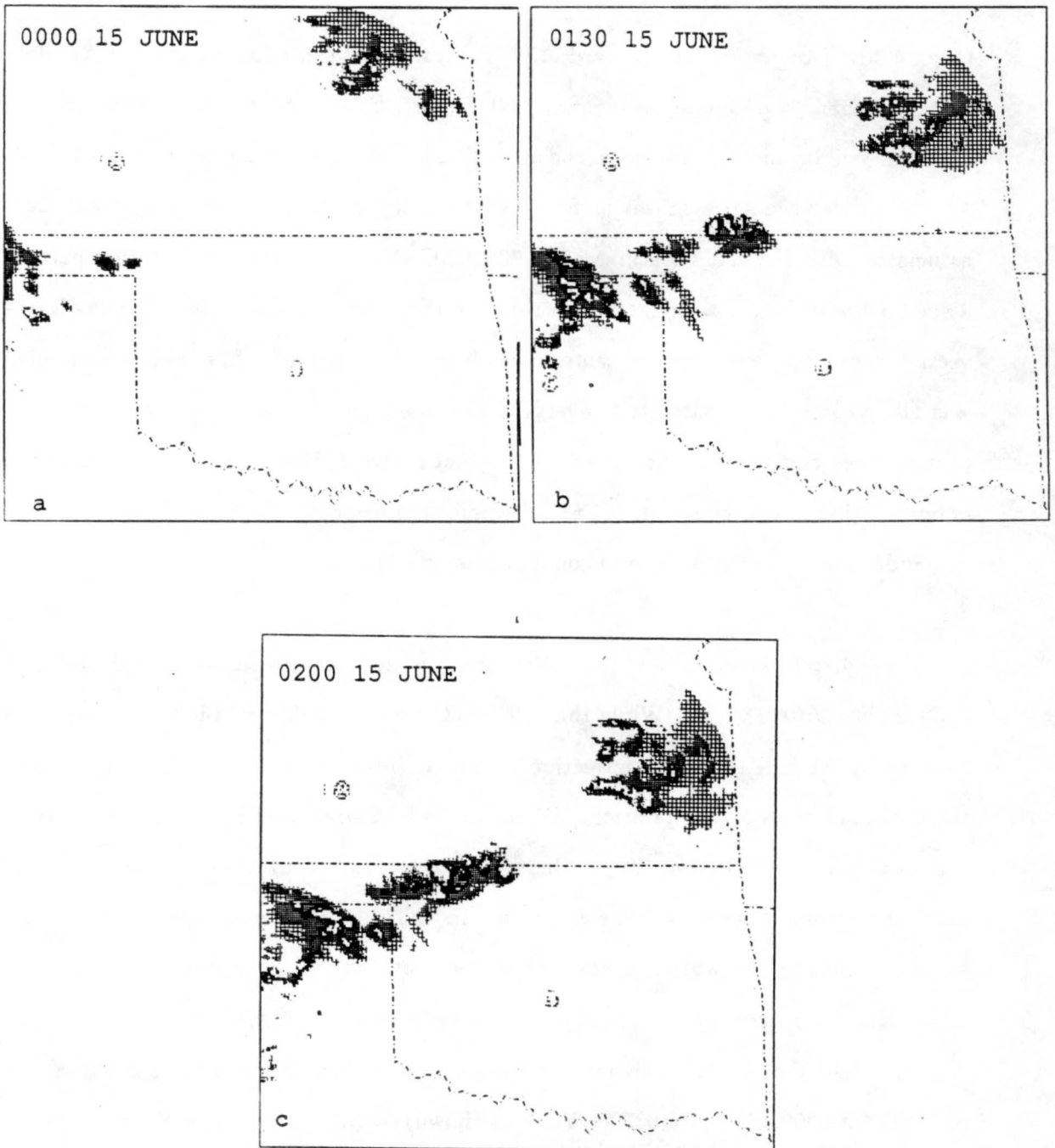


Figure 4.4: Radar composites of RADAP-II digitized data for 15 June 1985. Reflectivity contours are 15, 25, 40, and 50 dBz. Figures include: (a) 0000 UTC; (b) 0130 UTC; (c) 0200 UTC; (d) 0300 UTC; (e) 0500 UTC; (f) 0600 UTC; (g) 0700 UTC; (h) 0800 UTC; and (i) 0900 UTC.

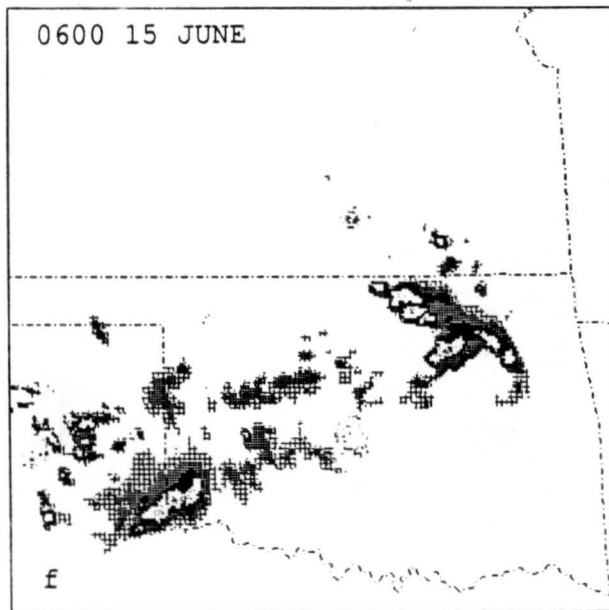
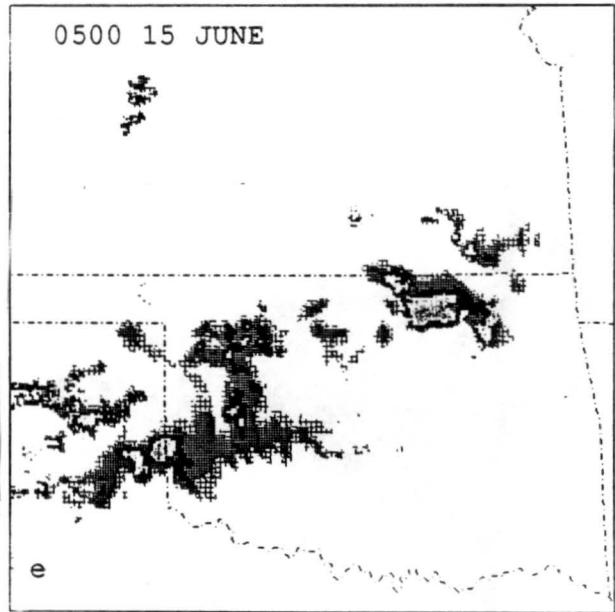
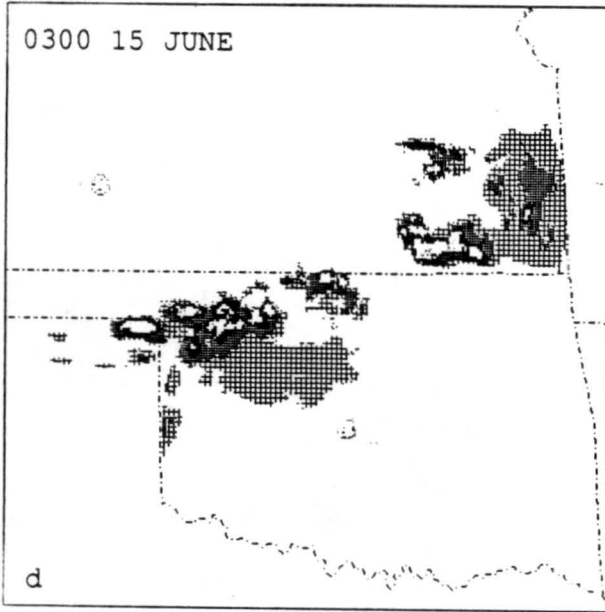


Figure 4.4: continued

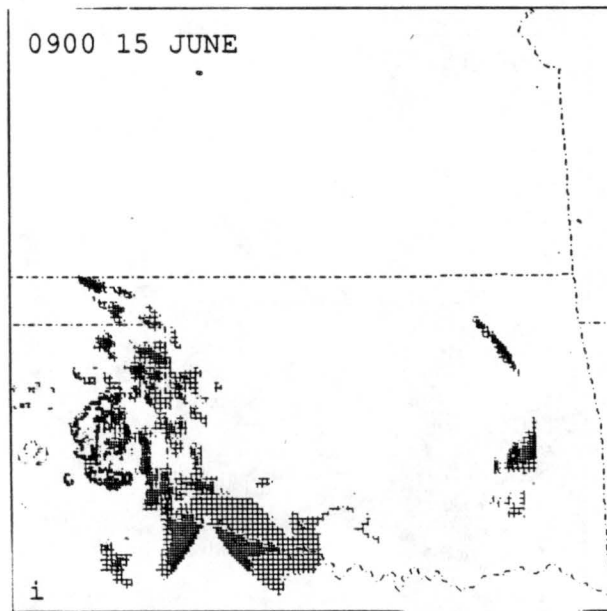
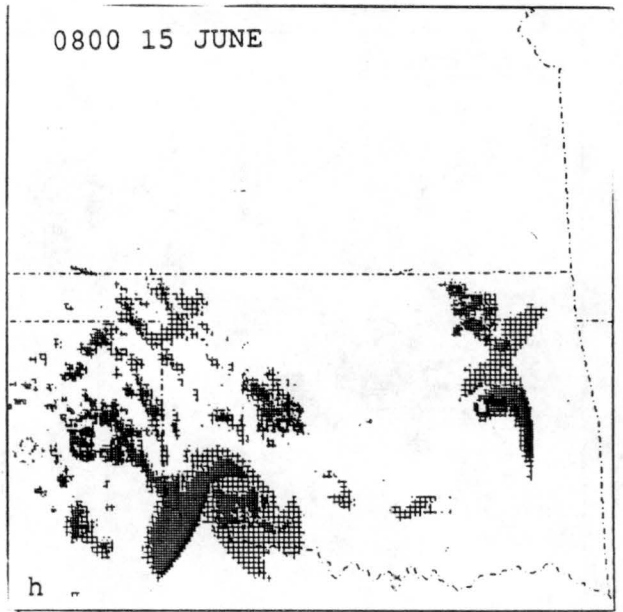
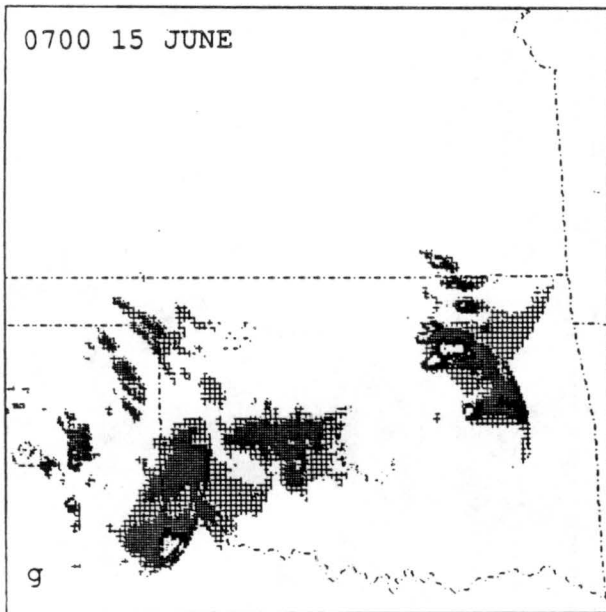


Figure 4.4: continued

began to dissipate, the convective regions weakened and moved out of radar range leaving behind stratiform precipitation (Figs. 4.4g-i).

Chapter 5

MESOSCALE ANALYSIS

The purpose of this chapter is to document the life cycles of the mesoscale surface and upper features of the two MCSs and the echo-free region between them on 14–15 June 1985. Although neither MCS was totally within the surface mesonet, the echo-free region, which is the main focus of this study, was within the mesonet throughout the period.

5.1 Surface observations

In this section a series of maps for 15 June are presented which show station plots of temperature, dewpoint, and winds, as well as contours of adjusted pressure. These plots were overlaid onto radar reflectivity composites to compare the surface features to the precipitation patterns. Radar reflectivity composites for the 14th were not available.

The sequence of surface analyses begins at 2100 UTC on 14 June 1985 (Fig. 5.1). At this time, the surface front was just within the surface mesonet. A trough of low pressure extended from the southwest corner of Kansas towards the northeast. The front lay within this trough. To the south of the line, the wind was from the south to southwest. The wind behind the front was from the north to northwest. There was very little temperature difference across the front; however, the dewpoints showed a 3 to 7 degree decrease. From 2100 UTC until 0000 UTC the northern portion of the front moved eastwards while the southern portion remained in southwest Kansas and the Oklahoma panhandle (not shown).

Convection was moving into the surface mesonet by 0000 UTC on the 15th (Fig. 5.2). MCS1 was near the northeast edge of the surface mesonet with three bands of convection. The strongest band of convection lay along the pressure trough and front

00Z

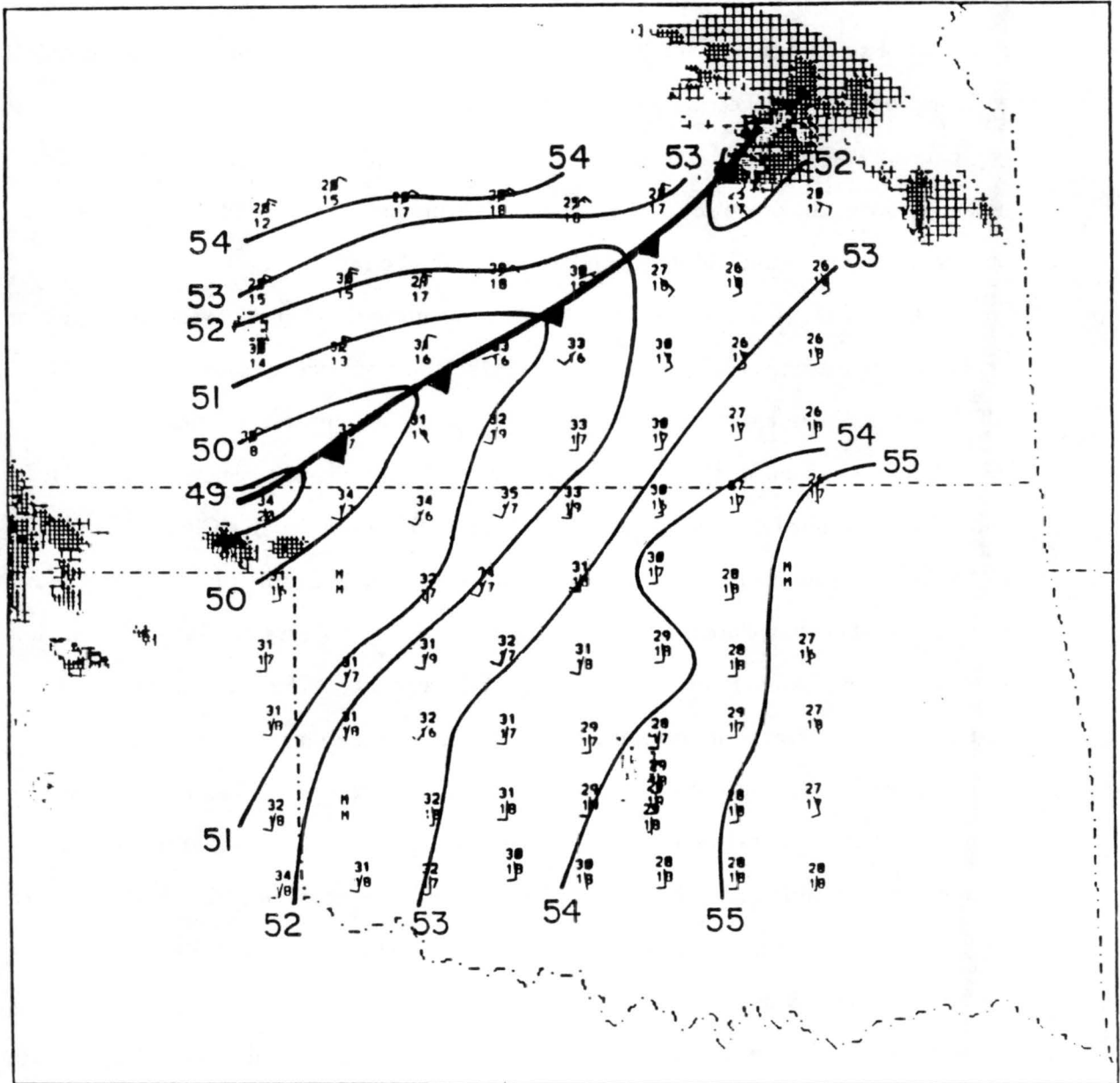


Figure 5.2: Surface analysis of adjusted pressure in mb (e.g. 54 = 954) at 0000 UTC 15 June 1985. Station plots include temperature and dewpoint (in $^{\circ}\text{C}$), and wind (one barb equals 5 m s^{-1}). Overlaid are radar reflectivity composites with intervals of 15, 25, 40, and 50 dBz.

that ran from northeast Kansas to the Oklahoma panhandle. MCS2 was just visible in the Oklahoma panhandle. A few cells had begun to develop between the two MCSs in the pressure trough. The front was only discernable by the windshift line. A 10 m s^{-1} wind ran parallel to and behind the front. The 0100 UTC (Fig. 5.3) analysis showed MCS1 with two bands of convection and an area of stratiform precipitation to the east of the two bands. The strongest convection was still associated with the windshift although it no longer lay in the pressure trough. MCS2 was still barely visible and disorganized. Two new areas of convection had developed between the two MCSs.

By 0200 UTC (Fig. 5.4) two mesolows had begun to develop. Convection in the area made precise placement of the front difficult, so the front was not analyzed after 0100 UTC. The first mesolow, near MCS1, developed near the southwest portion of the system in an area just ahead of the strongest convection. The echo-free region between MCS1 and MCS2 continued to have a mesolow in this area for several hours. Chapter 6 will look at the mechanisms behind the development of the mesolow in this region. There was a 10 m s^{-1} outflow associated with MCS1 (station P24) (see figure 3.2 for location). The stratiform precipitation remained to the east of the system. MCS2 and the convective line had no extensive stratiform precipitation at this time. A mesolow ahead of the convective line had developed, similar to the Hoxit et al. (1975) case. Fig. 5.5 shows the situation 30 minutes later. By this time (0230 UTC) the systems closely resembled the broken line convection that Bluestein and Jain (1985) describe. A strong mesohigh had developed with the strongest convection in the line. An 8 degree temperature decrease and weak outflow were also evident at station P35. Several small mesolows had developed between convective cells. The most significant of these lows was situated ahead of MCS1 and in the echo-free region.

The 0300 UTC (Fig. 5.6) analysis showed MCS2 and the convective line as one system with a strong mesohigh on the edge of the mesonet and strong outflow (12.5 m s^{-1}) (station S26). A second mesohigh was located in the leading stratiform precipitation. The presence of stratiform precipitation ahead of, as opposed to behind, the convective line was examined by Loehrer (1992). He found very strong rear to front flow above 800 mb

0100

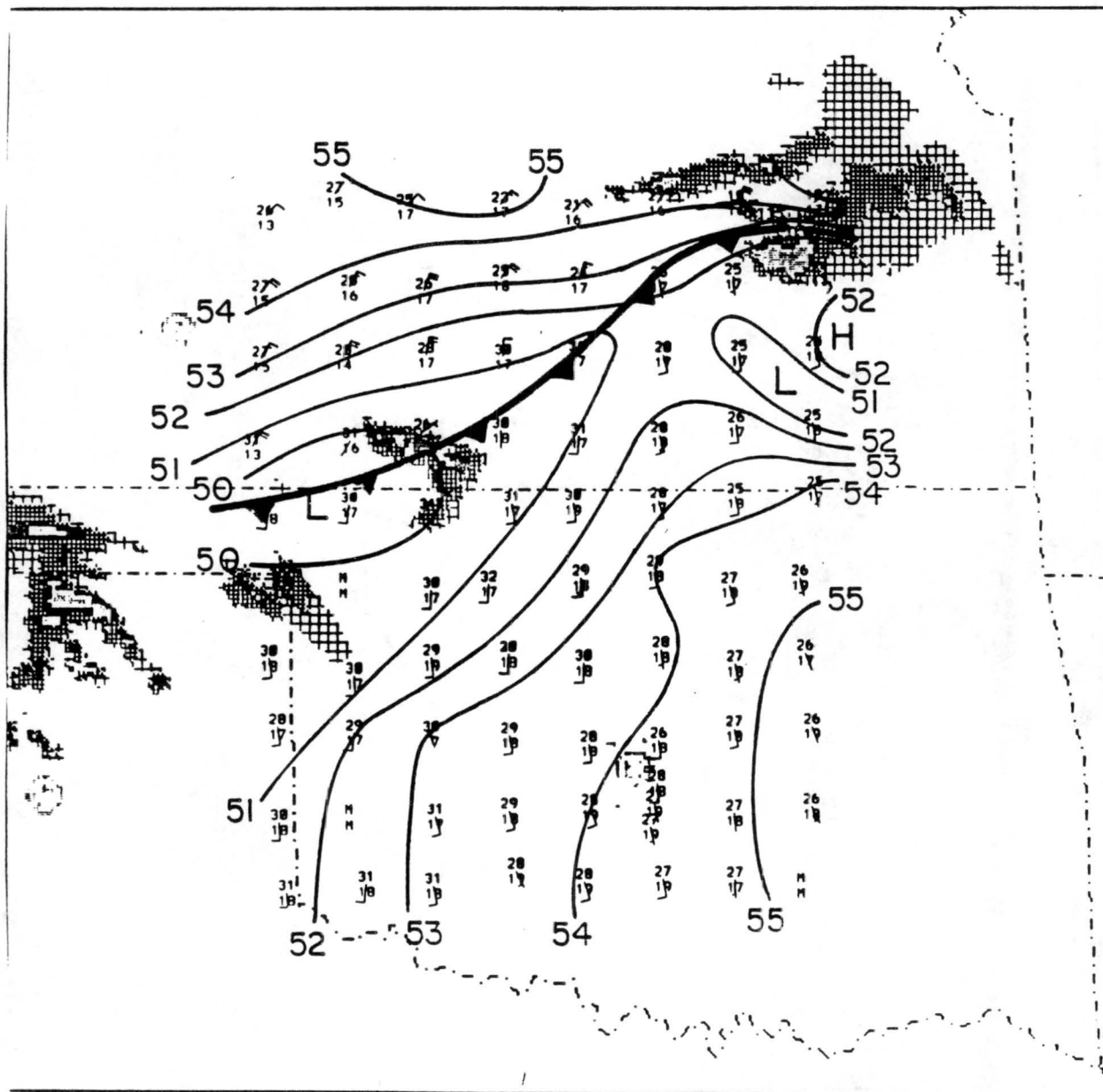


Figure 5.3: Same as Fig. 5.2 except for 0100 UTC 15 June 1985.

0200

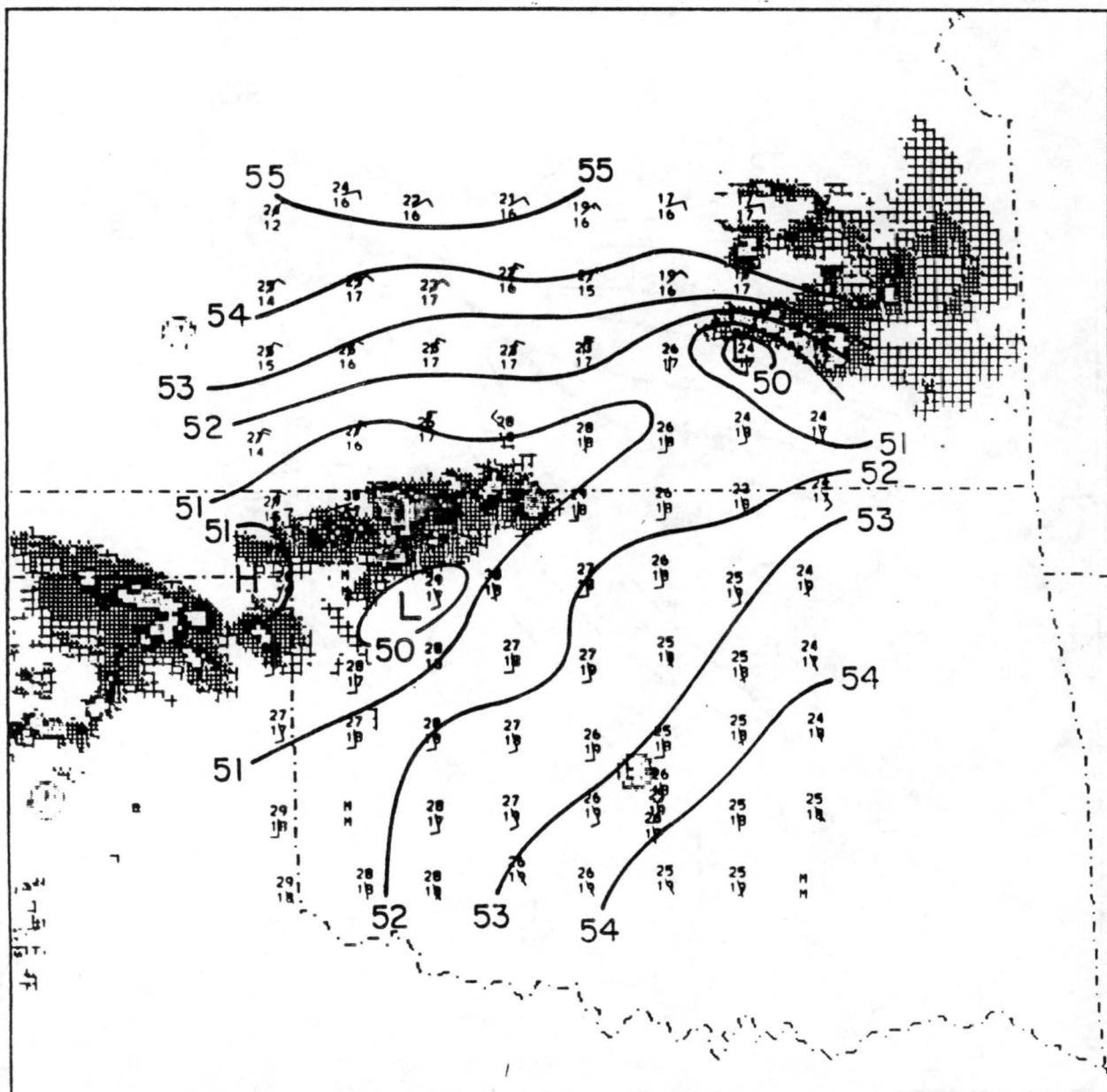


Figure 5.4: Same as Fig. 5.2 except for 0200 UTC 15 June 1985.

0230

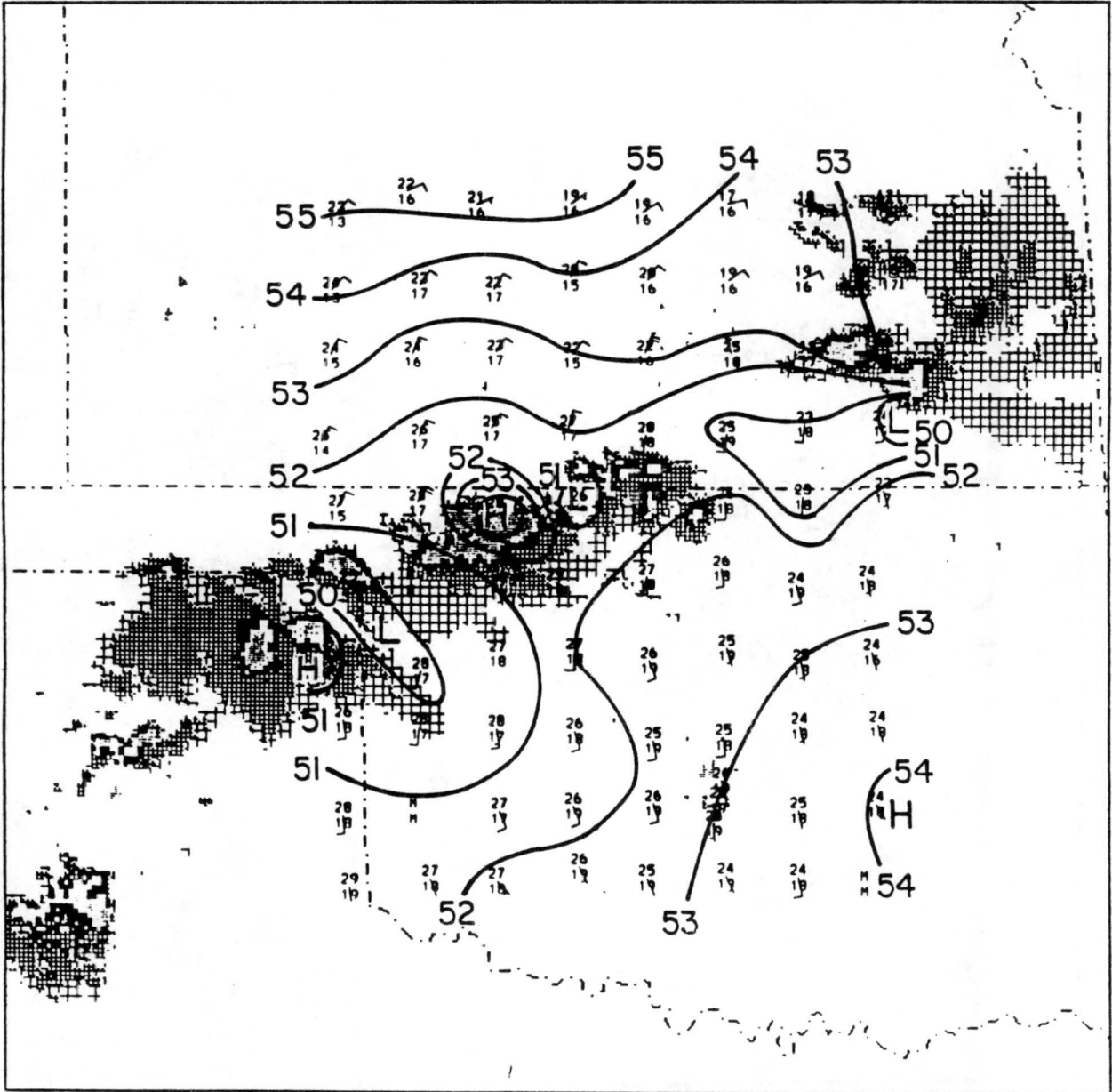


Figure 5.5: Same as Fig. 5.2 except for 0230 UTC 15 June 1985.

0300

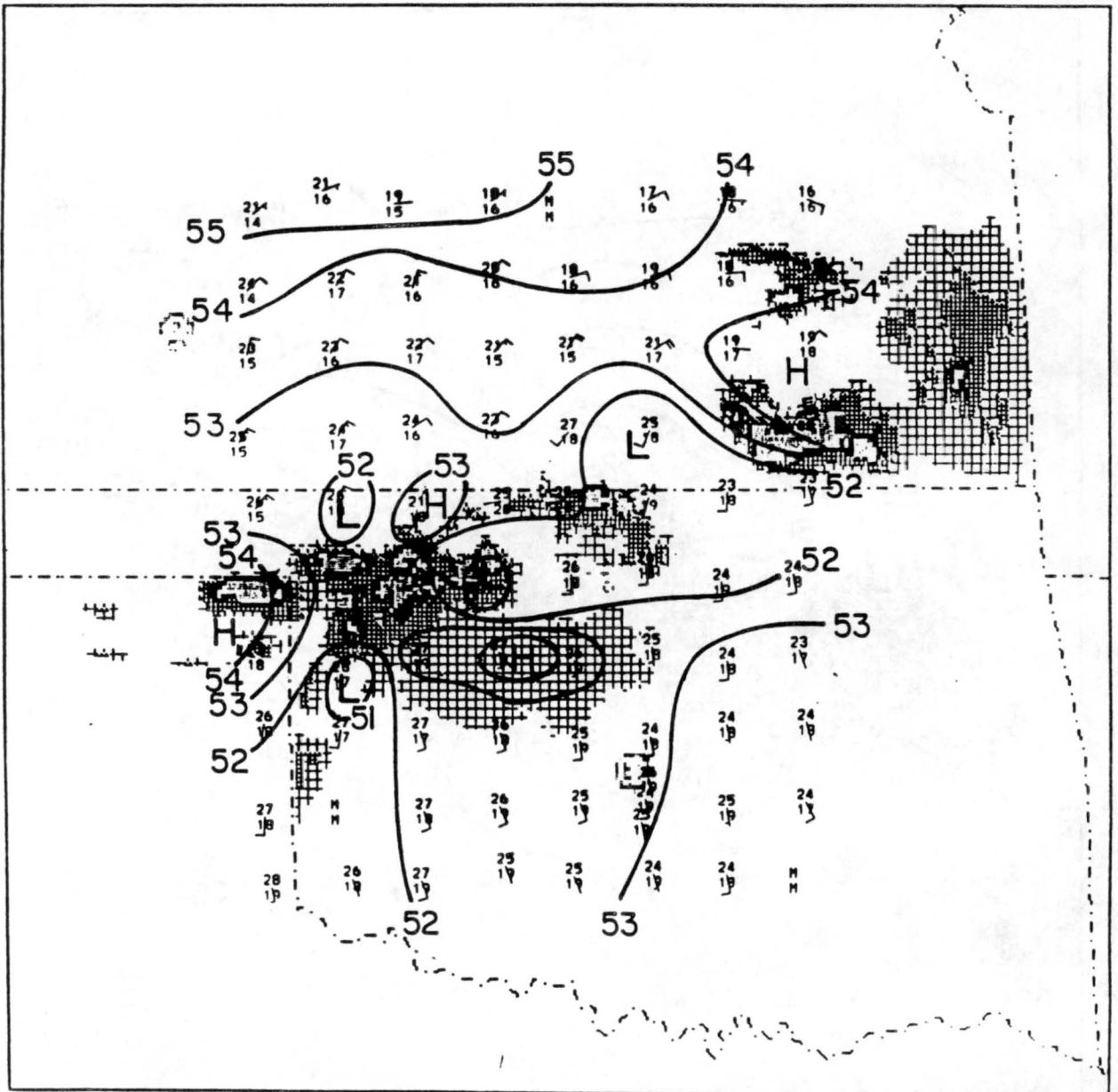


Figure 5.6: Same as Fig. 5.2 except for 0300 UTC 15 June 1985.

which advected the hydrometeors to the south and east of the two systems (Loehrer, 1992). There was a mesohigh associated with MCS1 with a strong 15 m s^{-1} north wind at the surface (station P32). The mesolow between MCS1 and MCS2 filled the echo-free region.

The 0430 UTC analysis (Fig. 5.7) showed the mesolow in the echo-free region to be nearly centered between the strong convective regions of the MCSs. MCS1 had a weak mesohigh and weak outflow (just evident on the edge of the mesonet). A mesohigh covered most of the precipitation region of MCS2, which showed two bands of convective precipitation at this time. Outflow of 10 m s^{-1} was found near the mesohigh. Weaker mesohighs were found with the second band of convection which formed behind the main band. The mesolow between the two systems conformed closely to regions where there was no echo or very weak stratiform precipitation. Two weaker mesolows were associated with echo-free regions of MCS2.

By 0500 UTC (Fig. 5.8) the stratiform precipitation associated with MCS1 had either dissipated or moved out of the radar's range. A mesohigh was between the two convective bands of this system. There was little stratiform precipitation with MCS2 at this time. Mesohighs were located along the north-south band of precipitation in MCS2. The echo-free region mesolow had begun to fill but was still quite strong. Scattered regions of stratiform precipitation were found to the north and east of the main convective cell of MCS2 at 0600 UTC (Fig. 5.9) Mesohighs were associated with the convective regions of both MCSs. Note that the mesolow was still present between the systems. By 0700 UTC (Fig. 5.10) both systems were weakening and the convective regions were moving out of the mesonet. By 0800 UTC (Fig. 5.11) only scattered stratiform precipitation remained although the mesolow remained quite strong. Both systems dissipated shortly after 0900 UTC (Augustine and Howard, 1988).

5.2 Upper Air Analyses

This section will present upper air analyses at constant pressure levels at 2100, 0000, 0300, and 0600 UTC. Plots include height, temperature, dewpoint, and wind. Calculated fields of divergence, moisture divergence, and vertical velocity (ω) will also be

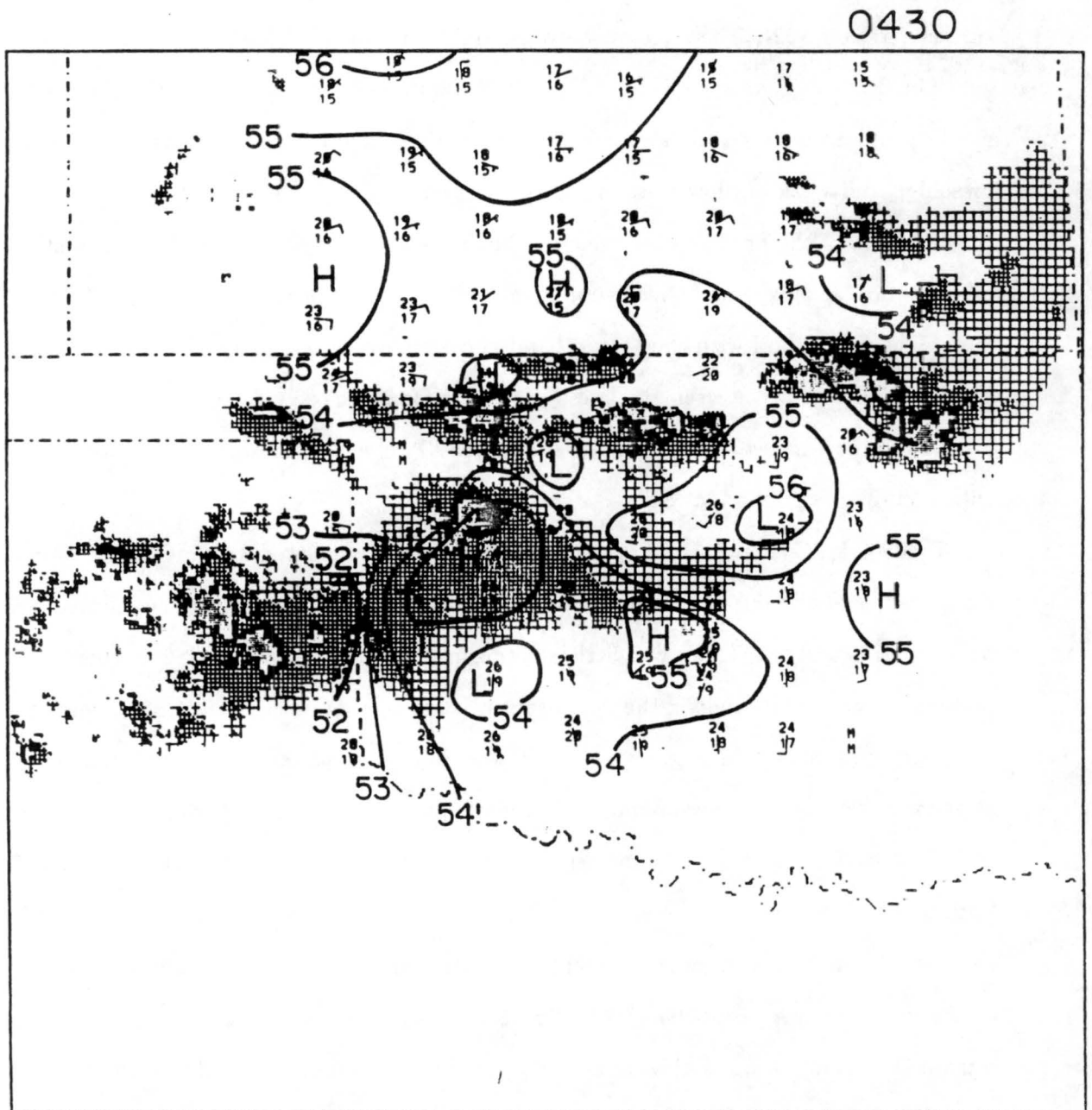


Figure 5.7: Same as Fig. 5.2 except for 0430 UTC 15 June 1985.

0500

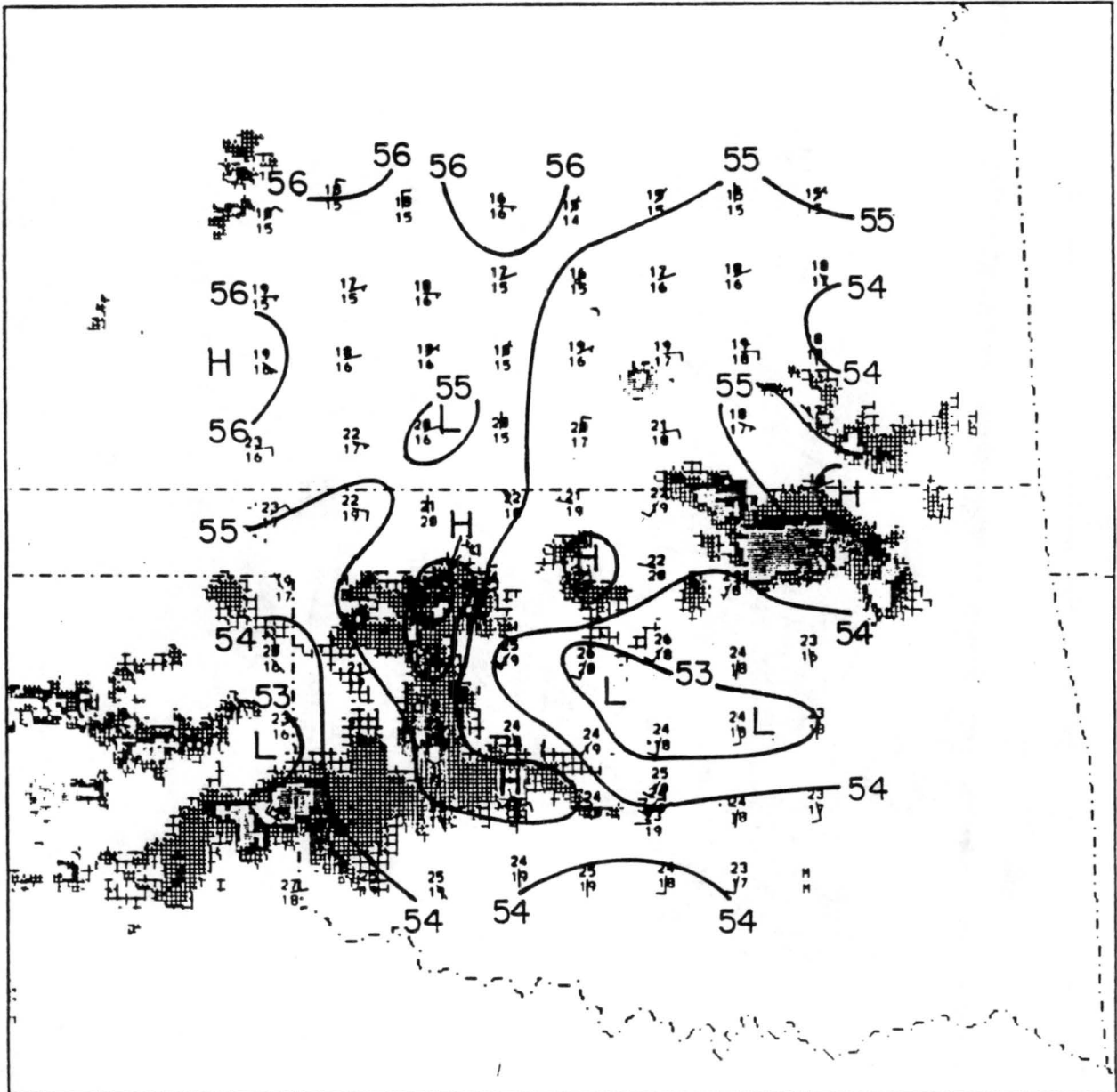


Figure 5.8: Same as Fig. 5.2 except for 0500 UTC 15 June 1985.

0600

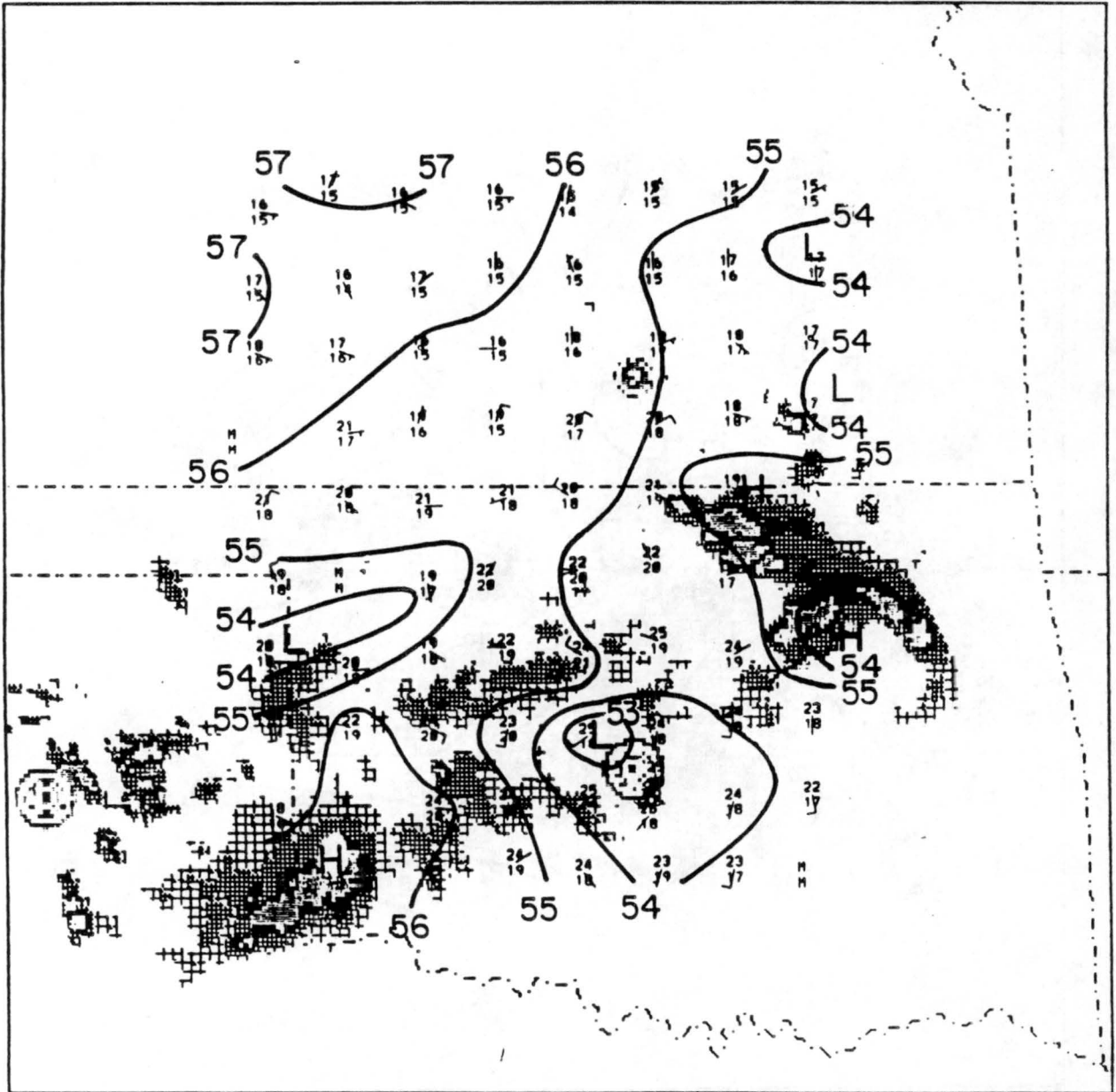


Figure 5.9: Same as Fig. 5.2 except for 0600 UTC 15 June 1985.

0700

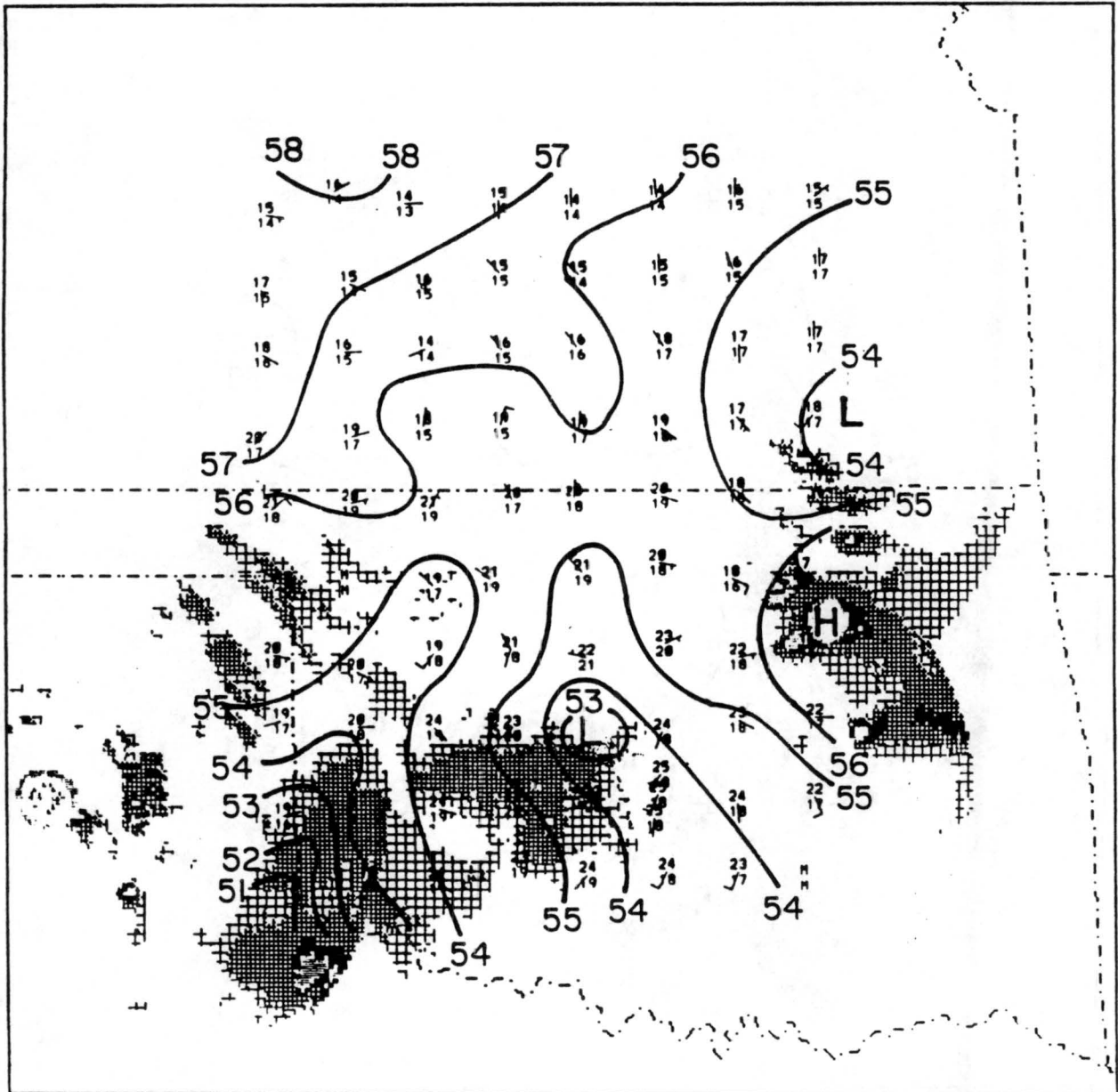


Figure 5.10: Same as Fig. 5.2 except for 0700 UTC 15 June 1985.

0800

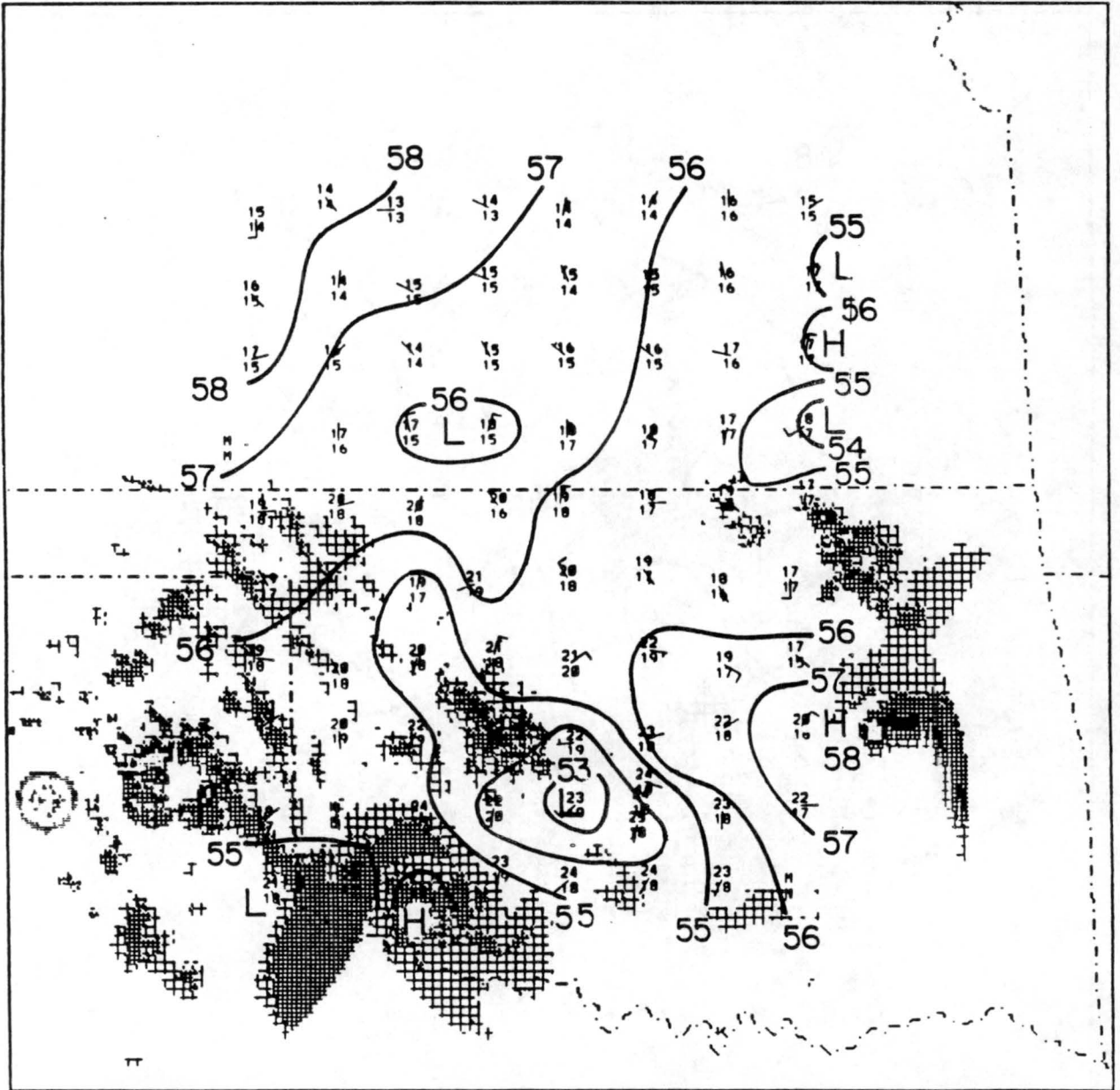


Figure 5.11: Same as Fig. 5.2 except for 0800 UTC 15 June 1985.

presented at constant pressure levels. These fields were overlaid onto radar reflectivity composites when available.

5.2.1 2100 UTC

Although radar composites were not available for this time period, light rain was occurring along the Kansas-Nebraska border, to the northeast of the mesonet network. The 850 mb analysis (Fig. 5.12a) showed the trough in northwest Kansas. A southwest, 12.5 m s^{-1} jet extended from Enid, Oklahoma to Wichita, Kansas. The southwest flow was quite moist with a large area where the dewpoint was at least 12° C . At 700 mb (Fig. 5.12b) the flow was from the west to northwest with a maximum of 15 m s^{-1} over Wichita, Kansas. The trough was still evident at this level. The 500 (not shown), 300 (not shown), and 200 mb analyses (Fig. 5.12c) showed northwest flow with the jet from northwest to southeast Kansas and a maximum of 35 m s^{-1} at 200 mb over Pratt, Kansas.

The divergence field showed convergence along and just ahead of the surface front at both the surface (Fig. 5.13a) and at 850 mb (Fig. 5.13b). The strongest convergence at the surface was northwest of Wichita, while at 850 mb the strongest convergence was to the west and southwest of this location. This region near Wichita is of particular interest because it is the area along the front where the echo-free region would later exist. Likewise, the strongest moisture convergence from the surface through 800 mb was also found near Wichita (Fig. 5.14 a-b) with the strongest moisture convergence at 800 mb in the Wichita area.

The omega field showed strong rising motion along and just ahead of the front at both 850 and 700 mb (Fig 5.15a-b). The two areas of rising motion at 850 mb occurred with the convection to the northeast and to the northwest of Wichita. The field was even stronger at 700 mb with values exceeding $-1.6 \times 10^{-2} \text{ mb s}^{-1}$ to the northwest of Wichita. The rising motion to the northwest of Wichita occurred at all levels at this time (Fig. 5.15 c-d) while subsidence persisted to the southeast of Wichita.

5.2.2 0000 UTC

The 850 mb plot at 0000 UTC (Fig. 5.16a) showed the trough through central Kansas

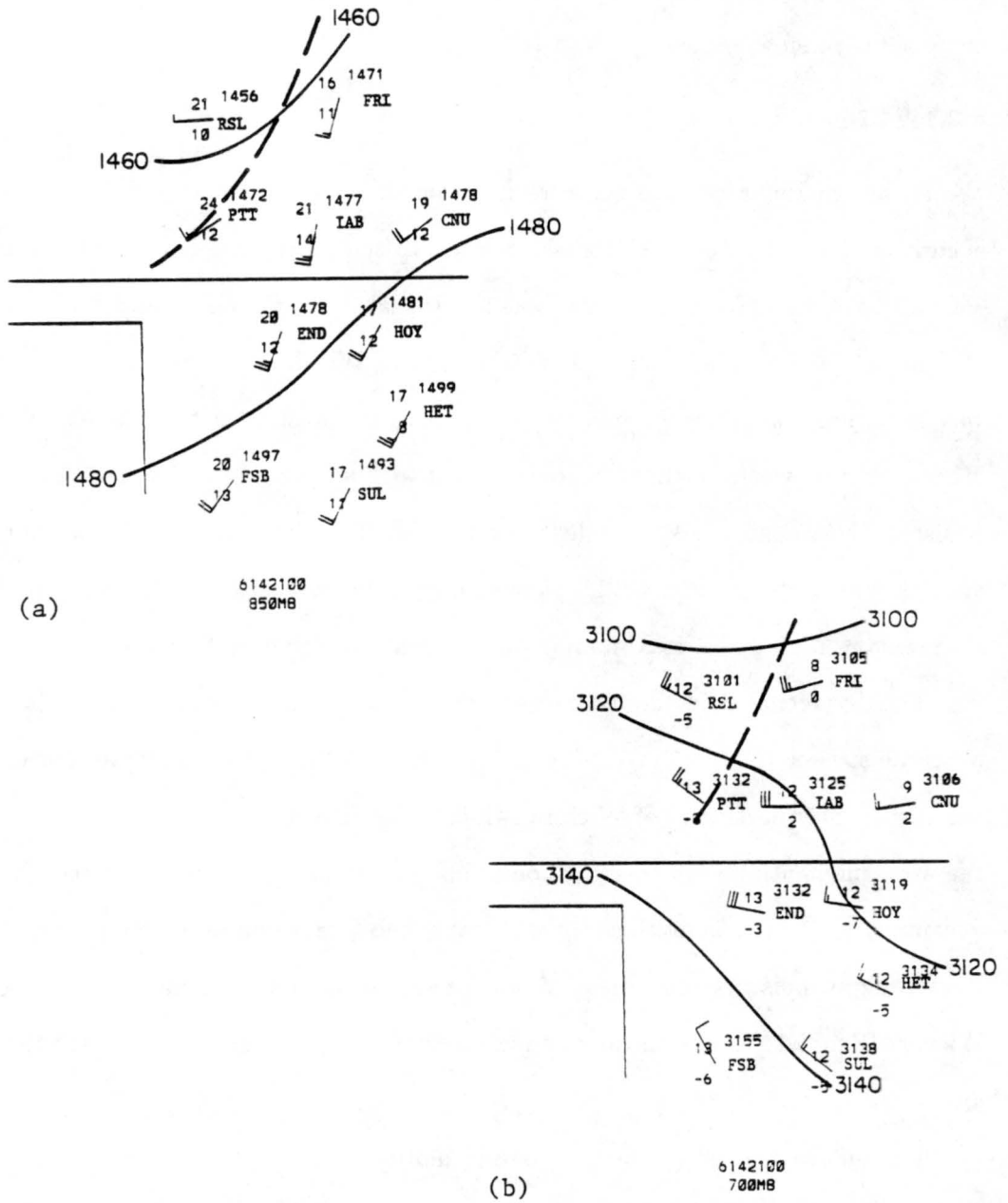
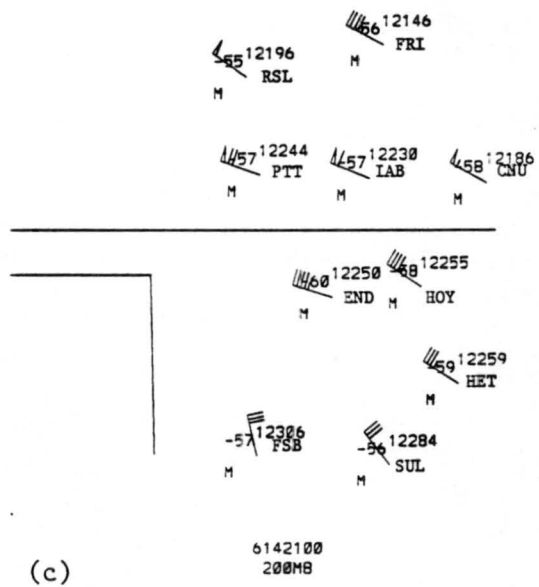


Figure 5.12: Constant pressure plots at 2100 UTC 14 June 1985; (a) 850 mb, (b) 700 mb and (c) 200 mb. Plots include temperature and dewpoint (in °C), wind (one barb equals 5 m s^{-1}) and height (in meters). Solid lines depict height in meters. Dashed lines show the position of the trough.



(c)

Figure 5.12: continued

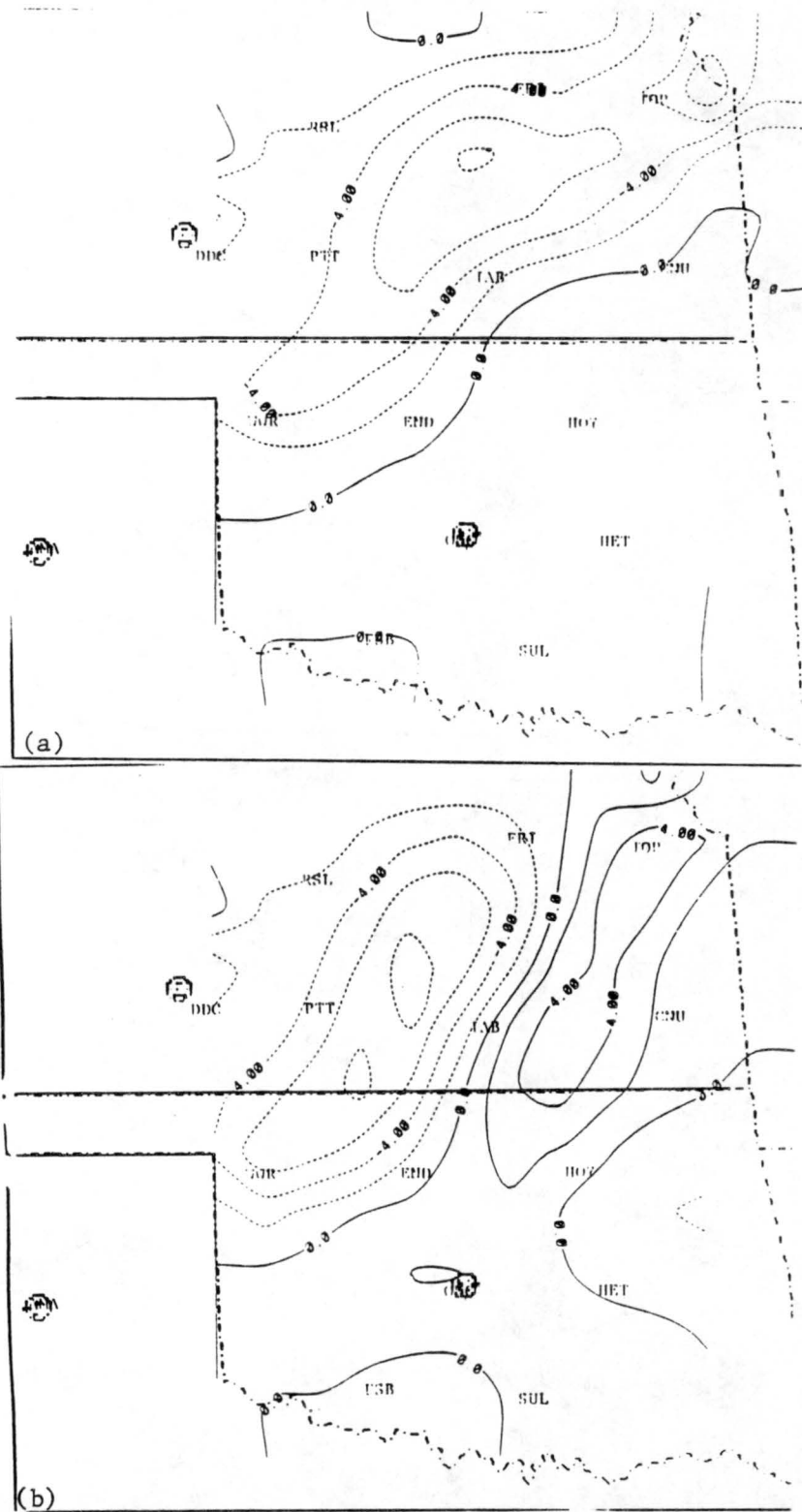


Figure 5.13: Divergence field (units: 10^{-5} s^{-1}) at 2100 UTC, 14 June 1985; (a) surface and (b) 850 mb. Solid lines (positive values) indicate divergence while dashed lines (negative values) indicate convergence.

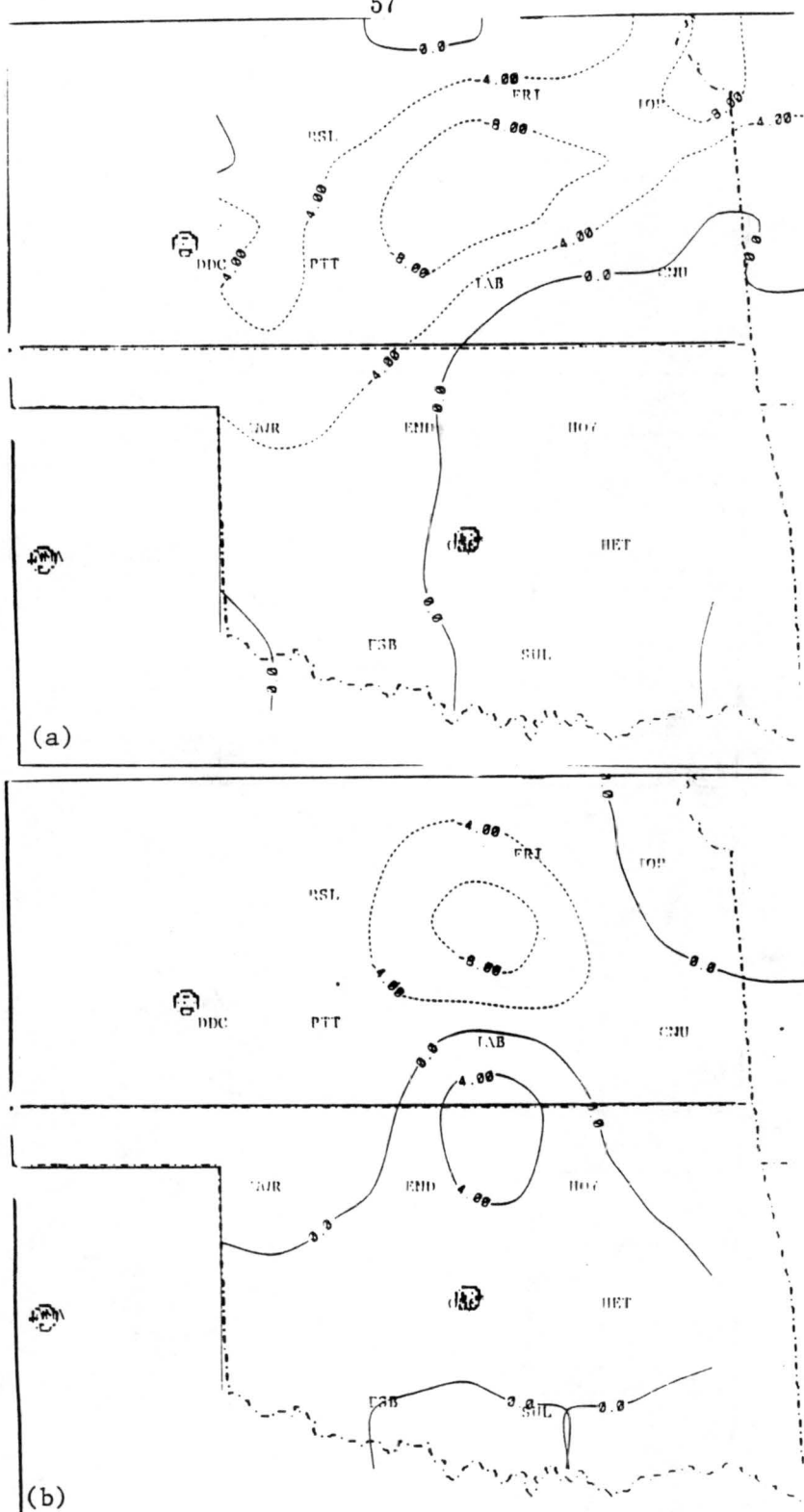


Figure 5.14: Moisture divergence (units: $10^{-5} \text{ g kg}^{-1} \text{ s}^{-1}$) at 2100 UTC, 14 June 1985; (a) surface and (b) 800 mb. Solid lines (positive values) indicate moisture divergence, while dashed lines (negative values) indicate moisture convergence.

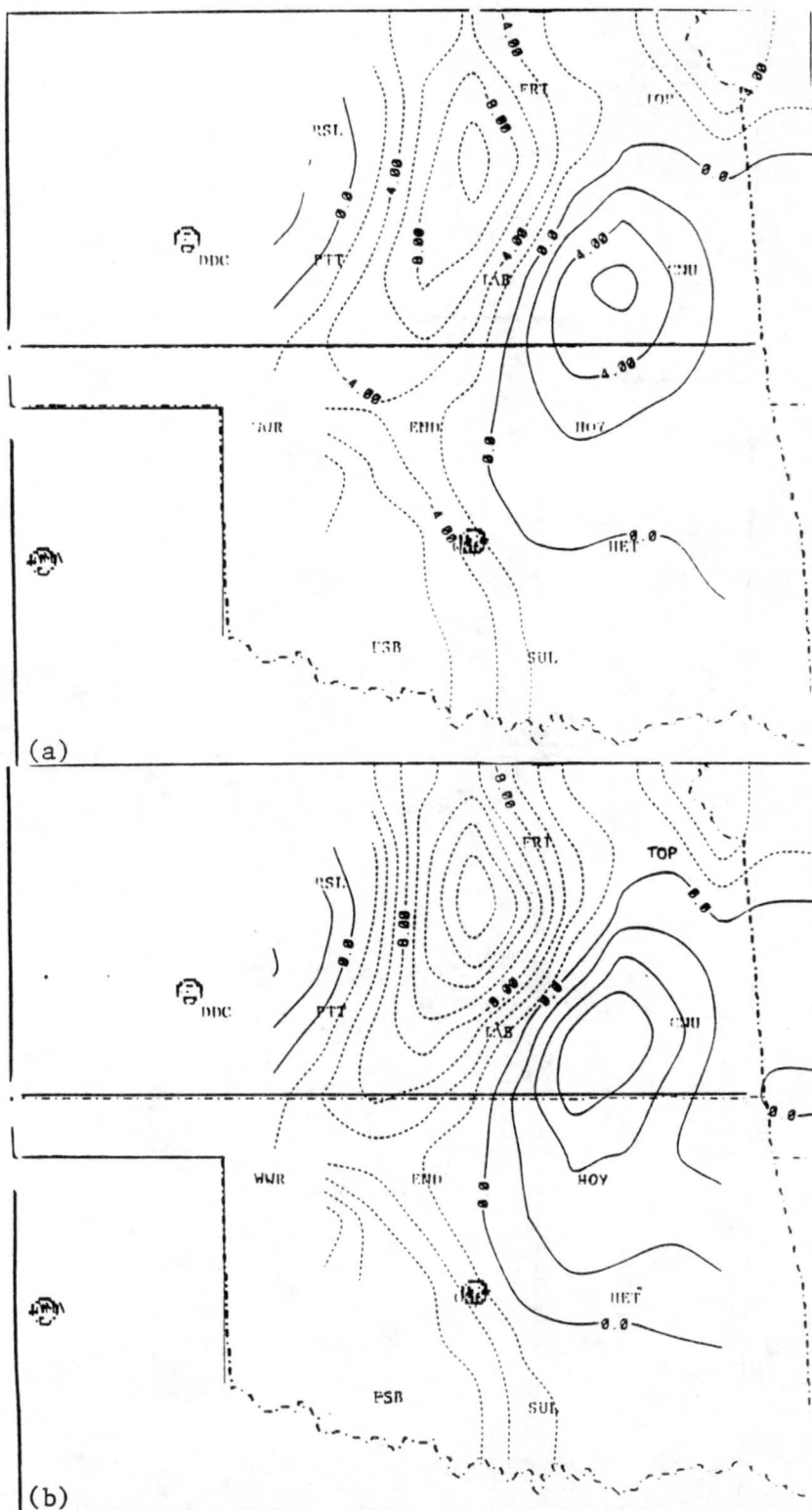
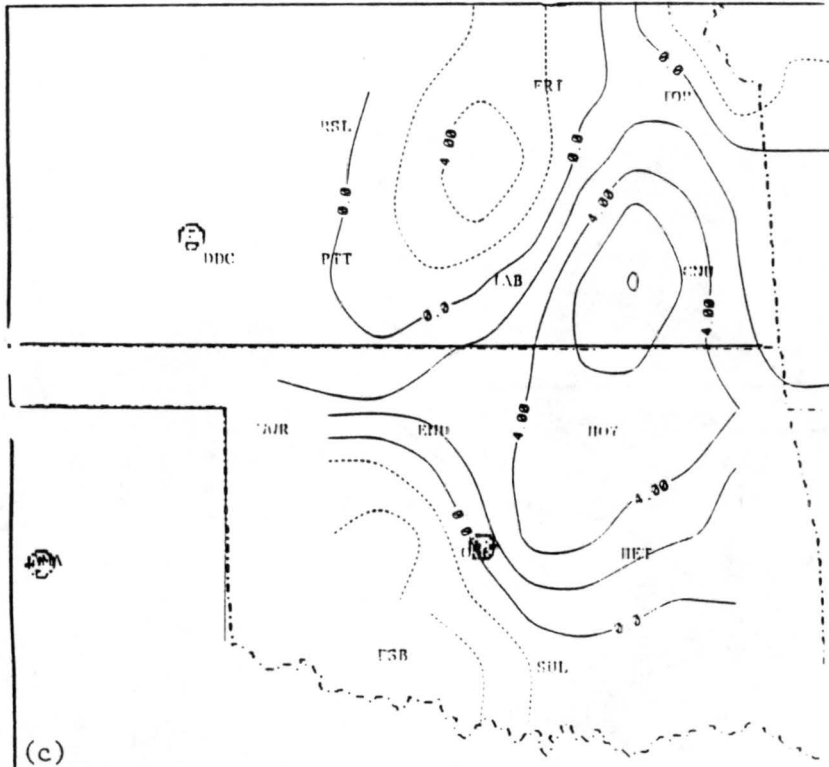
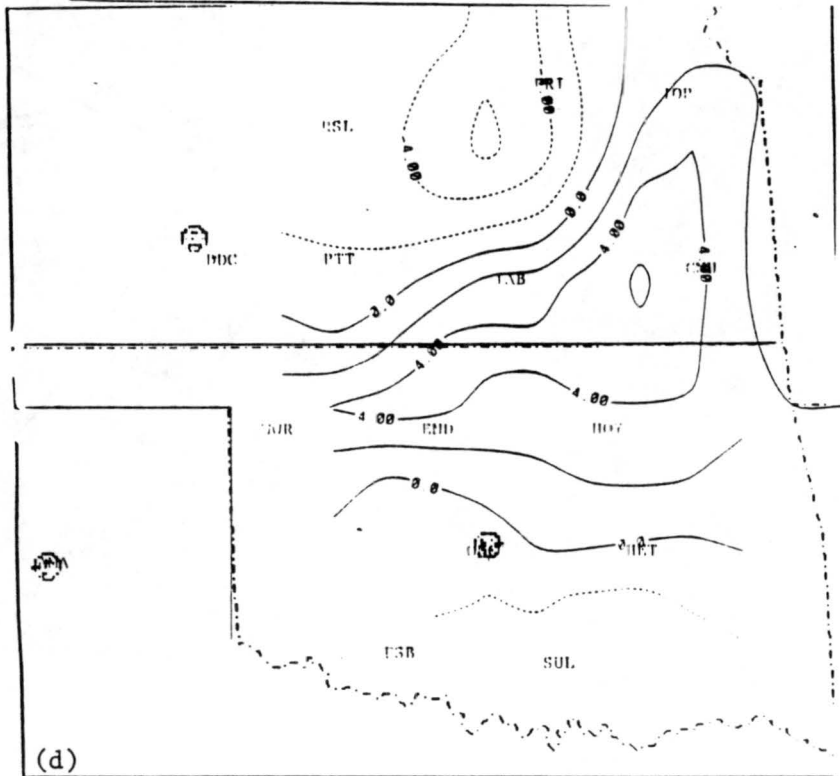


Figure 5.15: Omega (vertical velocity) field (units: $10^{-3} \text{ mb s}^{-1}$) at 2100 UTC, 14 June 1985; (a) 850 mb, (b) 700 mb, (c) 500 mb and (d) 300 mg. Solid lines (positive values) indicate sinking motion, while dashed lines (negative values) indicate rising motion.



(c)



(d)

Figure 5.15: continued

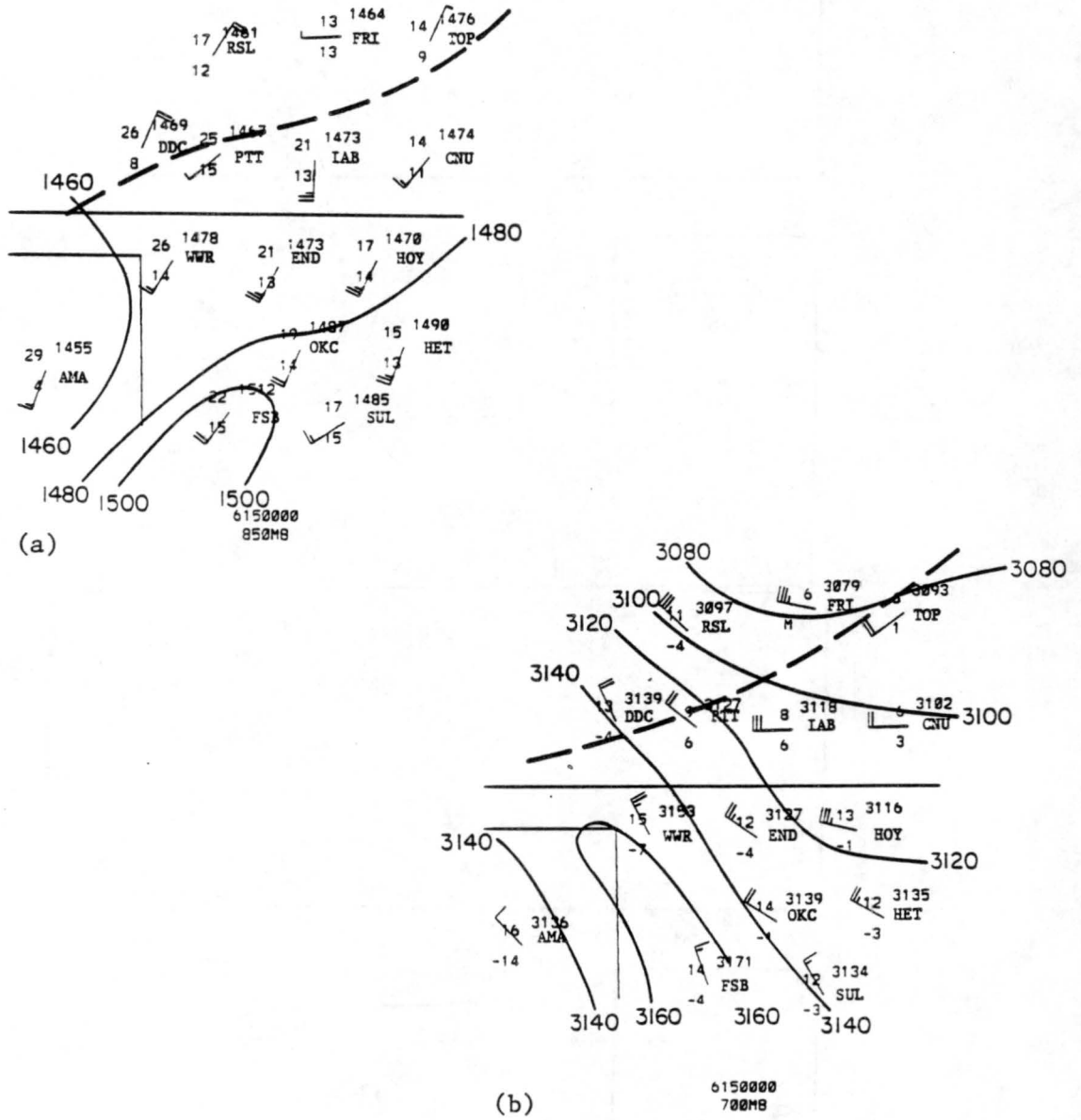


Figure 5.16: Same as Fig. 5.12 except at 0000 UTC, 15 June 1985.

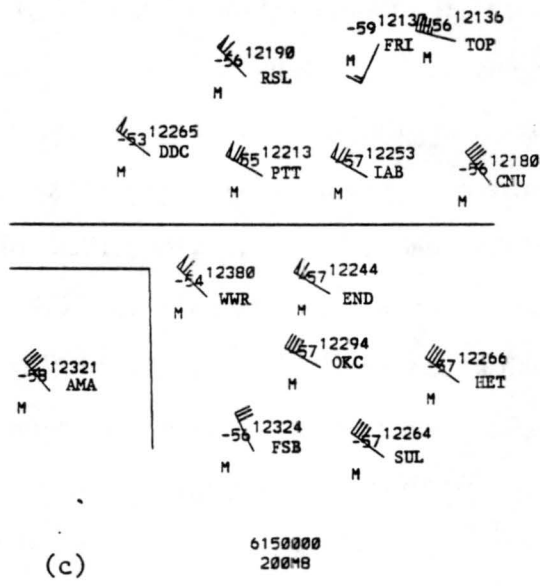


Figure 5.16: continued

with a warm ridge just ahead. Very moist air with dewpoints in excess of 12°C was also found in the warm ridge. Strong southwest flow of 12.5 m s^{-1} was to the south with northeast flow at 10 m s^{-1} to the north. The flow became northwesterly at 700 mb (Fig. 5.16b) and remained out of the northwest at higher levels. Very moist air was found at 700 mb along the trough, particularly near Pratt and Wichita. Flow was predominantly from the northwest with the jet penetrating into northern Oklahoma. The strongest wind was 35 m s^{-1} at 200 mb over Pratt and Wichita, Kansas (Fig. 5.16c). MCS1 formed in the left-exit region of the jet, a favorable position for development.

The surface divergence field showed the strongest convergence at the surface in the Oklahoma panhandle associated with MCS2, which was developing in that area (Fig. 5.17a).

A second area of convergence was northeast of Wichita and southwest of MCS1. The divergence at the northern edge of MCS1 indicates outflow from the system. At 850 mb (Fig. 5.17b) the strongest convergence occurred with MCS2 and northwest of Wichita. Strong divergence was to the west of MCS1. At 700 mb (Fig. 5.17c) weak convergence was associated with MCS2 while much stronger convergence was now in the MCS1 region. The strongest divergence at this level was south of Wichita, on the Oklahoma border. The 500 mb plot (not shown) showed weak convergence over both MCSs as well as the Wichita area. The 300 mb (not shown) and 200 mb (Fig. 5.17 d) plots showed divergence over MCS1 and MCS2 with weak convergence over Wichita.

Moisture convergence from the surface to 800 mb (Fig. 5.18 a-c) was found to be strong near the MCSs as one would expect, but also extended from MCS1 to the southwest of Wichita, from the surface up to 850 mb. In fact, the strongest convergence actually occurred in the echo-free region (Fig. 5.18 b). Assuming similar conditions aloft over the entire domain, one would expect subsequent convection to be preferred in this region of maximum low-level moisture convergence. It is seen, however, in Fig. 5.17 that conditions aloft varied considerably across the domain.

The omega field showed strong rising motion all along the front through 700 mb with maxima near MCS1 and MCS2 (Fig. 5.19 a-b) but also near the echo-free region. Rising motion was found through 200 mb with both MCSs while sinking motion was found above

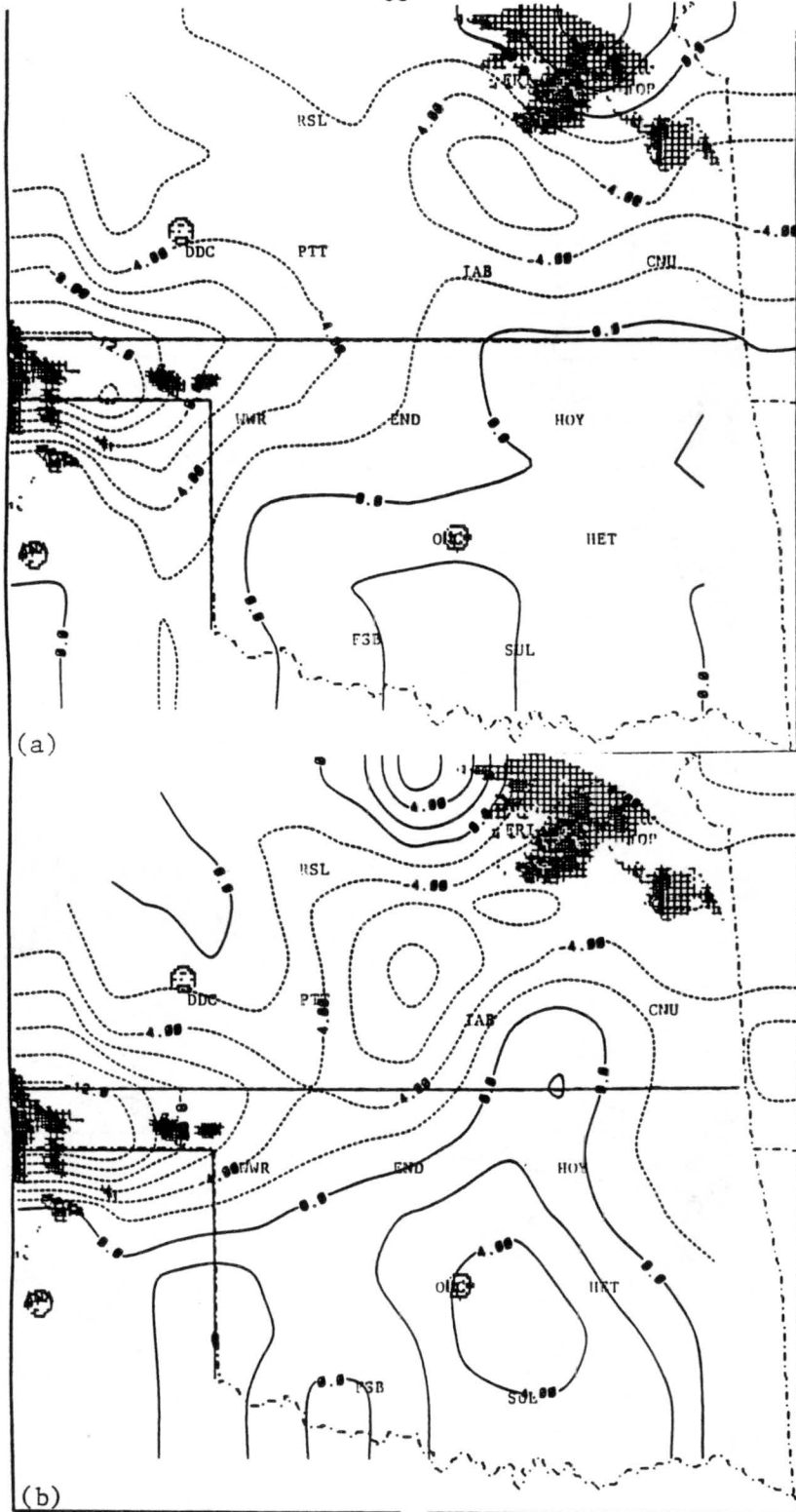


Figure 5.17: Divergence field (units: 10^{-5} s^{-1}) at 0000 UTC, 15 June 1985; (a) surface, (b) 850 mb, (c) 700 mb and (d) 200 mb. Solid lines (positive values) indicate divergence while dashed lines (negative values) indicate convergence. Overlaid are radar reflectivity composites with intervals of 15, 25, 40 and 50 dBz.

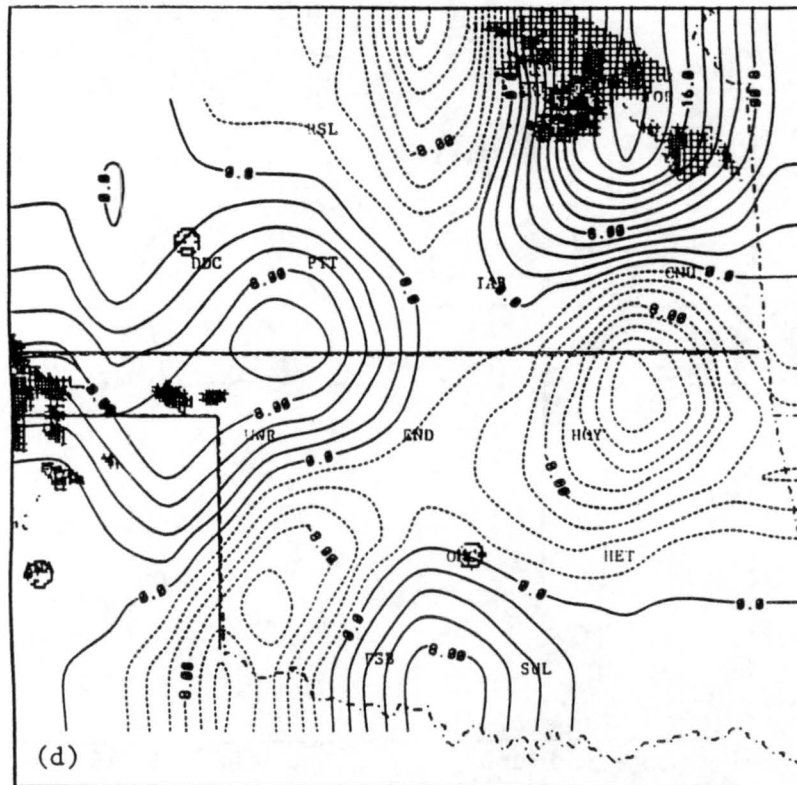
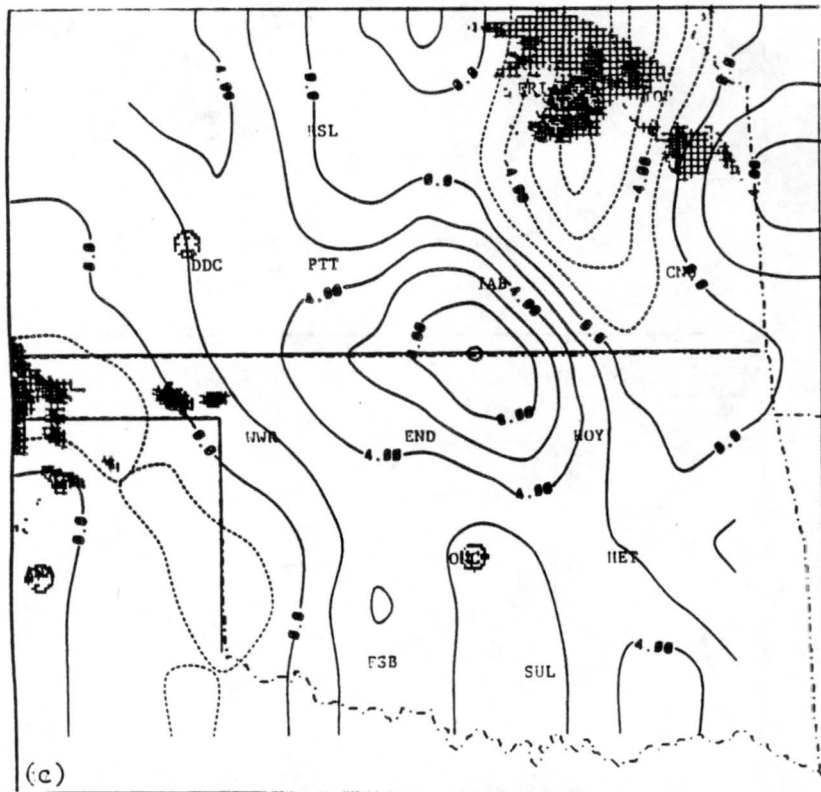


Figure 5.17: continued

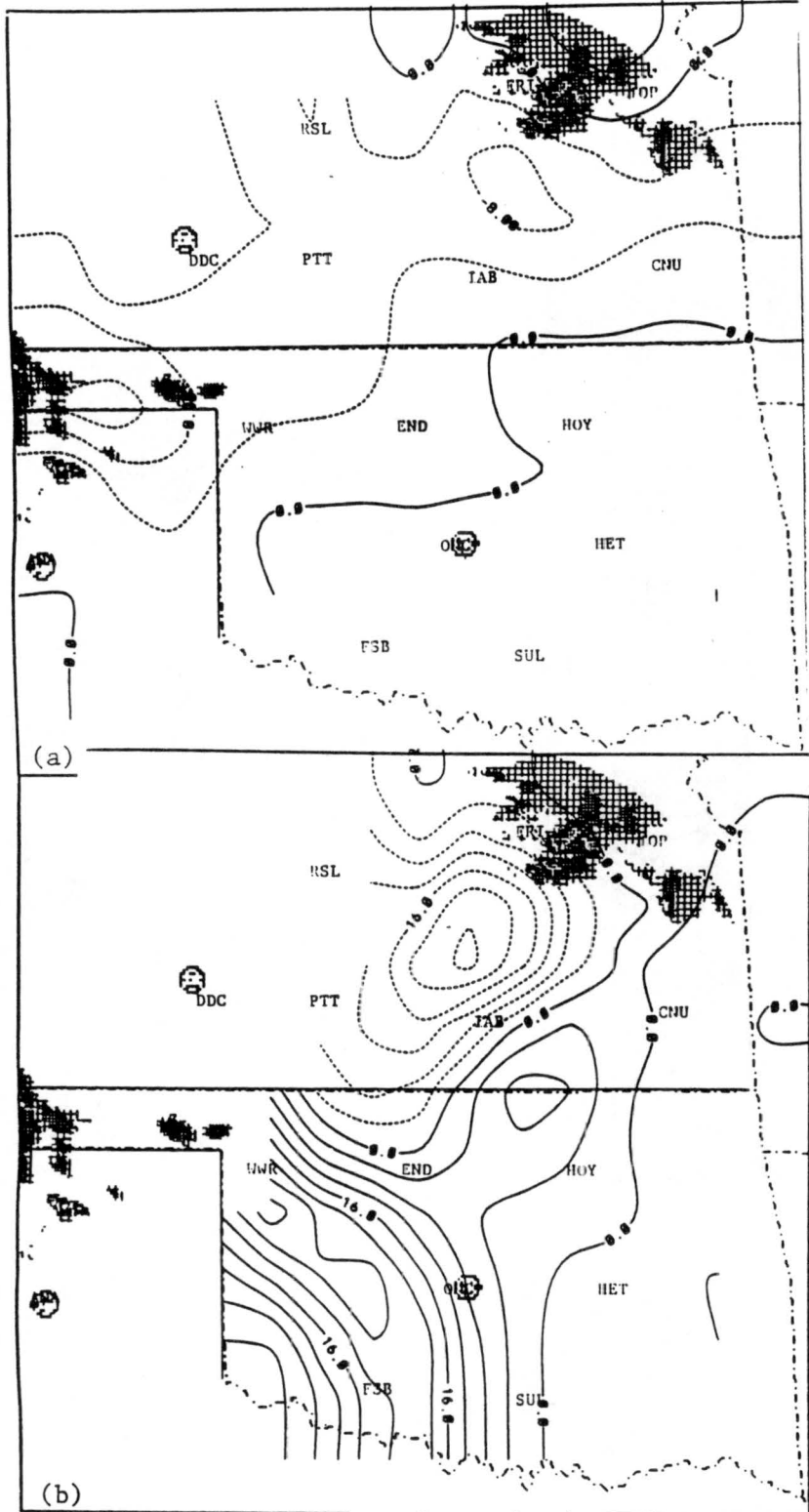


Figure 5.18: Moisture divergence (units: $10^{-5} \text{ g kg}^{-1} \text{ s}^{-1}$) at 0000 UTC, 15 June 1985; (a) surface, (b) 950 mb and (c) 800 mb. Solid lines (positive values) indicate moisture divergence, while dashed lines (negative values) indicate moisture convergence. Overlaid are radar reflectivity composites with intervals of 15, 25, 40 and 50 dBz.

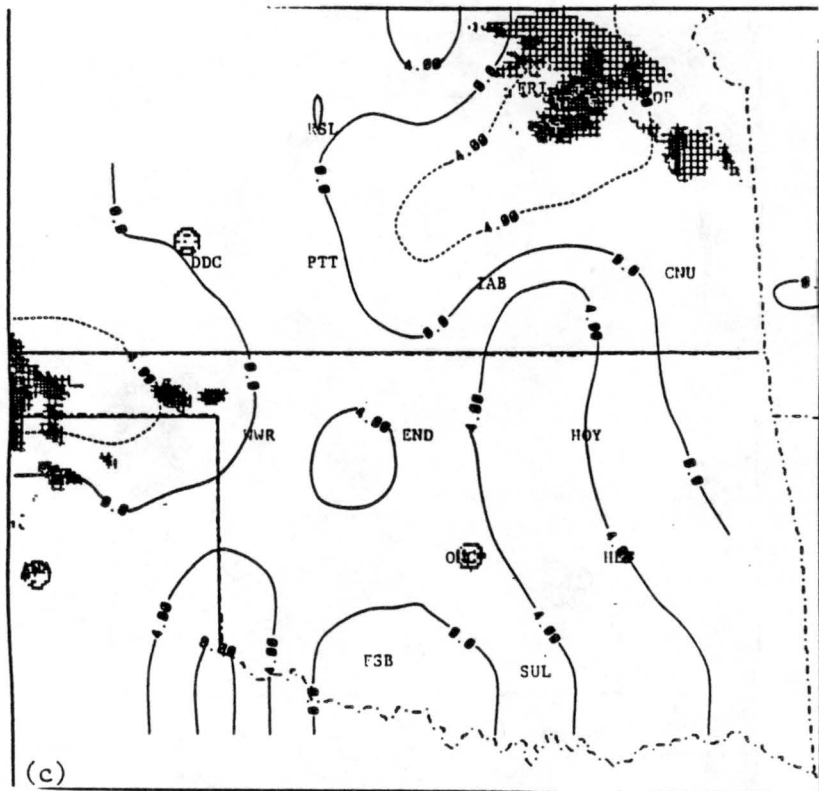


Figure 5.18: continued

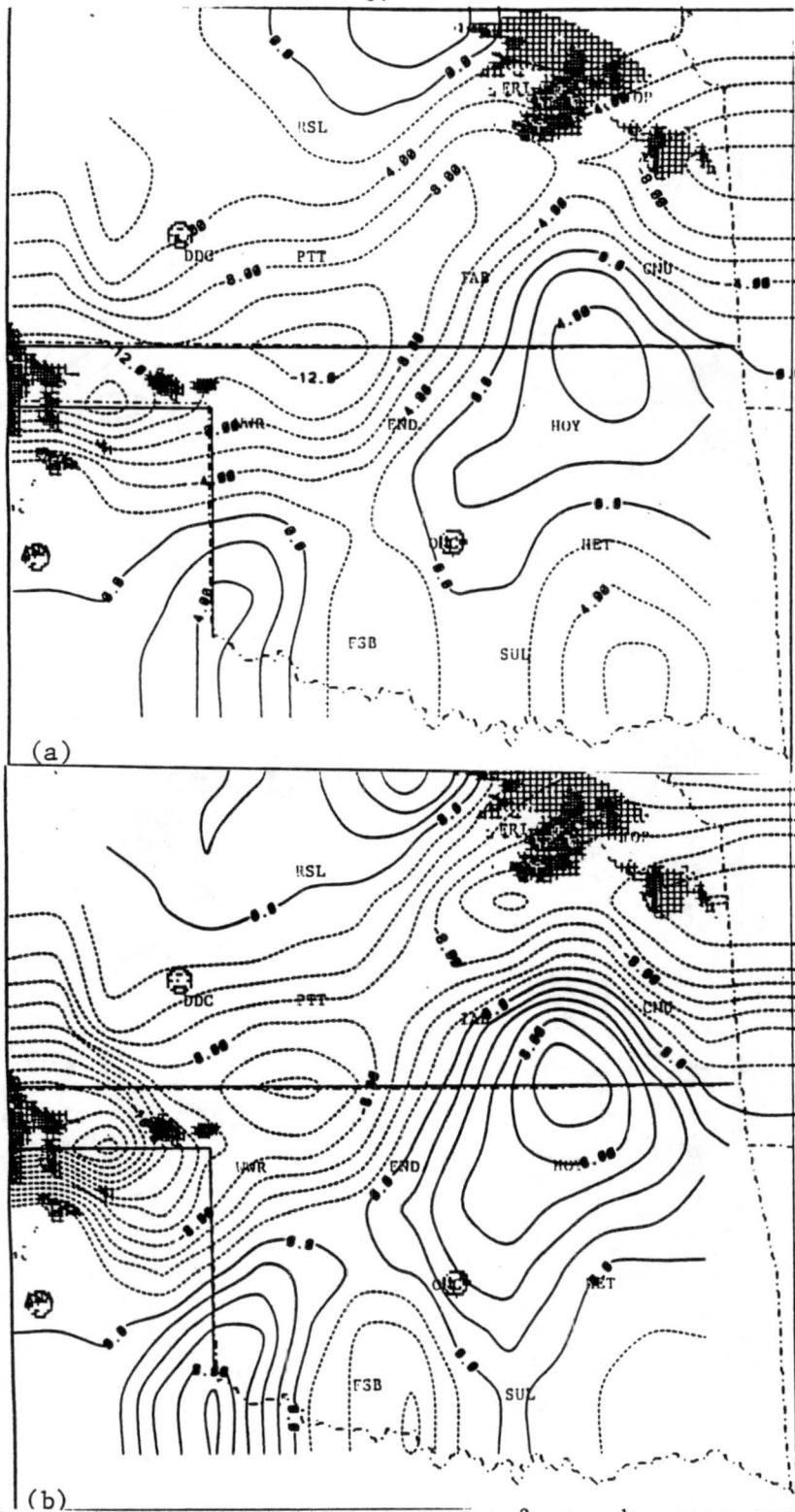


Figure 5.19: Omega (vertical velocity) field (units: $10^{-3} \text{ mb s}^{-1}$) at 0000 UTC, 15 June 1985; (a) 850 mb, (b) 700 mb, (c) 500 mb and (d) 200 mg. Solid lines (positive values) indicate sinking motion, while dashed lines (negative values) indicate rising motion. Overlaid are radar reflectivity composites with intervals of 15, 25, 40 and 50 dBz.

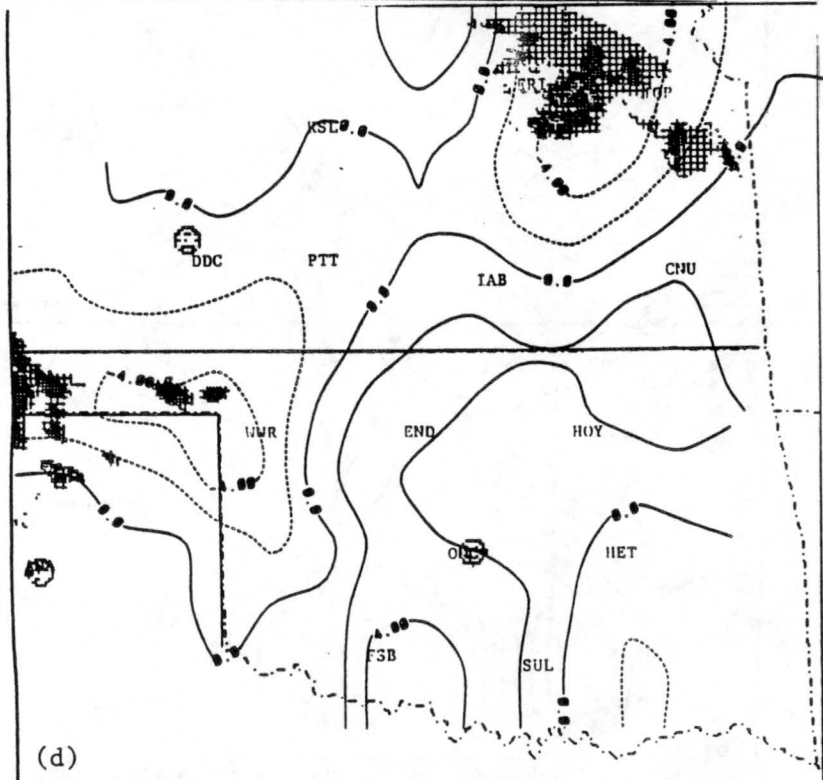
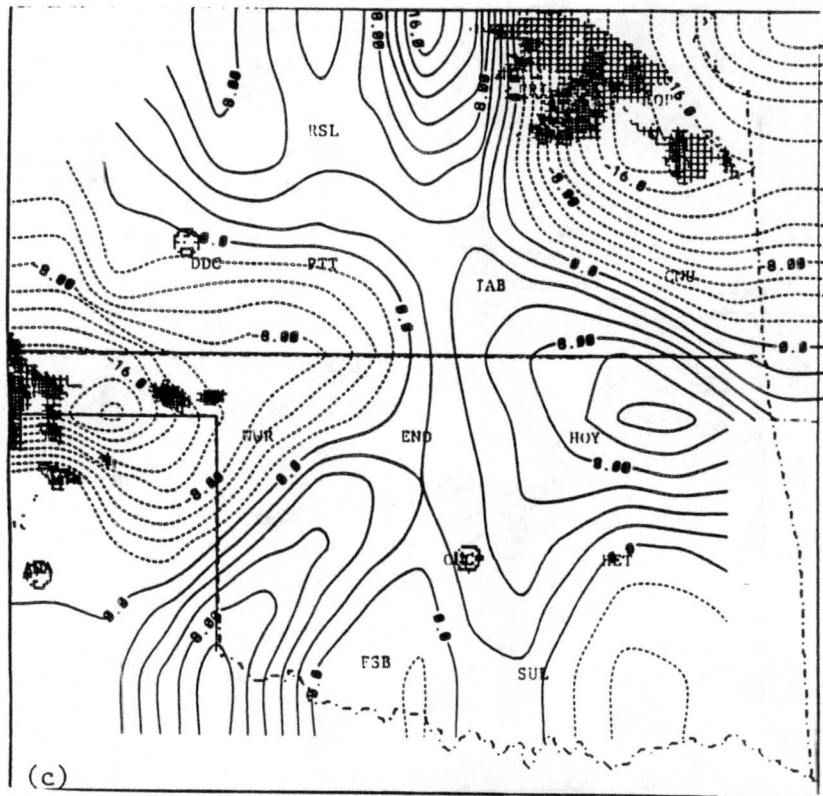


Figure 5.19: continued

500 mb in the Wichita area (Fig 5.19 c-d). The relationship of these vertical motion patterns to subsequent convective development will be discussed later.

5.2.3 0300 UTC

The trough at 850 mb lay from northeast to southwest Kansas (Fig. 5.20a). A strong southwest, low-level jet up to 17.5 m s^{-1} was in Oklahoma. Moist air was present throughout the area south of the trough. The 700 mb flow was from the northwest at 15 to 17.5 m s^{-1} with moist air just ahead of the trough (Fig. 5.20b). A very strong jet was found at 500 mb; nearly 40 m s^{-1} over Pratt, Kansas with 35 m s^{-1} over Wichita, Kansas (Fig. 5.20c). Note the slightly warmer but much drier air at Wichita as compared to Pratt or Chanute, Kansas. This feature will be studied in Chapter 6. The 200 mb level (Fig. 5.20d) showed the jet extending into Oklahoma.

Convergence existed within and behind the two systems at both the surface and 850 mb at this time (Fig. 5.21a, b). Some of the strongest convergence was present in the echo-free region between the two systems. Because of the strong convergence in this area, new convection would be expected, but it did not occur. Very strong convergence was directly over MCS2 at 500 mb while divergence was found along the rest of the line (Fig. 5.21 c). Finally, at 200 mb (Fig. 5.21 d) strong convergence was found over Wichita, extending into the echo-free region while very strong divergence was downstream of both MCSs.

As at 0000 UTC, there was strong moisture convergence from the surface (Fig. 5.22 a) through 800 mb associated with both MCSs. The echo-free region had fairly strong moisture convergence at 950 mb (not shown) and 900 mb (Fig. 5.22 b) with moisture divergence at 800 mb (not shown) at this time.

The omega field showed upward motion along the Kansas-Oklahoma border in the echo-free region at 850 mb (Fig. 5.23 a) and 700 mb (not shown). Upward motion was also associated with both MCSs. In contrast to the rising motion in the two MCSs, which extended through 200 mb (Fig. 5.23 c), sinking motion was found on the border of the echo-free region at 500 mb (not shown) and over the region at 300 mb (Fig. 5.23 b) inhibiting the growth of convection in this area.

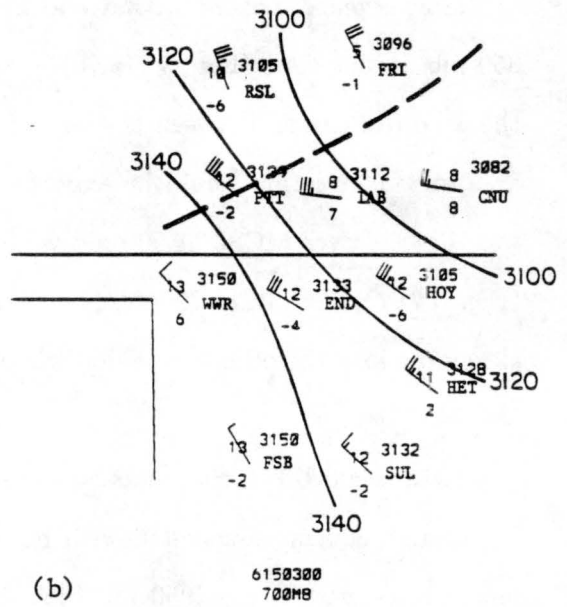
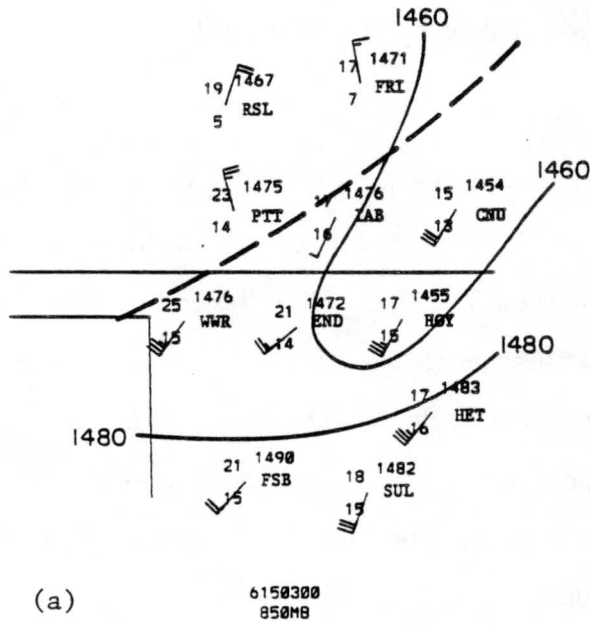


Figure 5.20: Same as Fig. 5.12 except at 0300 UTC, 15 June 1985; (a)850 mb, (b) 700 mb, (c) 500 mb and (d) 200 mb.

5794 RSL -29
5763 FRI -11
-32

5839 PTT -12
5807 IAB -30
5758 CNU -12
-18

5828 END -10
5804 HOY -11
-19

5839 HET -21

5967 FSB -7
5844 SUL -6
-21
-23

(c)

6150300
530MB

12180 RSL -54
12157 FRI -56

12269 PTT -54
12278 IAB -55

12266 END -57

12282 HET -58

12320 FSB -56
12320 SUL -58

(d)

6150300
200MB

Figure 5.20: continued

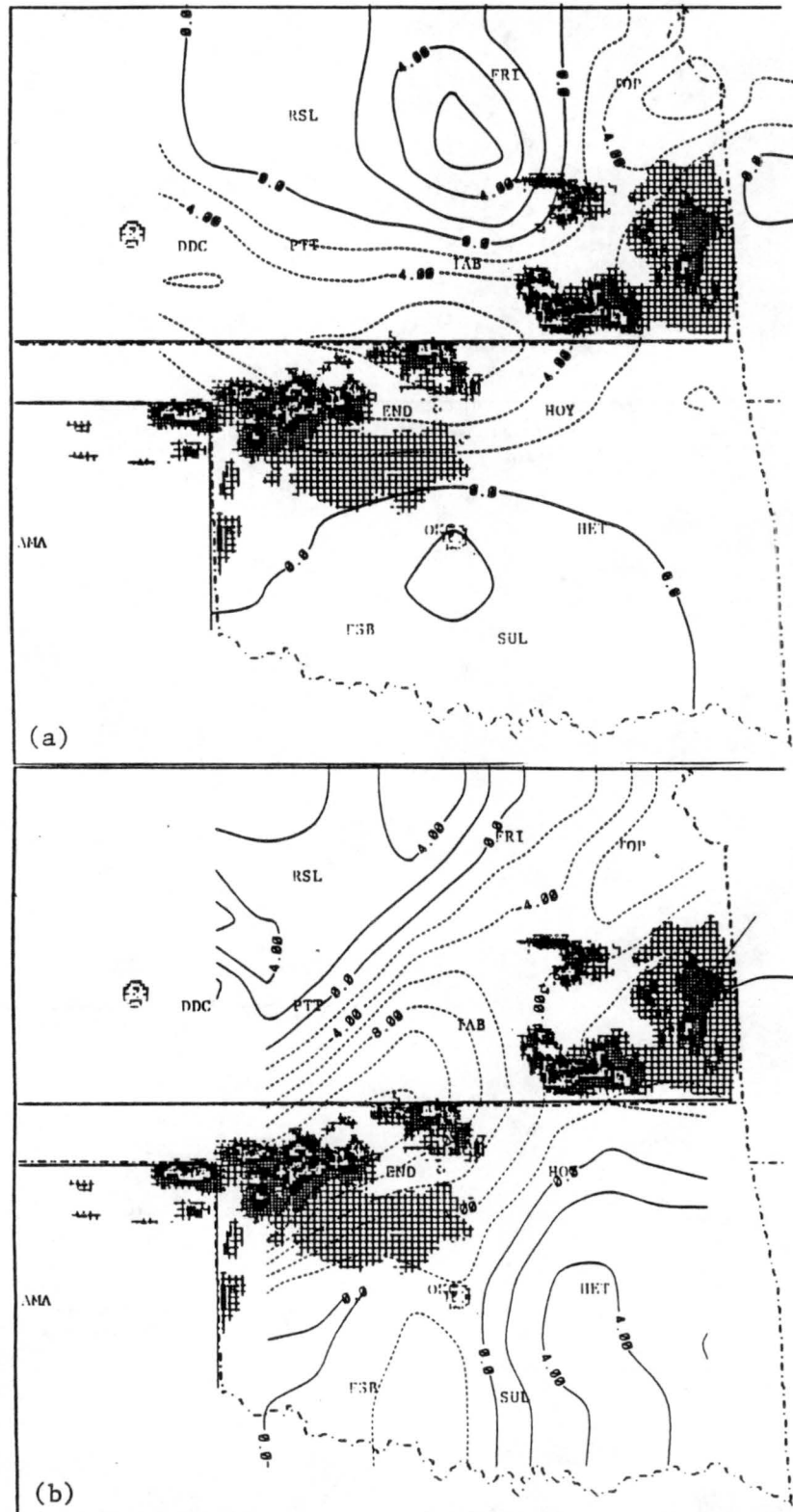


Figure 5.21: Divergence field as in Fig. 5.17 except at 0300 UTC, 15 June 1985: (a) surface, (b) 850 mb and (c) 200 mb.

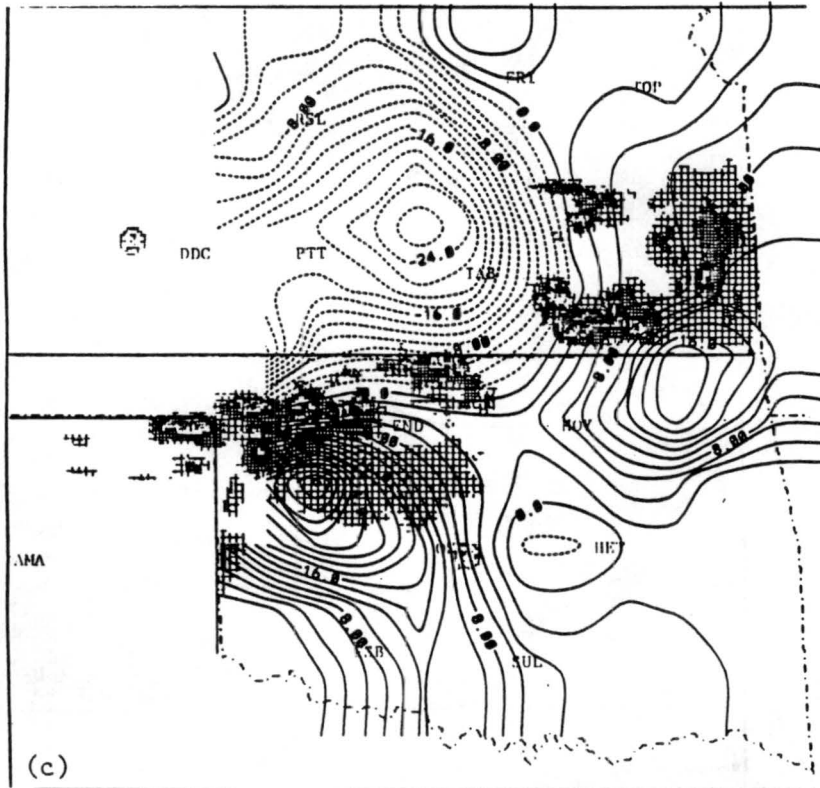


Figure 5.21: continued

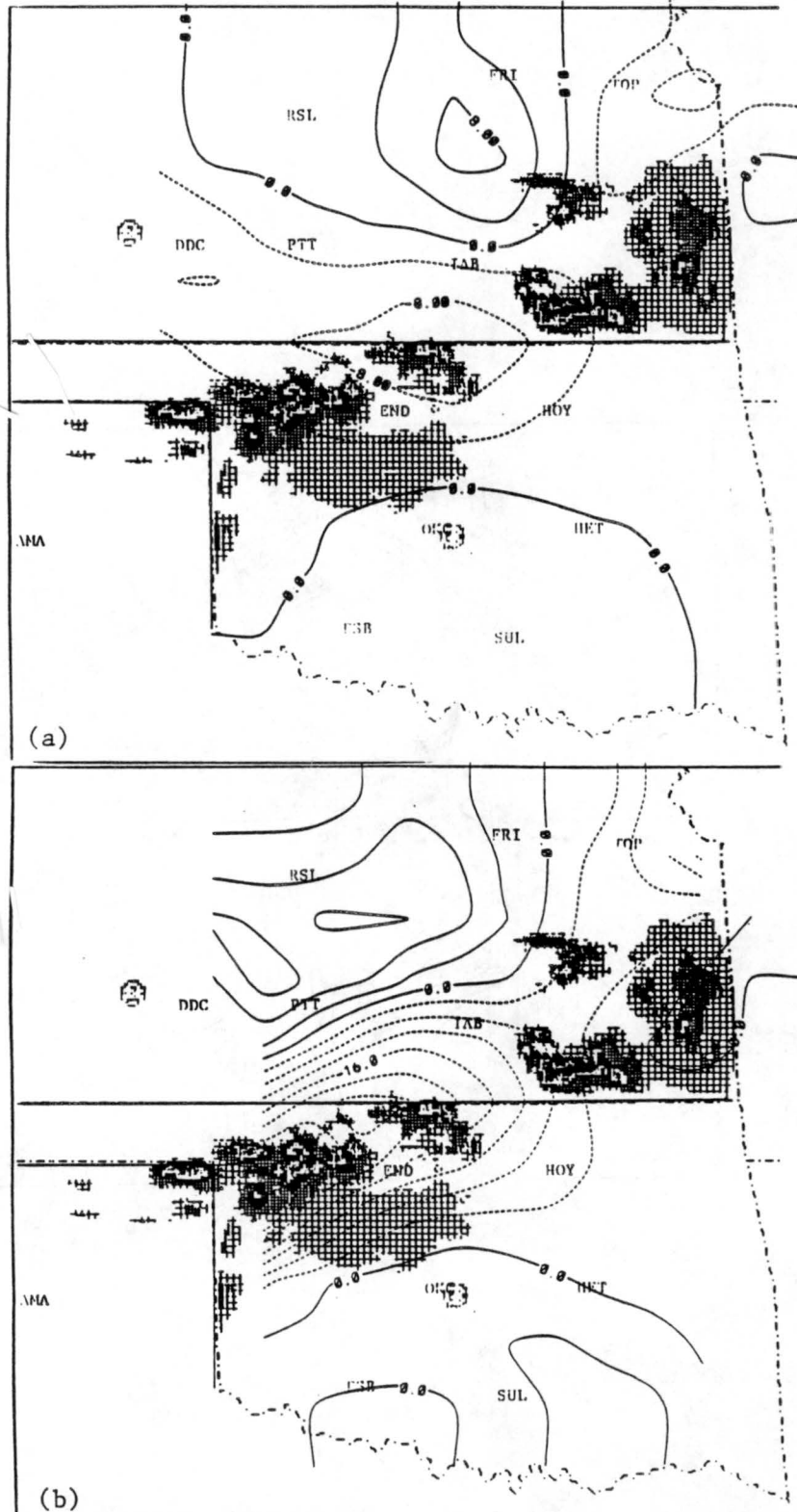


Figure 5.22: Moisture divergence field as in Fig. 5.18 except at 0300 UTC, 15 June 1985; (a) surface and (b) 900 mb.

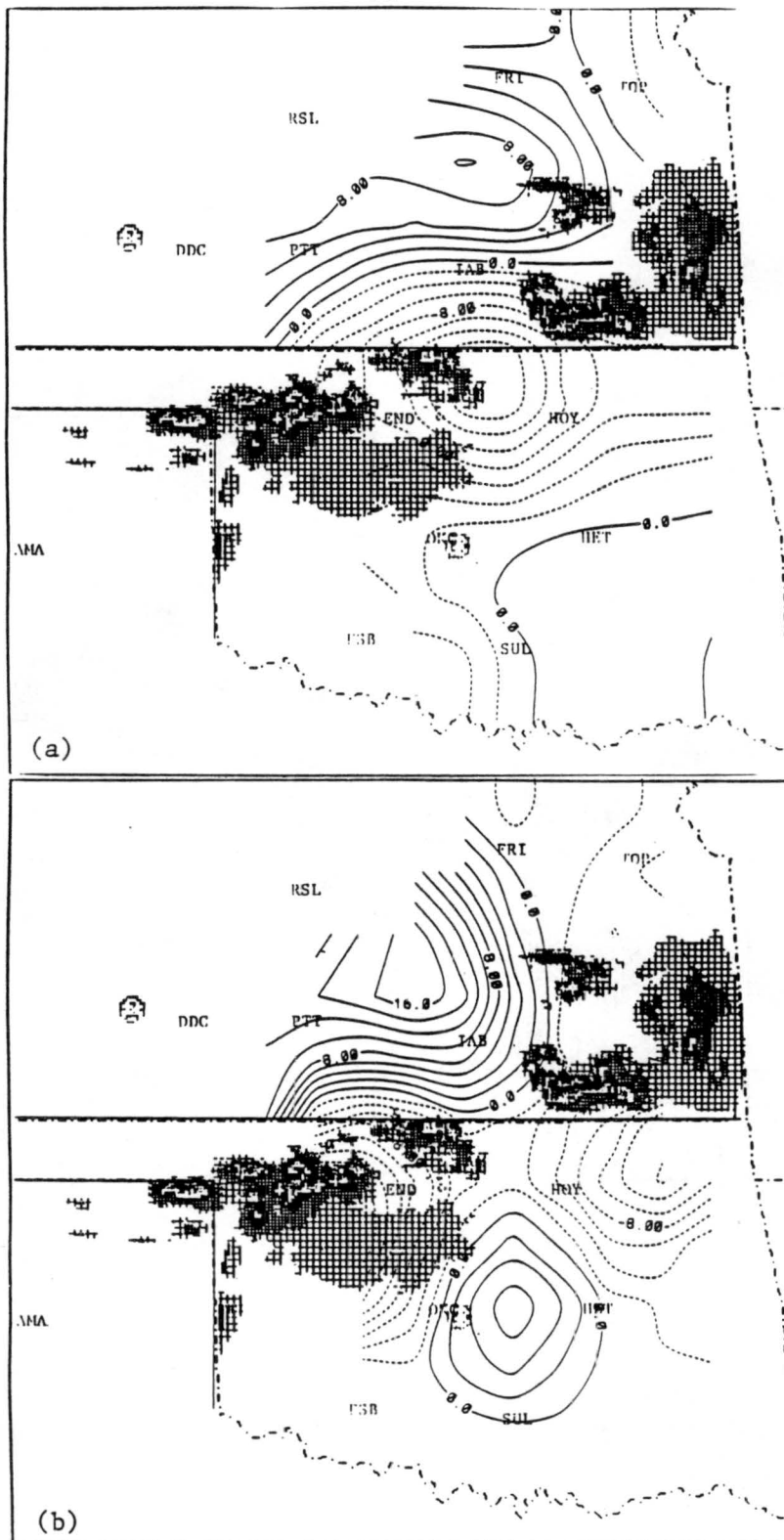


Figure 5.23: Omega field as in Fig. 5.19 except at 0300 UTC, 15 June 1985; (a) 850 mb, (b) 300 mb and (c) 200 mb.

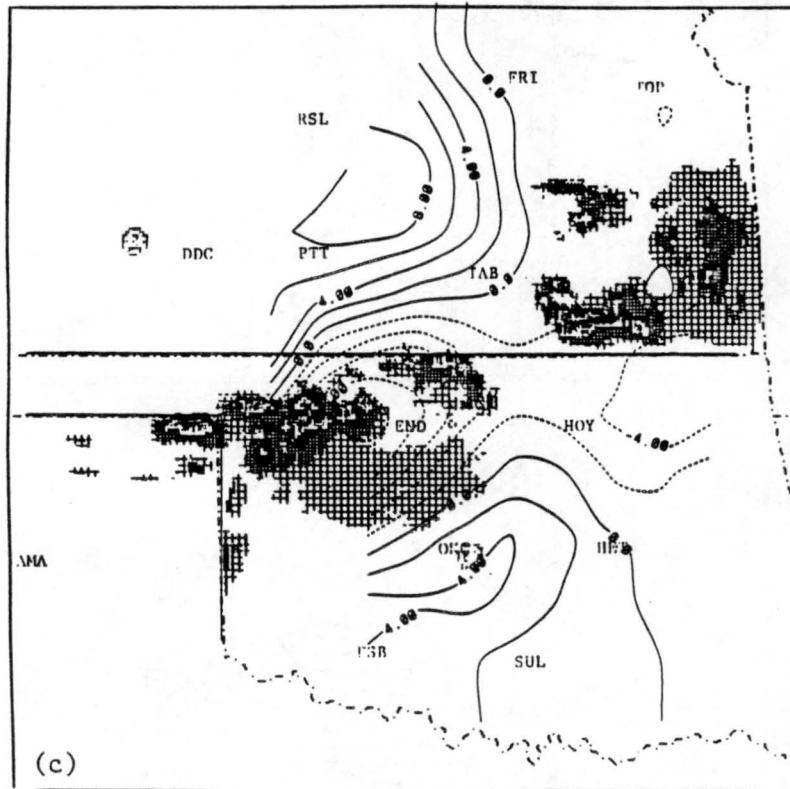


Figure 5.23: continued

5.2.4 0600 UTC

The divergence pattern at 0600 UTC (Fig. 5.24 a - c) showed convergence associated with MCS1 at the surface and 850 mb, and strong divergence at 200 mb. The low-level divergence pattern over MCS2 could not be defined as no special soundings were taken in the Texas panhandle at this time and data in this area is therefore unreliable. The echo-free region had strong low-level convergence from the surface through 850 mb and divergence above. There was strong moisture convergence associated with both MCS1 and the echo-free region from the surface through 900 mb (Fig. 5.25 a - b).

The omega field (Fig. 5.26 a - b) along the western boundary seemed very unrealistic when compared to the precipitation pattern at this time. There may be errors in the field due to a sparsity of data near the edge of the domain. However, the field over MCS1 seemed more realistic with rising motion from 850 mb (Fig. 5.26 a) through 200 mb (Fig. 5.26 b). Weaker rising motions over the echo-free region at all levels while weak subsidence was associated with the eastern portion of the decaying MCS2.

5.3 Surface and Upper Air Synopsis

The 14-15 June case was characterized by low-level (surface to 850 mb) southwesterly flow with northwesterly flow above 700 mb. The strong northwesterly jet above 500 mb, giving system relative rear-to-front flow aloft, most certainly contributed to the stratiform regions being ahead of the two MCSs. The divergence field was characterized by strong low-level convergence along the front, in both the MCSs and in the echo-free region. Likewise, some of the strongest low-level moisture convergence and upward motion were also found in the echo-free region. Normally these conditions would strongly favor convection in the echo-free region yet no convection developed. We must therefore look to the mid- and upper-levels to find the cause.

Mid- and upper-level convergence and subsidence were found over the echo-free region after 0000 UTC. It is a simple deduction that the subsidence suppressed any convection in that area. However, the cause of the subsidence is not yet clear. Chapter 6 will use vertical cross-sections along the front to examine the interactions between the two MCSs and the echo-free region.

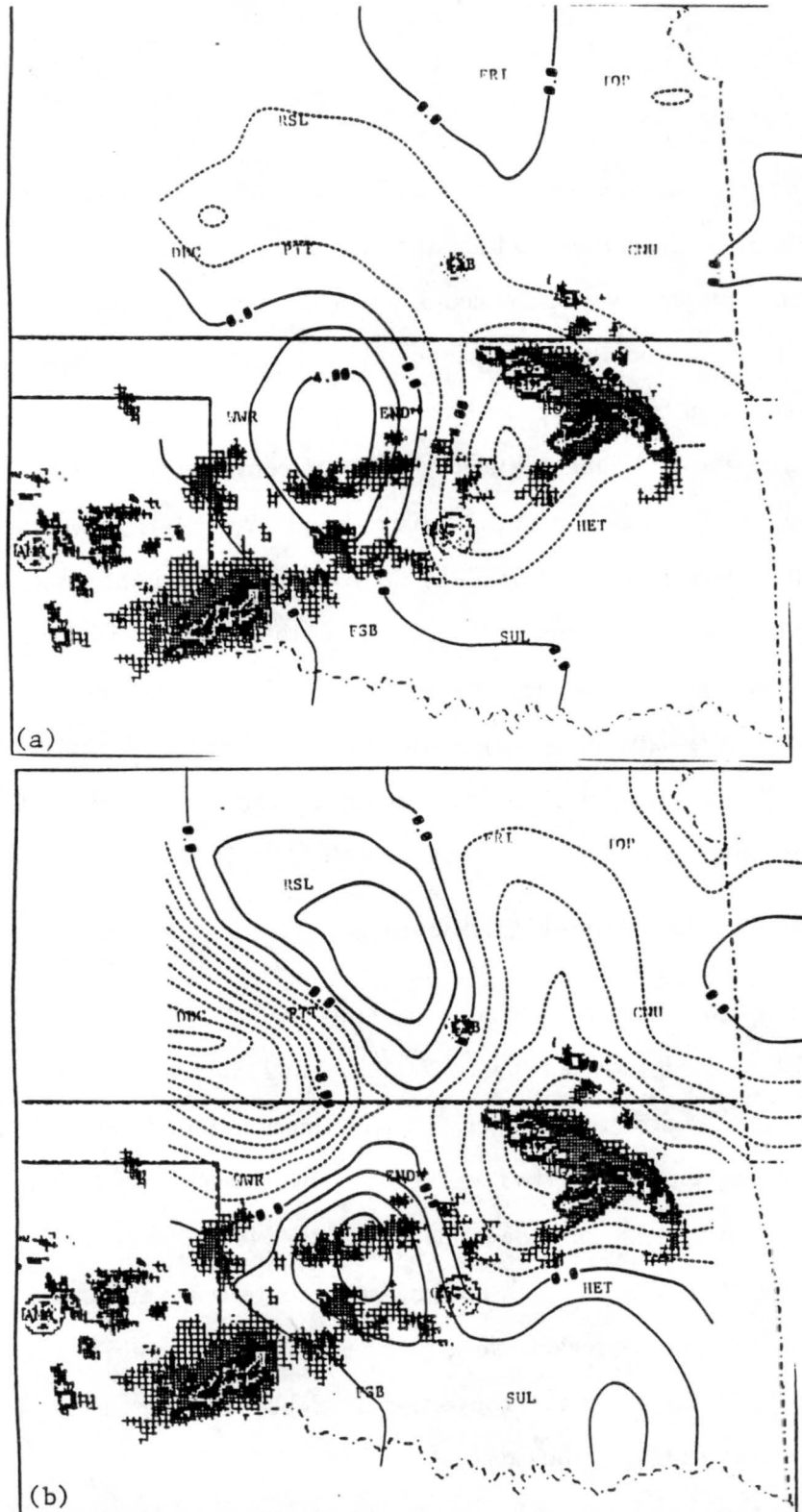


Figure 5.24: Divergence field as in Fig. 5.17 except at 0600 UTC, 15 June 1985; (a) surface, (b) 850 mb and (c) 200 mb.

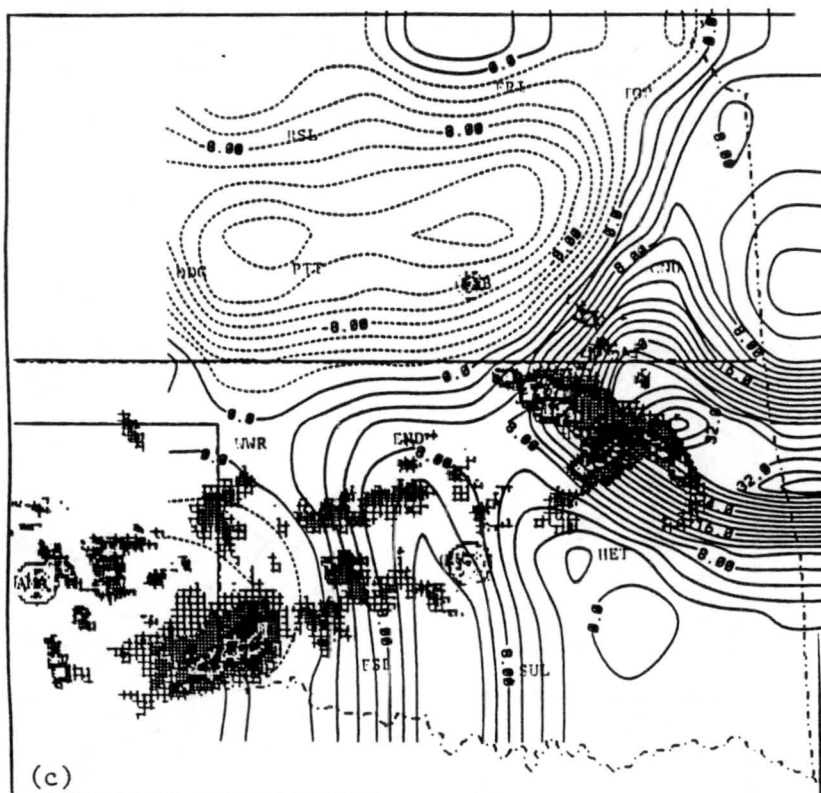


Figure 5.24: continued

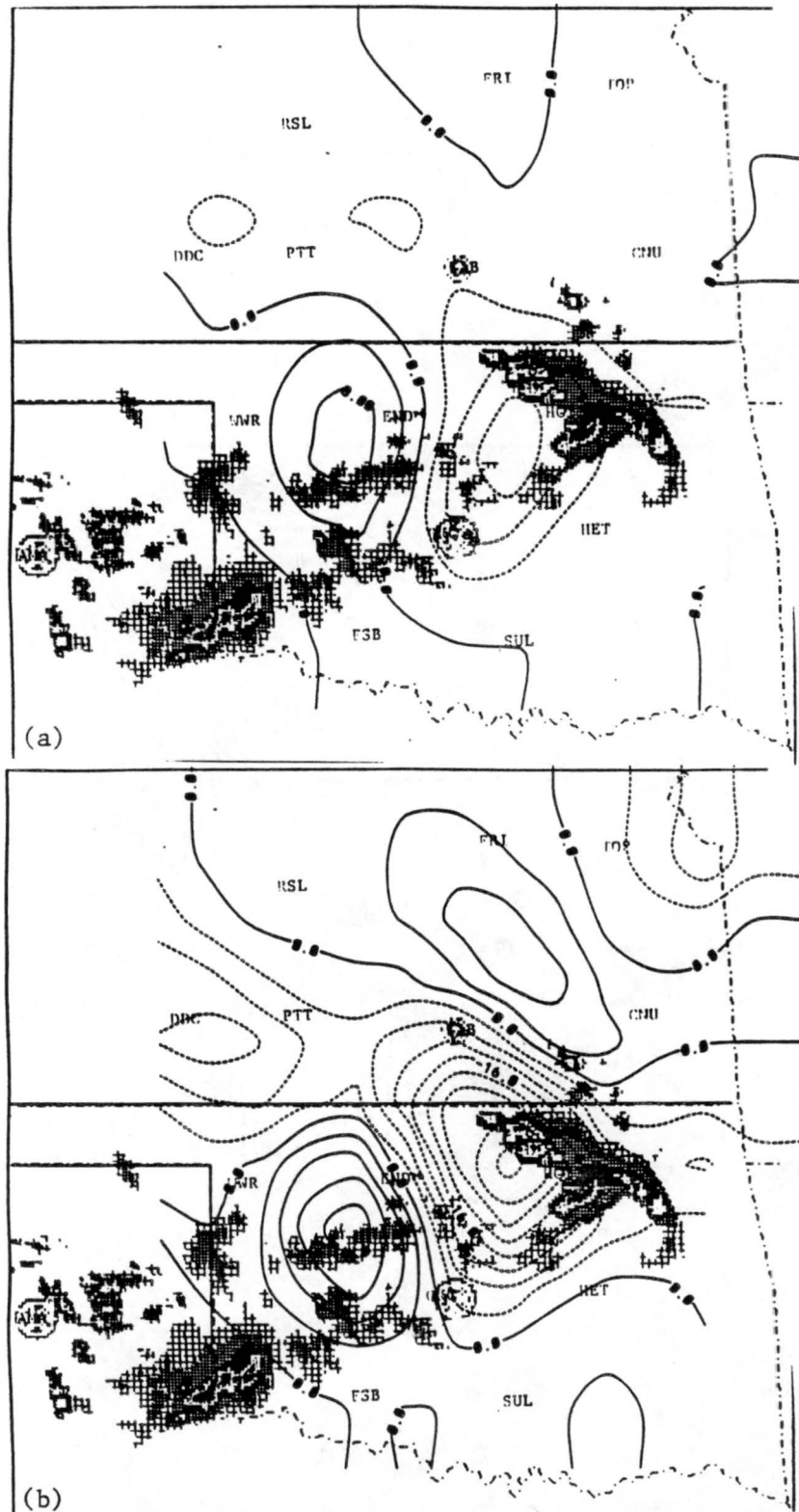


Figure 5.25: Moisture divergence field as in Fig. 5.18 except at 0600 UTC, 15 June 1985; (a) surface and (b) 900 mb.

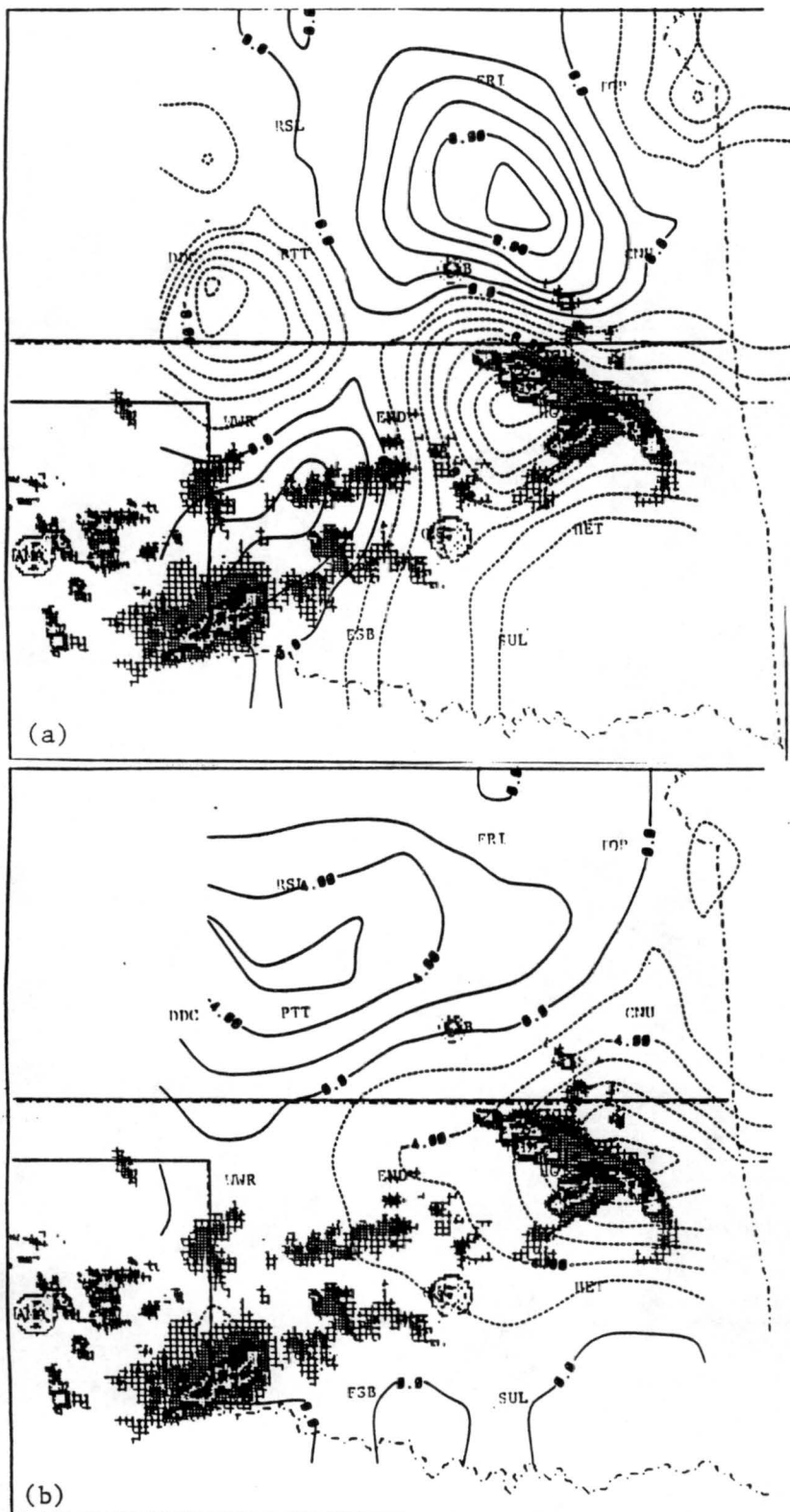


Figure 5.26: Omega field as in Fig. 5.19 except at 0600 UTC, 15 June 1985; (a) 850 mb and (b) 200 mb.

Chapter 6

MESOSCALE ANALYSIS OF ECHO-FREE REGION AND MESOLOW

This chapter will investigate the probable cause of the echo-free region in the squall line and the development of the surface mesolow within this region. The first section uses vertical cross-sections along the line of convection to examine the flow fields in the echo-free region. The second section will examine conditions at 0300 UTC to show that upper tropospheric subsidence warming could partially account for the development of the surface mesolow. The final section will present a schematic of the 14–15 June surface and upper-air flow patterns.

6.1 Development of the echo-free region

Vertical cross-sections derived from the gridded data were taken along the front at 2100, 0000, 0300, and 0600 UTC to examine the circulations within the echo-free region as well as within the two MCSs. Fields that were examined include divergence, vertical velocity, relative humidity and the departure from the mean wind along the line (or wind perturbation).

6.1.1 2100 UTC

The portion of the front examined at this time ran from northwest of Pratt, Kansas to northeast of Russell, Kansas, roughly 300 km (see Fig. 5.1). Although no convection was occurring along this section of the front at this time, it provides information on the pre-storm conditions. Further portions of the front were not studied due to a lack of data. Data was averaged over a 100 km wide band parallel to the front for this time period. Fig. 6.1 shows the region used in the cross-section. Numbers indicated in the figure correspond to the points along the cross-section found in the following figures.

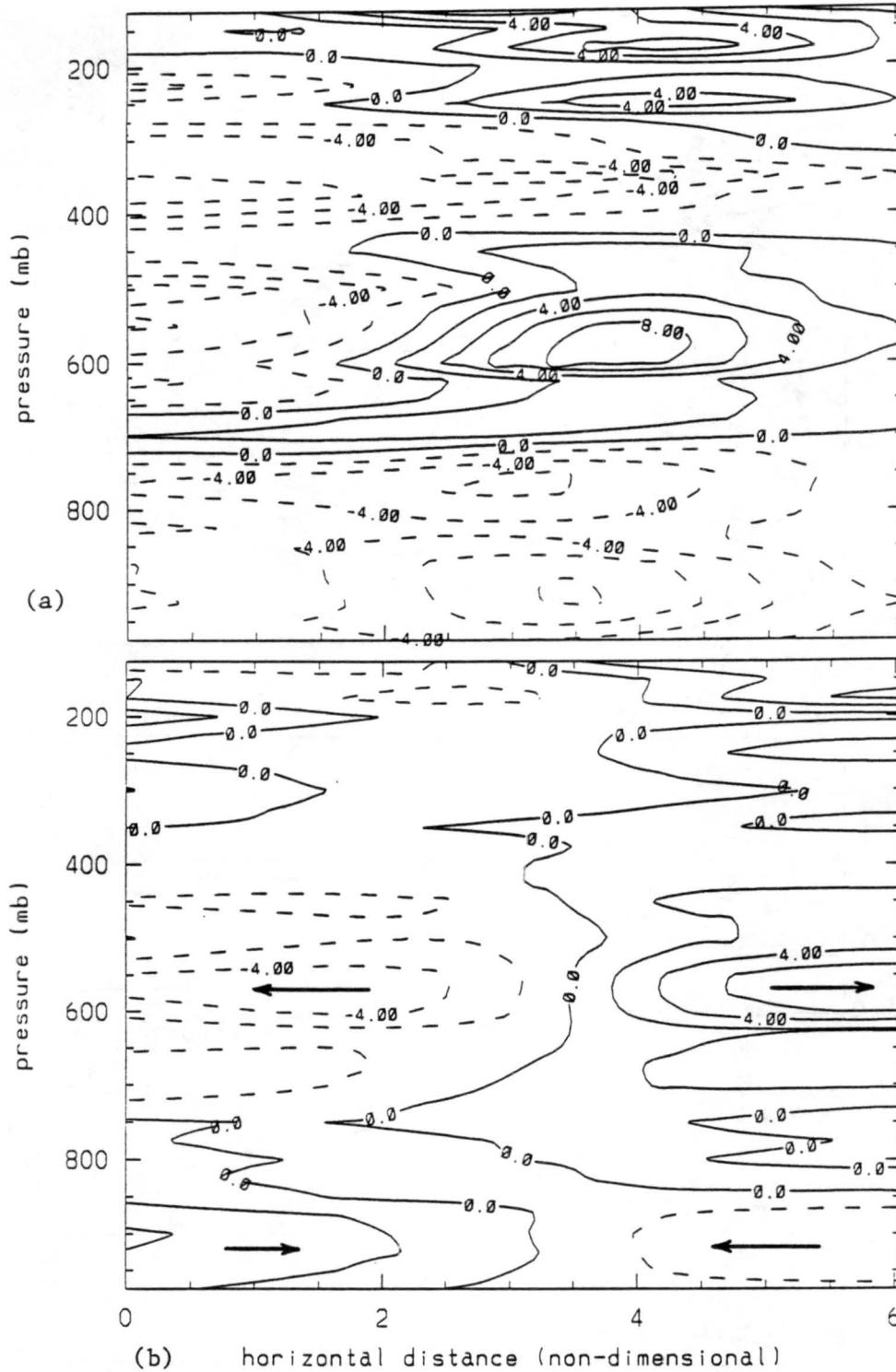


Figure 6.2: Vertical cross-sections of (a) divergence (10^{-5} s^{-1}): positive values (solid lines) indicate divergence, negative values (dashed lines) indicate convergence; (b) wind perturbation (m s^{-1}): positive values (solid lines) indicate motion to the right, negative values (dashed lines) indicate motion to the left; (c) omega ($10^{-3} \text{ mb s}^{-1}$): positive values (solid lines) indicate downward motion, negative values (dashed lines) indicate upward motion; and (d) relative humidity (percent). Lines are drawn at increments of 2, except for relative humidity which has lines drawn at increments of 20.

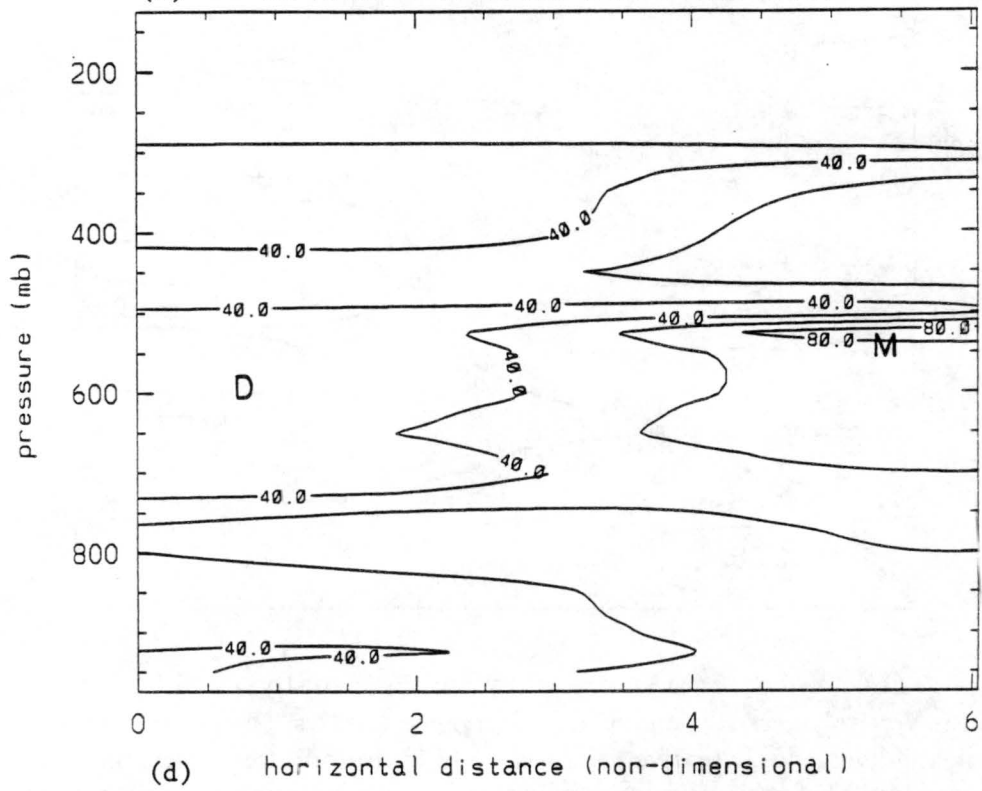
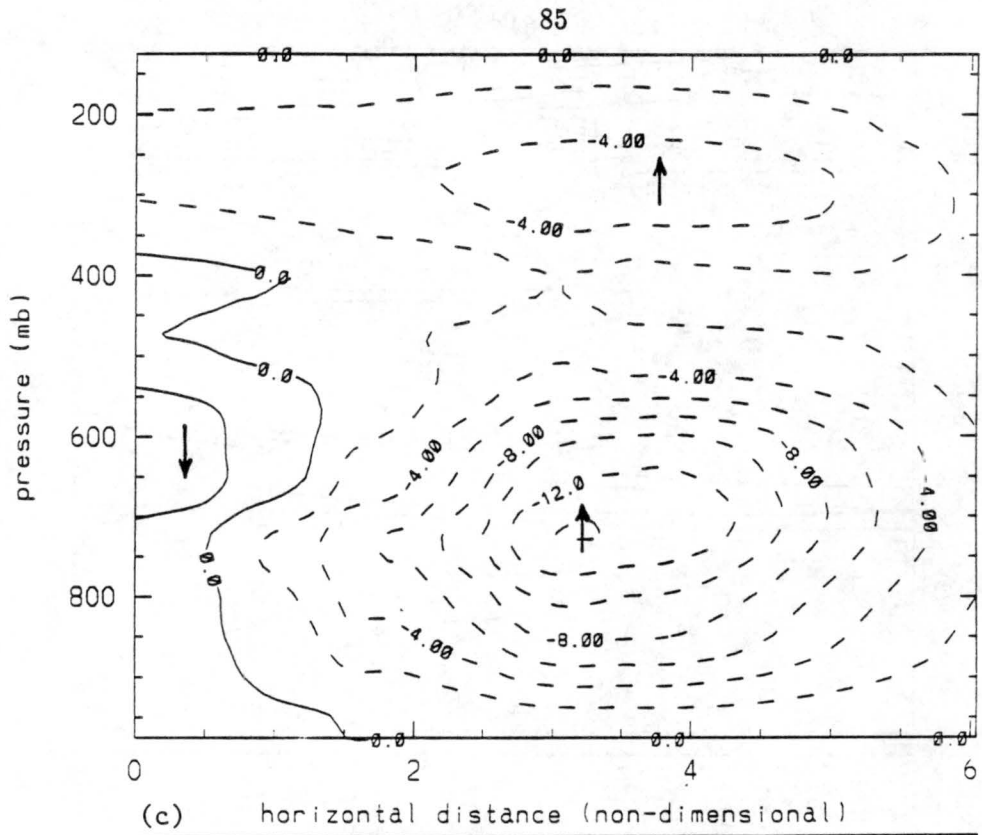


Figure 6.2: continued

Fig. 6.2a shows the vertical cross-section of the divergence field. Convergence was found from the surface to roughly 700 mb along the line with maximum convergence located north-northwest of Wichita, Kansas in the area between points 2 and 4. A maximum of $-8 \times 10^{-5} \text{ s}^{-1}$ was found at 900 mb with a second maximum of $-6 \times 10^{-5} \text{ s}^{-1}$ at 750 mb. Divergence in this same region was found from 700 mb to 450 mb with the maximum of $8 \times 10^{-5} \text{ s}^{-1}$ over point 4. This pattern is also well demonstrated in the wind perturbation field (Fig. 6.2b) where convergent flow was found near point 3 from the surface to 850 mb and divergent flow at point 3.5 from 650 mb to 400 mb. The omega field (Fig. 6.2c) showed strong upward motion from point 2 to point 6 throughout the depth of the atmosphere with a maximum of $-1.4 \times 10^{-2} \text{ mb s}^{-1}$ at 750 mb above point 3.

The relative humidity field is often an indication of vertical motion associated with ascending air by a higher relative humidity and subsidence with drier air. Drier air is found from point 0 to point 2 near 600 mb, an area of subsidence. The area from point 2 to point 6 has a higher relative humidity in the area of upward motion (Fig. 6.2d). A maximum found at 550 mb from point 5 to point 6 was most likely a result of the cloud shield in northeast Kansas.

6.1.2 0000 UTC

The vertical cross section at 0000 UTC was the most extensive in length because of the large number of soundings available at that time period. The cross-section begins in the Texas panhandle where MCS2 was developing to northeast Kansas, through MCS1 (Fig. 6.3). The length of the cross-section is approximately 700 km and is averaged over a width of 100 km to encompass the width of the two MCSs. The regions of prime interest at this time period were from point 0 to point 3, where MCS2 was developing; point 7 to point 10, where the echo-free region would lie; and point 11 to point 13, along the main line of convection associated with MCS1.

The divergence field (Fig. 6.4a) showed low-level convergence from the surface to 700 mb associated with MCS2 (point 0 to point 3) and divergence above. MCS1 (point 11 to point 13) showed divergence close to the surface indicating downdraft outflow from the system with convergence from 900 mb to 500 mb. Divergence was found above 500 mb

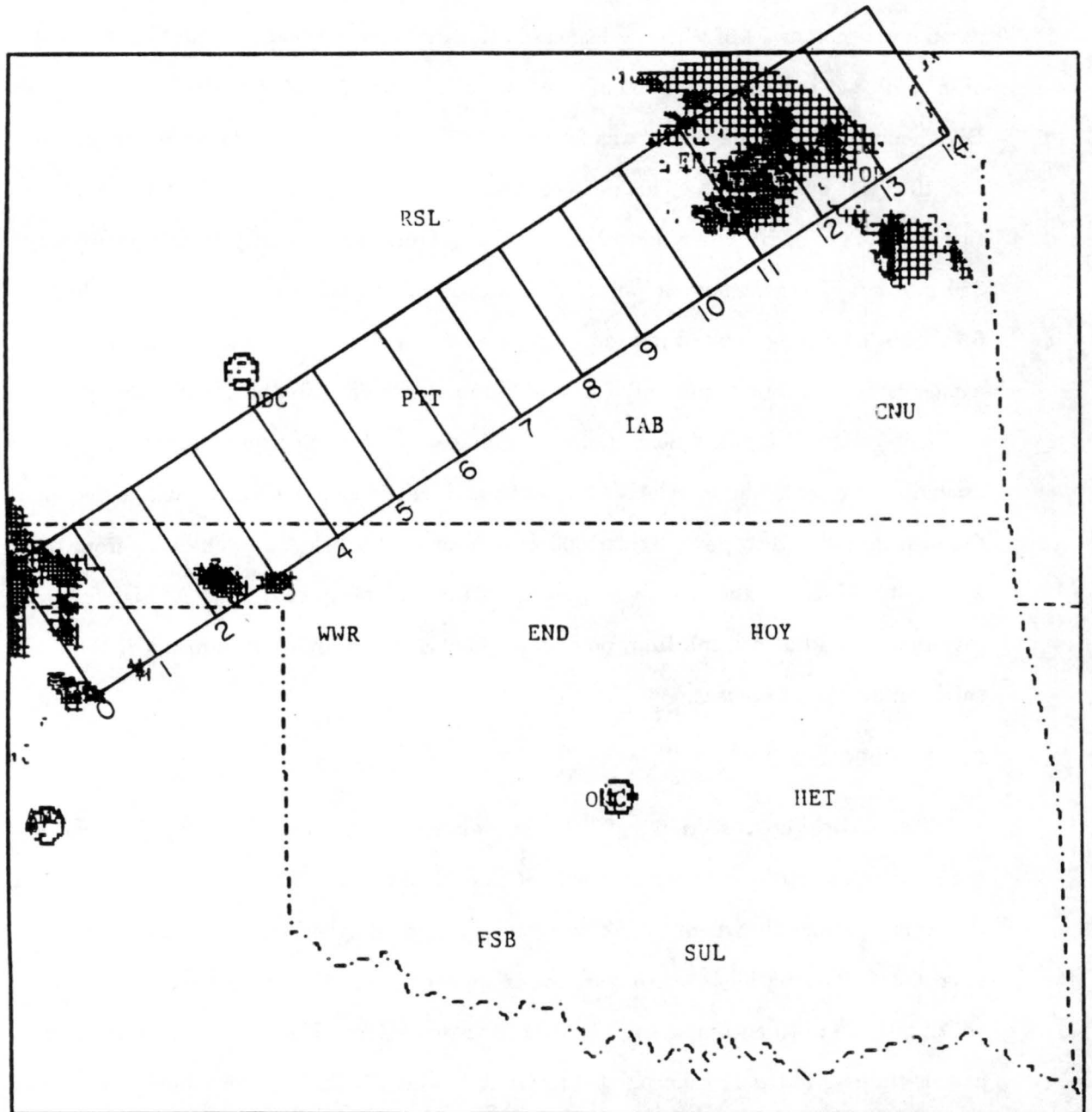
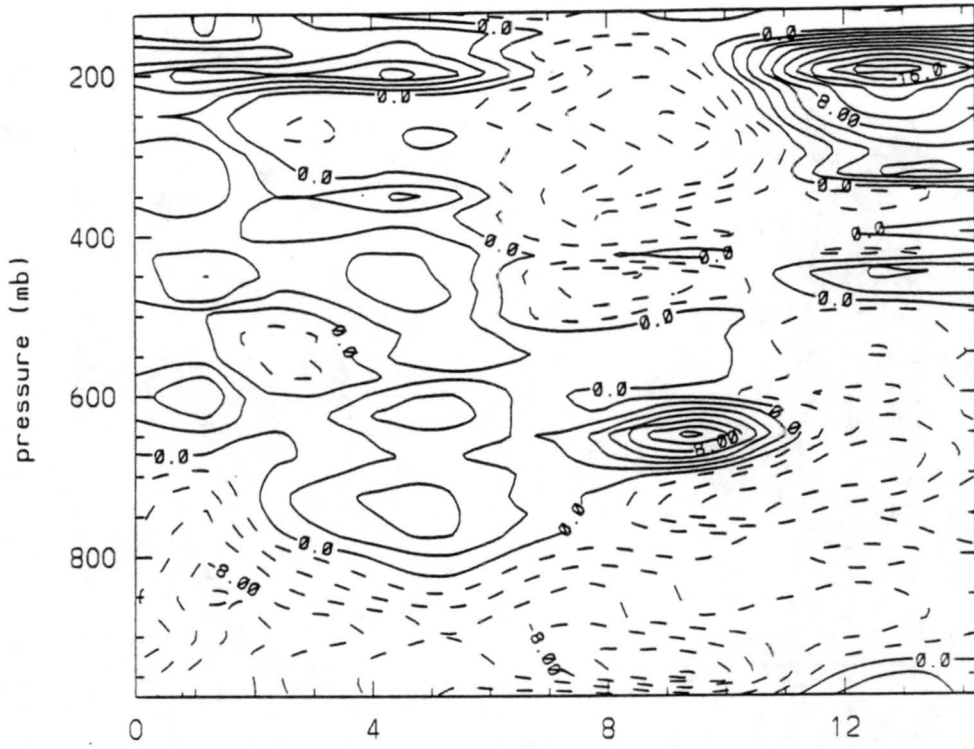
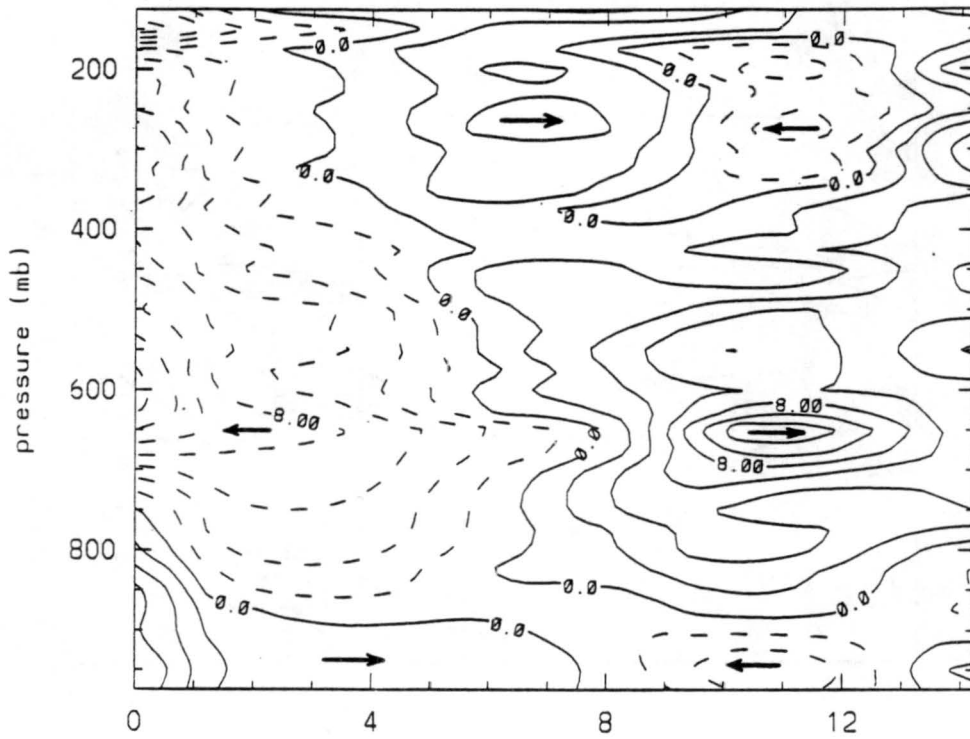


Figure 6.3: Same as Figure 6.1 except for 0000 UTC, 15 June 1985.



(a) horizontal distance (non-dimensional)



(b) horizontal distance (non-dimensional)

Figure 6.4: Same as figure 6.2 except for 0000 UTC, 15 June 1985.

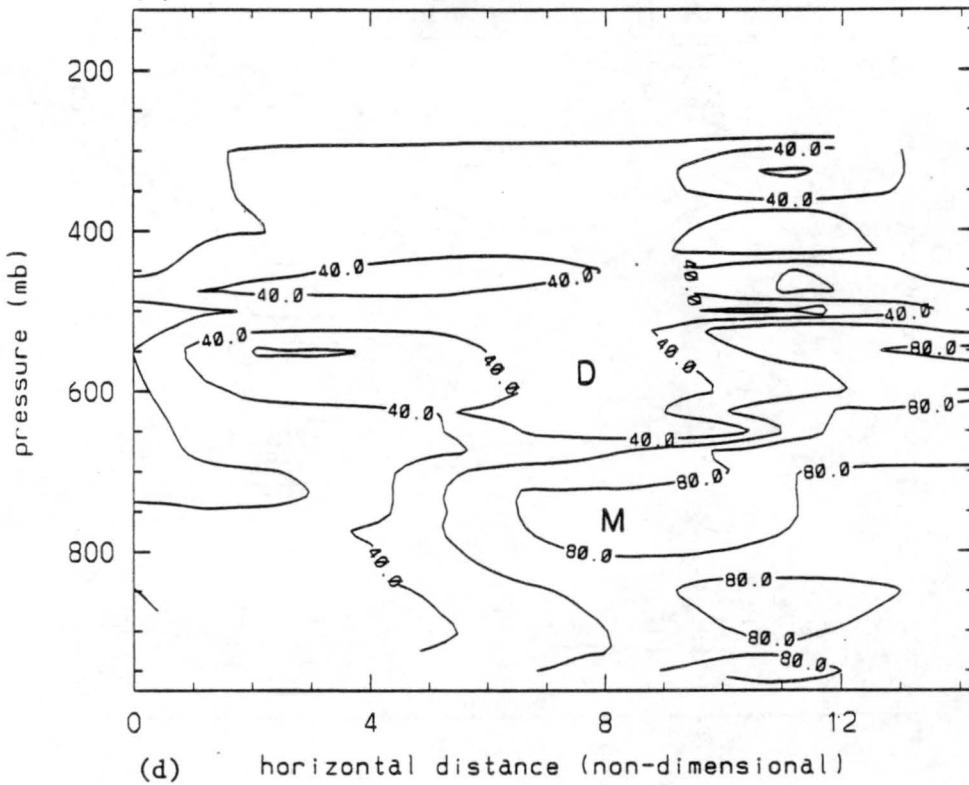
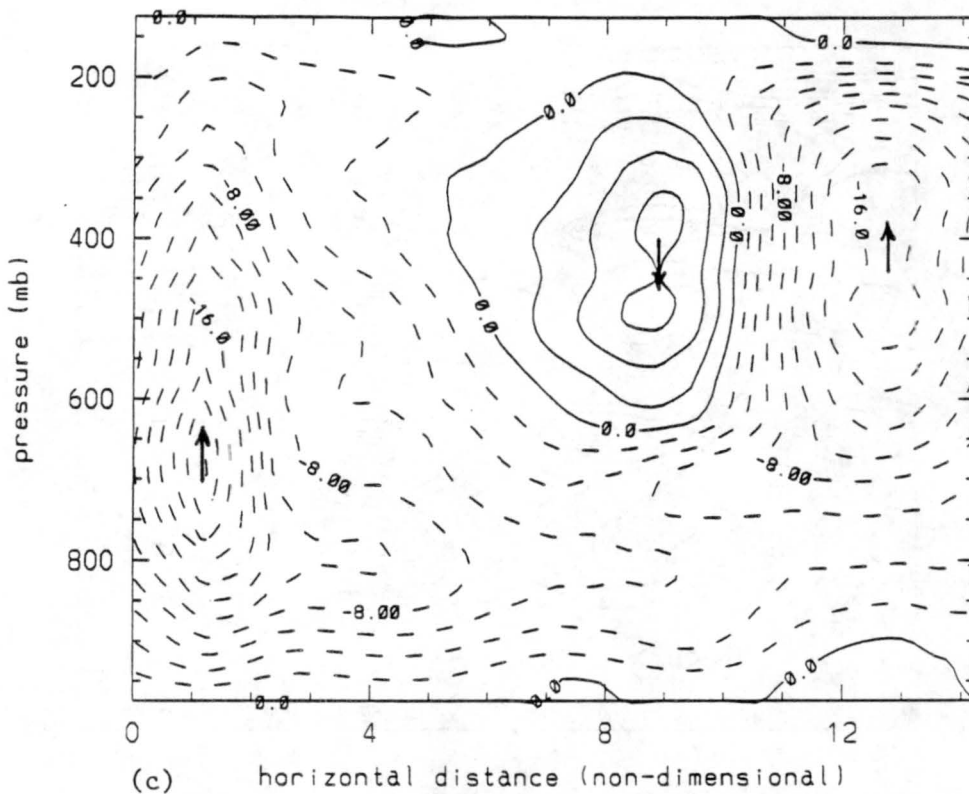


Figure 6.4: continued

with a maximum at 200 mb near the storm top. The echo-free region actually had the strongest low-level convergence along the line at this time with $-1 \times 10^{-4} \text{ s}^{-1}$ (point 7 to point 10)! Convergence was evident from the surface to 700 mb, much the same as MCS2 and strong divergence from 700 mb to 500 mb. However, unlike MCS2, the echo-free region showed convergence above 500 mb. The wind perturbation field (Fig. 6.4 b) showed this convergence very likely to be due to the opposing upper-level outflows above 350 mb from MCS1 and MCS2. Thus; while favorable conditions existed for convection in the echo-free region based on low-level convergence, convergent flow at the upper levels was not favorable. Similar opposing flows between two MCSs were found by Stensrud and Maddox (1988).

The vertical velocity field (Fig. 6.4c) showed very strong rising motion ($-2.2 \times 10^{-2} \text{ mb s}^{-1}$ in the mid-levels over MCS2, with rising motion throughout the depth of the troposphere. MCS1 had low-level sinking motion due to precipitation downdrafts, but strong rising motion from 900 mb to 150 mb. The strongest vertical velocity was near 400 mb with $-1.6 \times 10^{-2} \text{ mb s}^{-1}$. While there was rising motion from the surface to 600 mb in the echo-free region, a well defined area of subsidence was found from 600 mb to 200 mb above the echo-free region, preventing the growth of convective cells in this region. The subsidence region was also evident in the relative humidity field (Fig. 6.4d) where drier air was found in this same region.

Upper air soundings from Pratt (PTT) and Wichita (IAB) (Fig. 6.5 a, b) show subsidence inversions at 700 mb at Pratt and at 675 mb at Wichita. Note the very dry layers associated with the subsidence.

6.1.3 0300 UTC

The vertical cross-section at this time extended from east of Woodward, Oklahoma to east of Chanute, Kansas. Unfortunately, the Woodward sounding was found to be unreliable (balloon went up between two cells, moved into one cell and was discontinued above 600 mb) and had to be removed from the data. Therefore, a full cross-section of MCS2 could not be done. Furthermore, a full analysis of the stratiform region associated with MCS1 was not available due to a lack of data. The length of the cross-section was

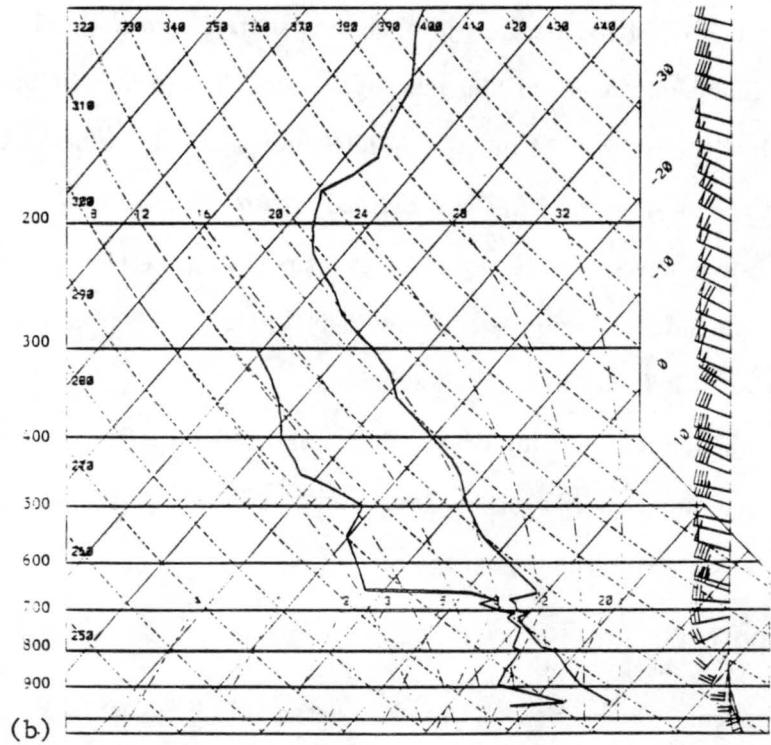
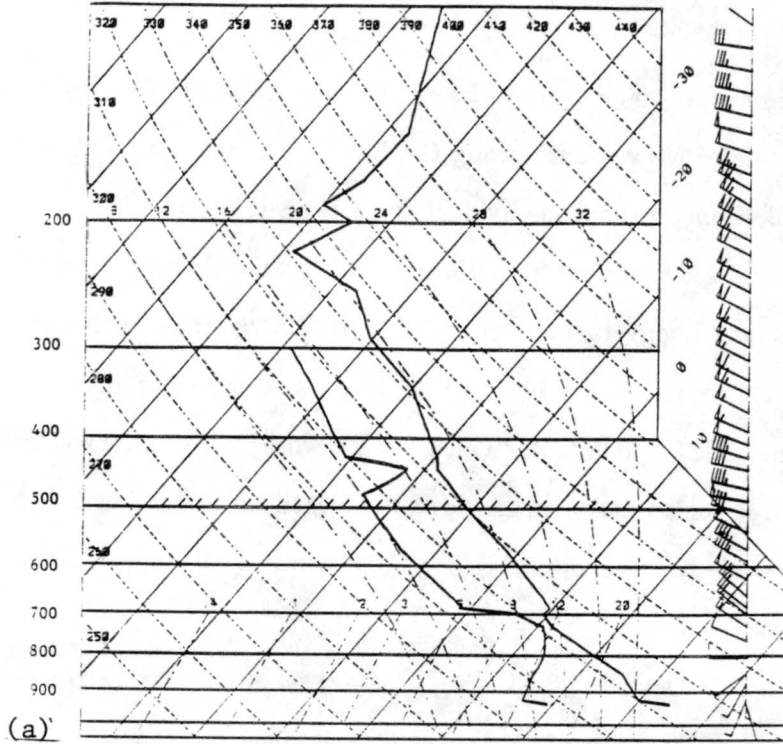


Figure 6.5: Upper-air soundings from (a) Pratt, Kansas and (b) Wichita, Kansas at 0000 UTC, 15 June 1985.

350 km and was averaged over a width of 100 km. The regions of interest at this time were from point 0 to point 2.5 (MCS2); point 3 to point 4 (echo-free region); and point 4.5 to point 6 (MCS1) (Fig. 6.6).

The divergence field (Fig. 6.7a) showed strong low-level convergence along the entire line. The strongest low-level convergence ($1.4 \times 10^{-4} \text{ s}^{-1}$) was associated with MCS2 and found at 900 mb. The southwestern portion of MCS2 had convergence from the surface to 200 mb where divergence values of $1.8 \times 10^{-4} \text{ s}^{-1}$ were found. The northern portion of MCS2, near point 2, had divergence from 800 mb to 500 mb. The echo-free region (point 3 to point 4) had low-level convergence (maximum of $1.2 \times 10^{-4} \text{ s}^{-1}$) from the surface to 800 mb and divergence from 800 mb to 400 mb, with convergence above to 200 mb. MCS1 had several layers of convergence and divergence at this time.

The wind perturbation field (Fig. 6.7b) indicated divergent flow in the region from point 2 to point 3 from 850 mb to 500 mb, and very strong convergent flow above 400 mb over the region from point 2.5 to point 4.5. As at 0000 UTC the convergent flow in the upper levels led to subsidence over the echo-free region.

The vertical velocity field (Fig. 6.7c) had rising motion throughout the troposphere associated with MCS1. MCS2 had descending motion due to downdrafts at the surface, with rising motion above. Weak subsidence was found at 600 mb and may be due to some aliasing of data in the area. The echo-free region had strong ascending motion (a maximum of $1.2 \times 10^{-2} \text{ mb s}^{-1}$ at 800 mb) from the surface to 650 mb, but mid- and upper-level subsidence of $4 \times 10^{-3} \text{ mb s}^{-1}$ from 650 mb to 250 mb. The peak of both the ascending motion and subsidence occurred at the same levels found by Stensrud and Maddox (1988), while the strength of the subsidence was somewhat weaker than that found by them. A minimum in relative humidity was found below the base of the subsidence maximum (Fig. 6.7d).

6.1.4 0600 UTC

The final set of cross-sections at 0600 UTC examine MCS1, the echo-free region and portions of the decaying stratiform precipitation region of MCS2. The convective portion of MCS2 is not presented due to a lack of sounding data in the Texas panhandle at this

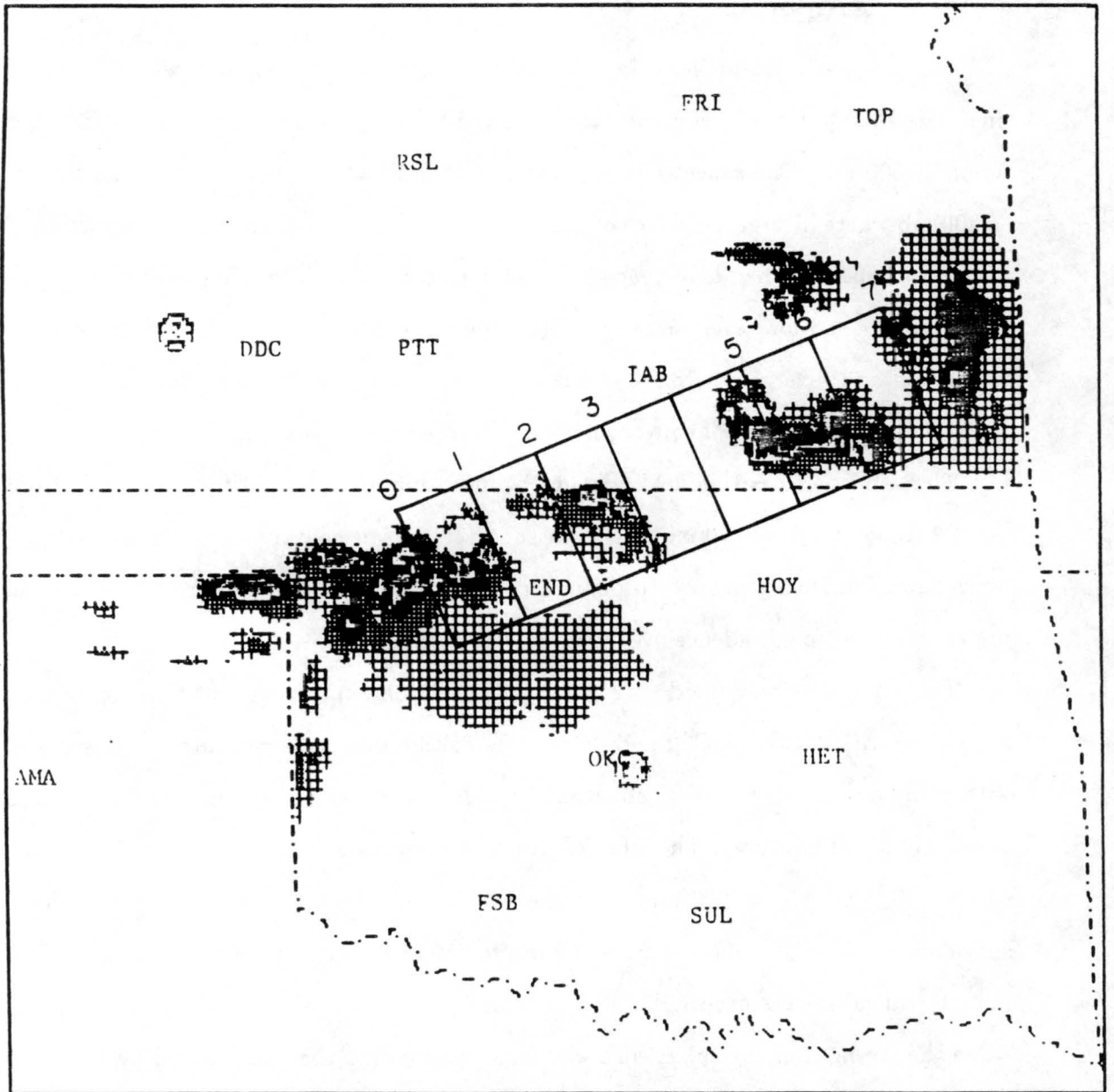
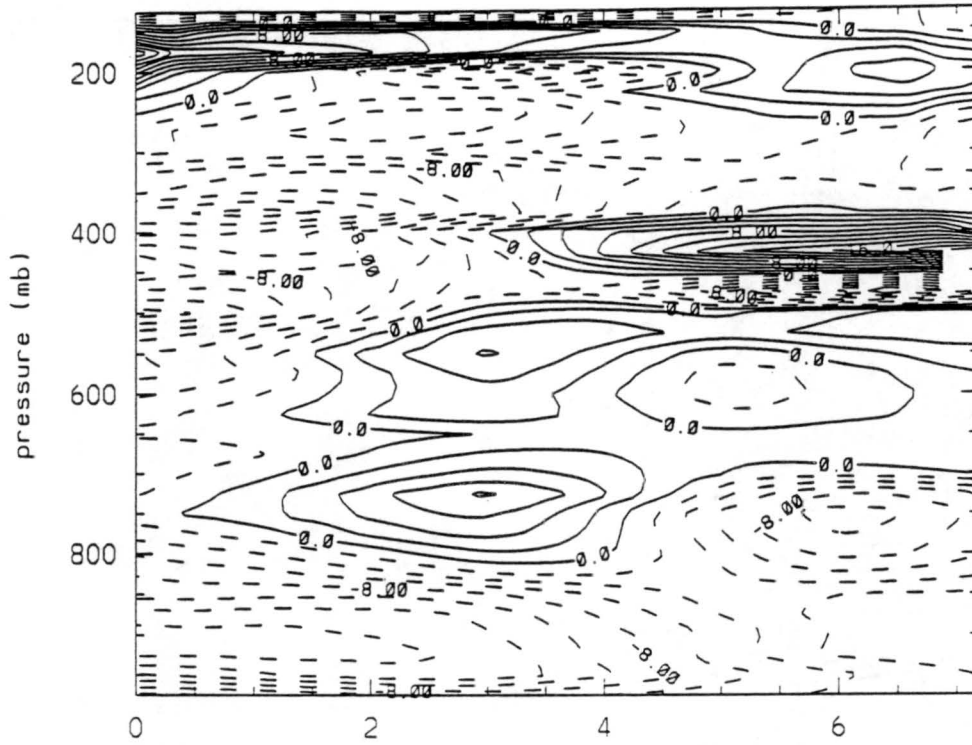
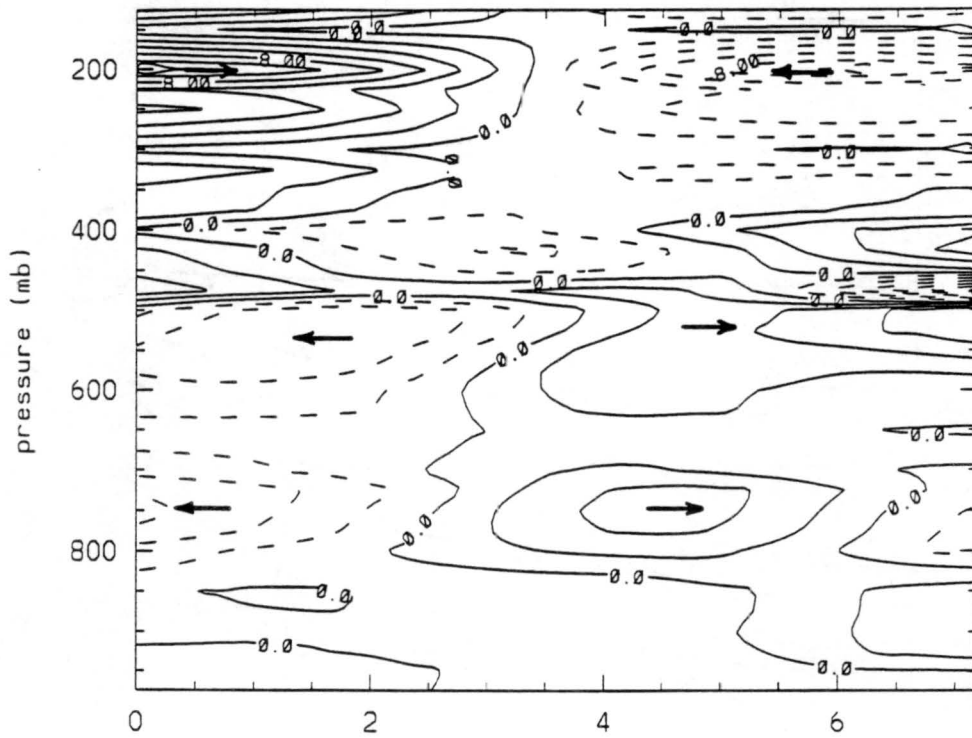


Figure 6.6: Same as figure 6.1 except for 0300 UTC, 15 June 1985.



(a) horizontal distance (non-dimensional)



(b) horizontal distance (non-dimensional)

Figure 6.7: Same as figure 6.2 except for 0300 UTC, 15 June 1985.

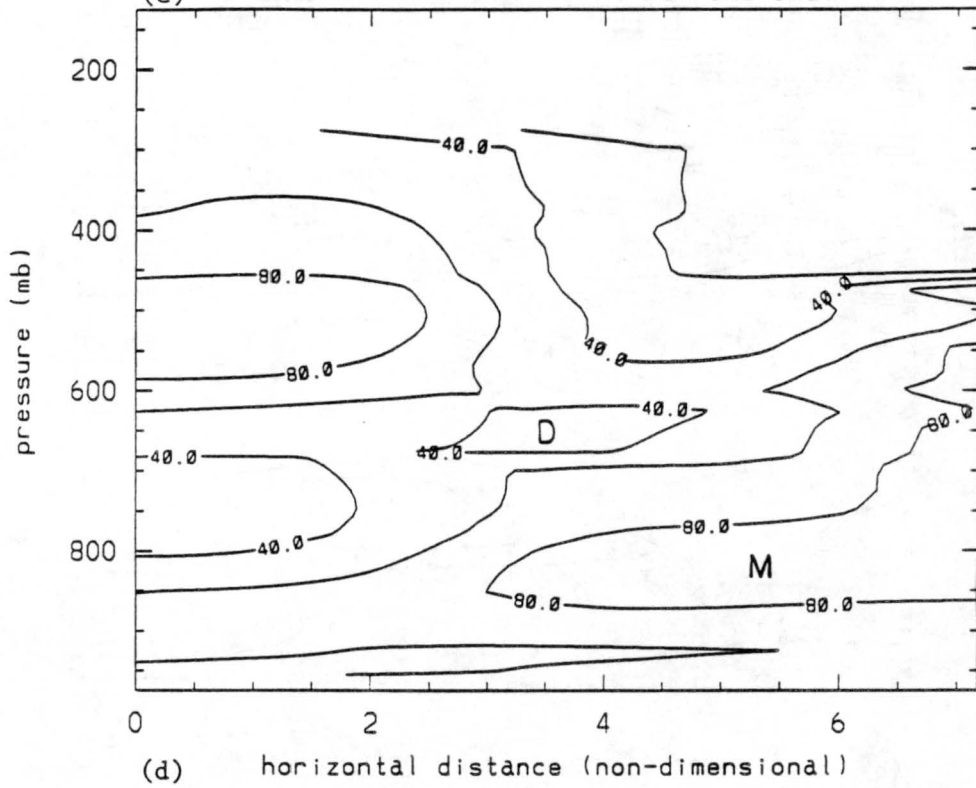
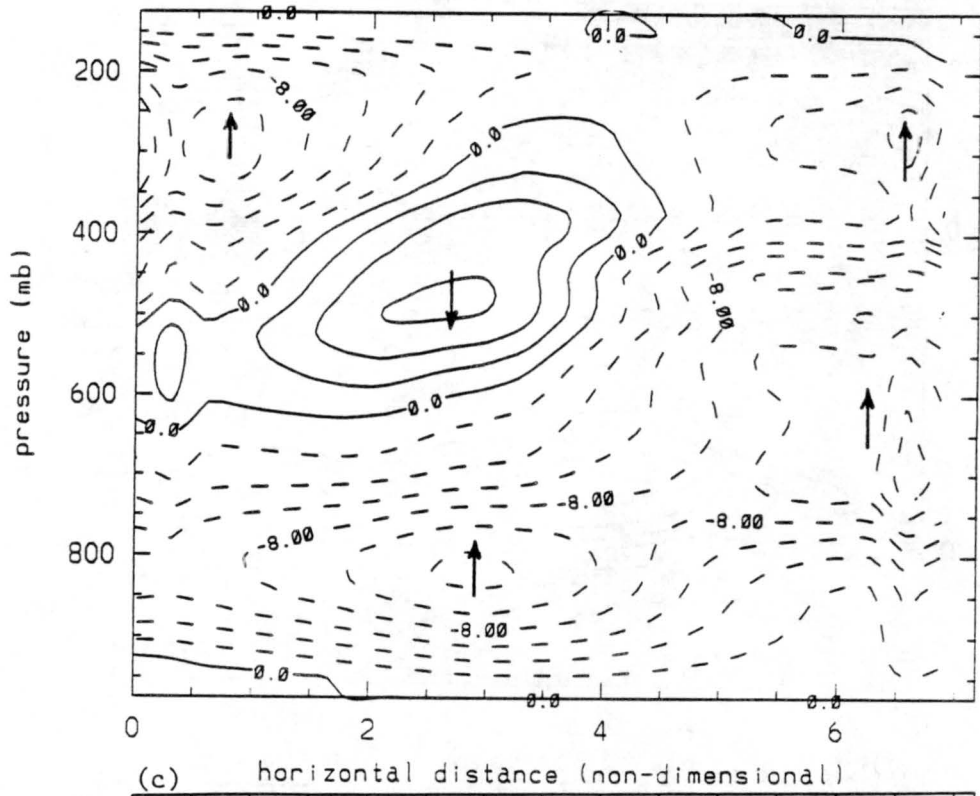


Figure 6.7: continued

time. The length of the cross-section is 300 km and was averaged over a 100 km width. Point 0 to point 3 covers MCS2, the echo-free region is found from point 3.5 to point 4.5, and MCS1 from point 5 to point 6 (Fig. 6.8)

Fig. 6.9a shows the divergence field. Divergence was found from the surface to 600 mb beneath the stratiform precipitation region of MCS2. MCS1 showed convergence through most of the troposphere and divergence above 300 mb. The echo-free region did show the strong pattern of low-level convergence seen at earlier times, but the mid-level divergence is much weaker. The wind perturbation field (Fig. 6.9b) was also weaker at this time. While the upper-level outflow from MCS1 is not as prominent as at 0300 UTC, outflow from MCS2 is still present.

While MCS1 was still quite strong at this time, MCS2 had begun to dissipate after 0400 UTC and was much weaker. Subsidence was found in the stratiform region of MCS2 from the surface to 450 mb with a maximum at 650 mb (Fig. 6.9c). Weak rising motion was found above 450 mb. MCS1 was just reaching its maximum extent in cloud cover at this time (Augustine and Howard, 1988) and had ascending motion throughout its depth. MCS1 began to dominate the area and the echo-free region became smaller. Rising motion was also found throughout the echo-free region. The relative humidity field (Fig. 6.9d) became more a reflection of the precipitation and cloud features than a reflection of strong ascension or subsidence.

6.2 Formation of the surface mesolow in the echo-free region

It was found in the previous section that upper-level subsidence was very strong over the echo-free region at both 0000 UTC and 0300 UTC. A surface mesolow developed in the echo-free region by 0230 UTC and persisted until 0500 UTC. The pressure in the mesolow at 0300 UTC was roughly 2 mb lower than the surrounding areas. Could the upper-tropospheric subsidence have produced enough upper level warming to produce a surface mesolow of this strength? This section will make use of the temperature differences along the line of convection and the hypsometric equation to calculate the surface pressure change due to subsidence warming.

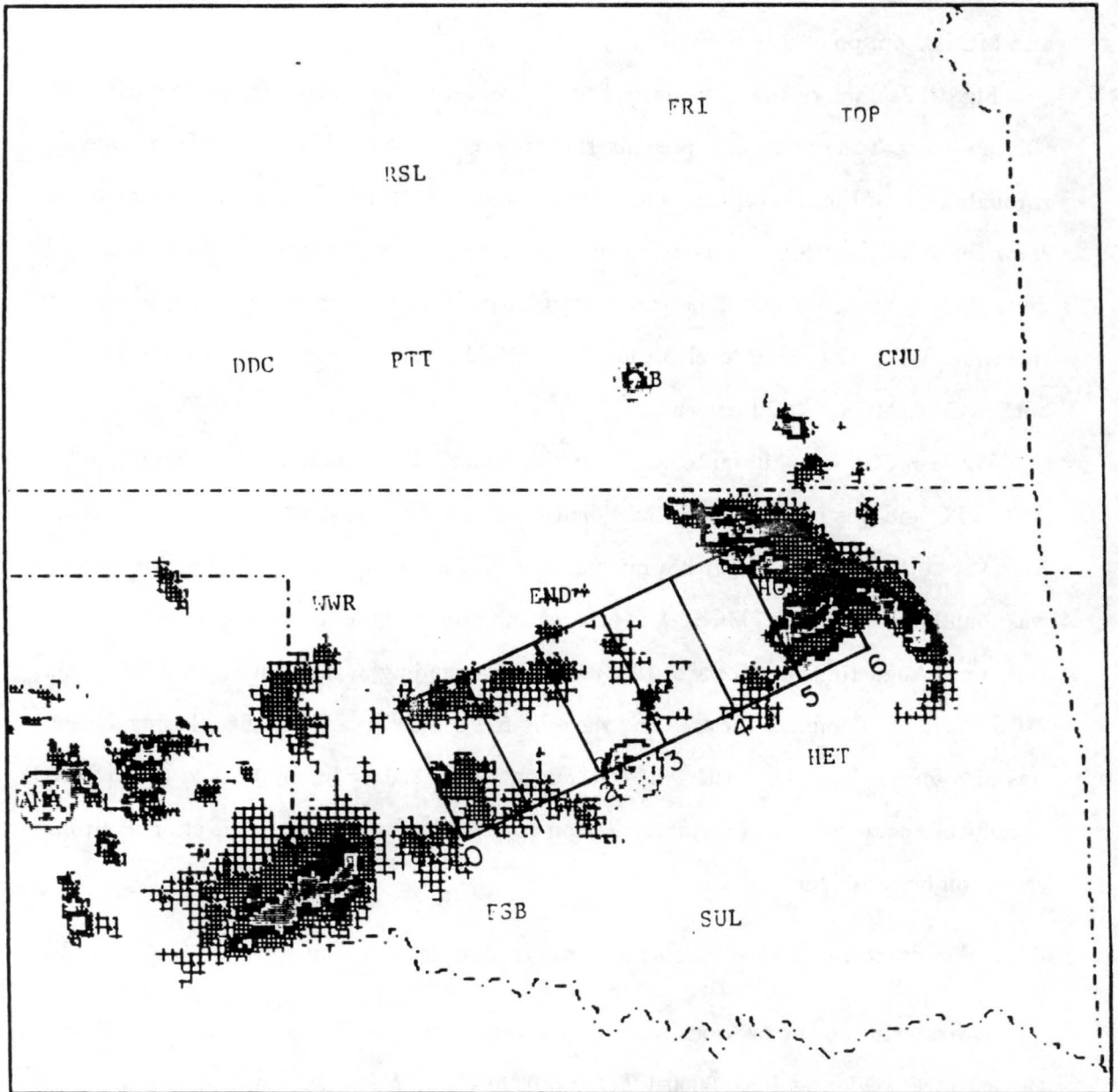
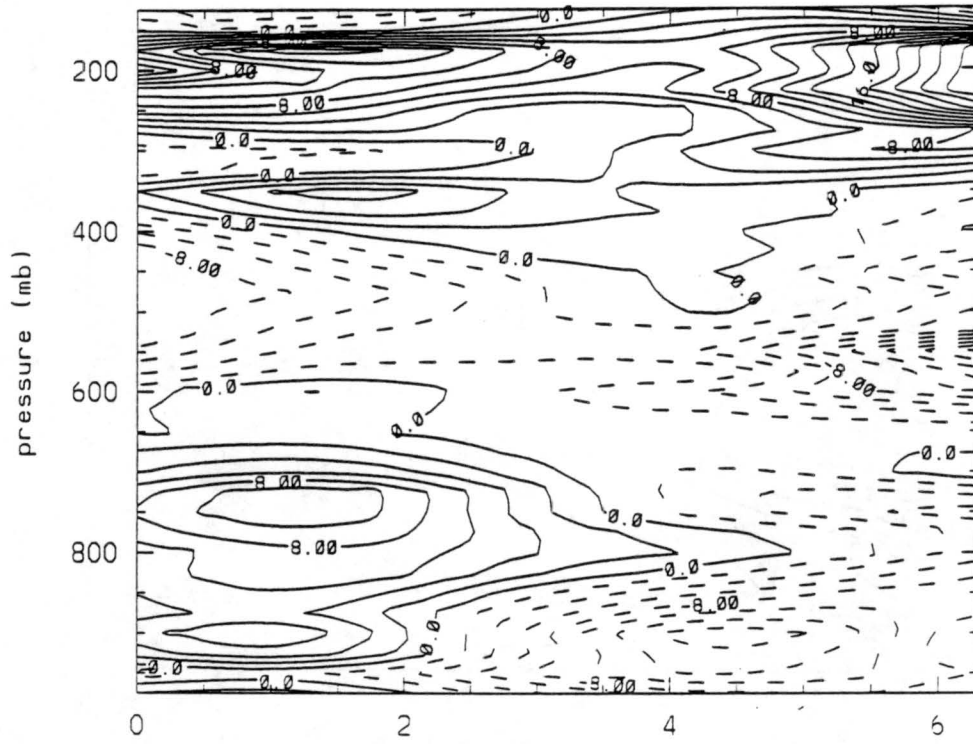
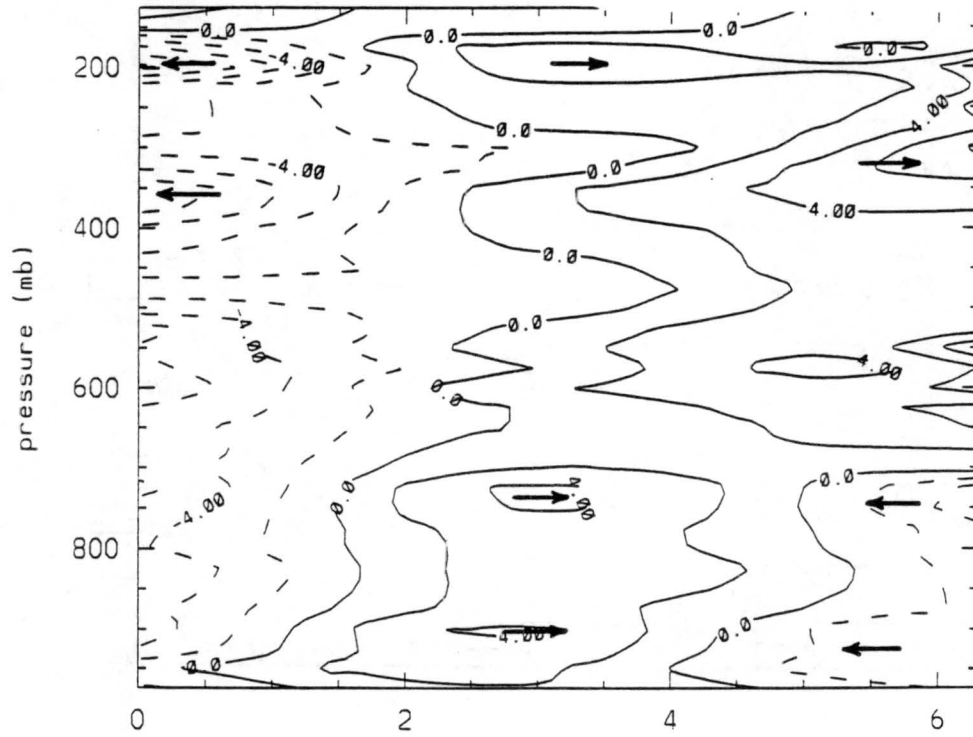


Figure 6.8: Same as figure 6.1 except for 0600 UTC, 15 June 1985.



(a) horizontal distance (non-dimensional)



(b) horizontal distance (non-dimensional)

Figure 6.9: Same as figure 6.2 except for 0600 UTC, 15 June 1985.

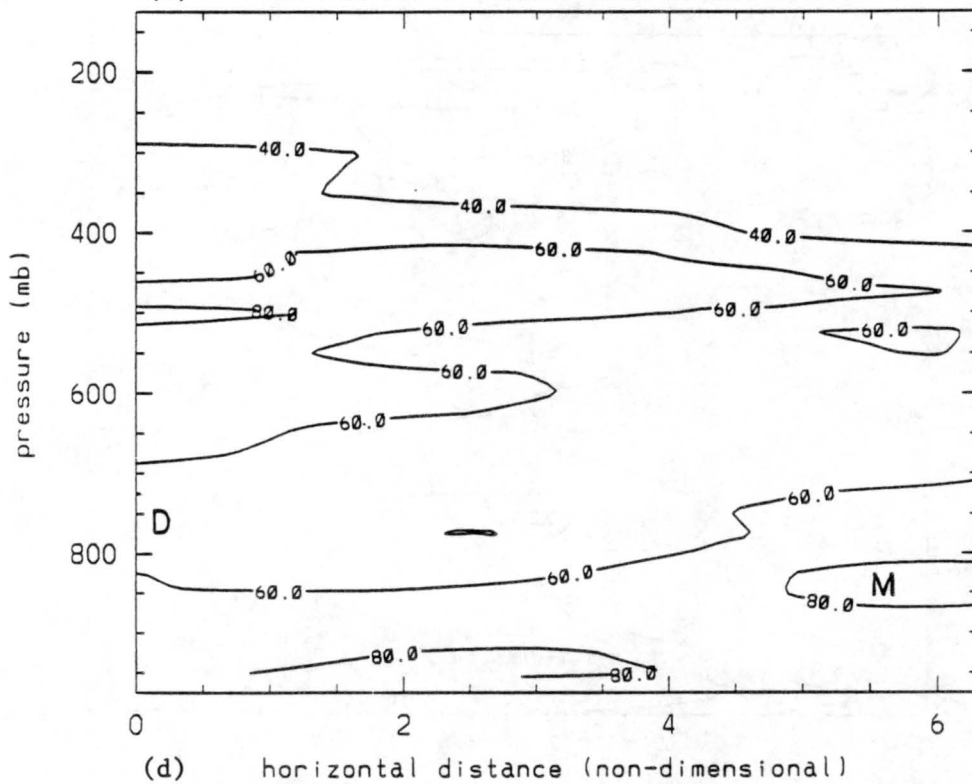
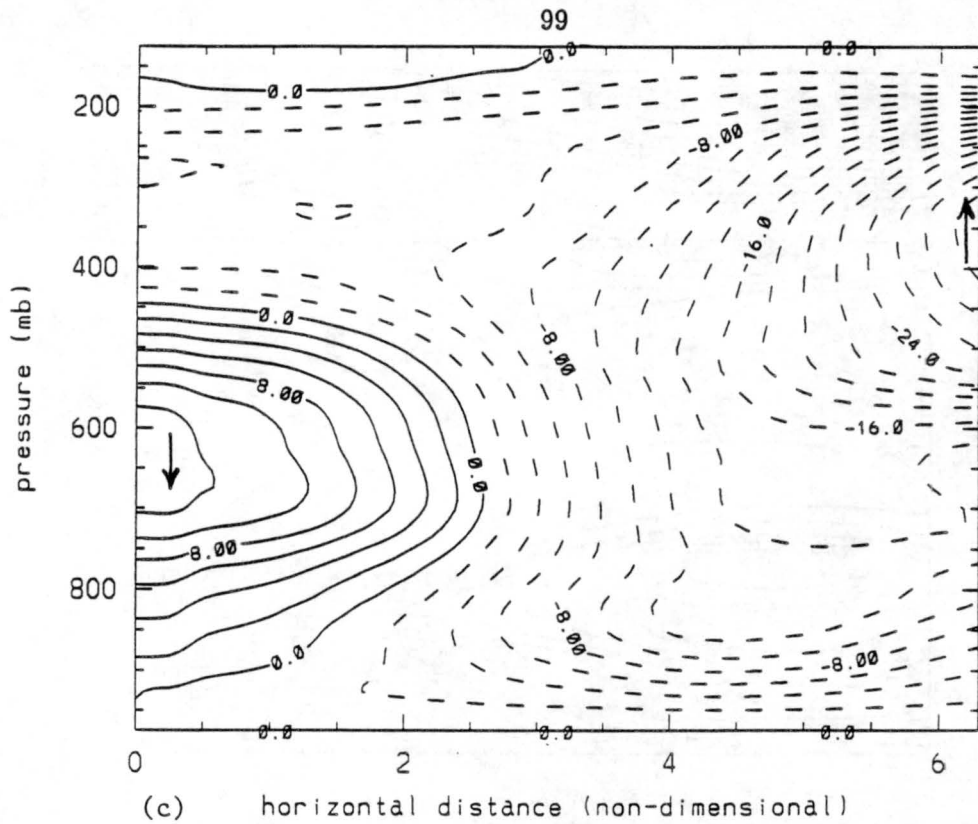


Figure 6.9: continued

In order to calculate the surface pressure fall a vertical cross-section was taken through the line of convection and the mesolow at 0300 UTC (Fig. 6.10). Temperature deviation along the line was calculated by subtracting the actual temperature from the mean temperature along the line at each level at 25 mb increments. Thickness and layer mean virtual temperature were taken from the 0300 UTC Wichita sounding. Fig. 6.11 a-b shows the vertical velocity and temperature deviation fields for this cross-section. A warm anomaly appears aloft in the subsident region. A strong gradient in perturbation temperature appears at low levels. This gradient is a result of low-level temperature gradients in the vicinity of the front and aliasing of data. These gradients complicate the analysis to follow. The temperature deviation column above the mesolow (point 1 to point 2.5) was divided into six layers; one above the subsidence layer, three within the subsidence layer, one just below the subsidence layer, and a surface layer.

The equation used to calculate the change in pressure in a layer due to the change in temperature is:

$$\Delta P = P_0 \left[\exp \left(\frac{g \Delta z}{R_d \bar{T}_{v(new)}} \right) - \exp \left(\frac{g \Delta z}{R_d \bar{T}_v} \right) \right] \quad (6.1)$$

where ΔP is the change in pressure in the layer, P_0 is the pressure at the upper limit of the layer, Δz is the thickness of the layer in meters, \bar{T}_v the mean virtual temperature of the layer and $\bar{T}_{v(new)}$ the mean virtual temperature plus the temperature deviation. R_d is the dry gas constant ($287 \text{ J kg}^{-1} \text{ K}^{-1}$) and $g = 9.8 \text{ m s}^{-2}$.

Using the above equation and then summing the pressure change over the six layers gave a total pressure change of -2.4 mb, very close to the actual difference, 2 mb, in this region. The change in pressure due to warming within the subsidence layer itself was -.75 mb while the layer just below produced a pressure drop of 1.5 mb. The effect of the lower layer is obviously greater; however upper-level subsidence did contribute at least one third to the formation of the surface mesolow. This supports findings by Hoxit et al. (1975) and Fritsch and Chappell (1980).

6.3 Schematic

Given the results of the two previous sections, a schematic of the mesoscale circulation, along the line of convection, can be made for the 14-15 June case (Fig. 6.12). The

0300

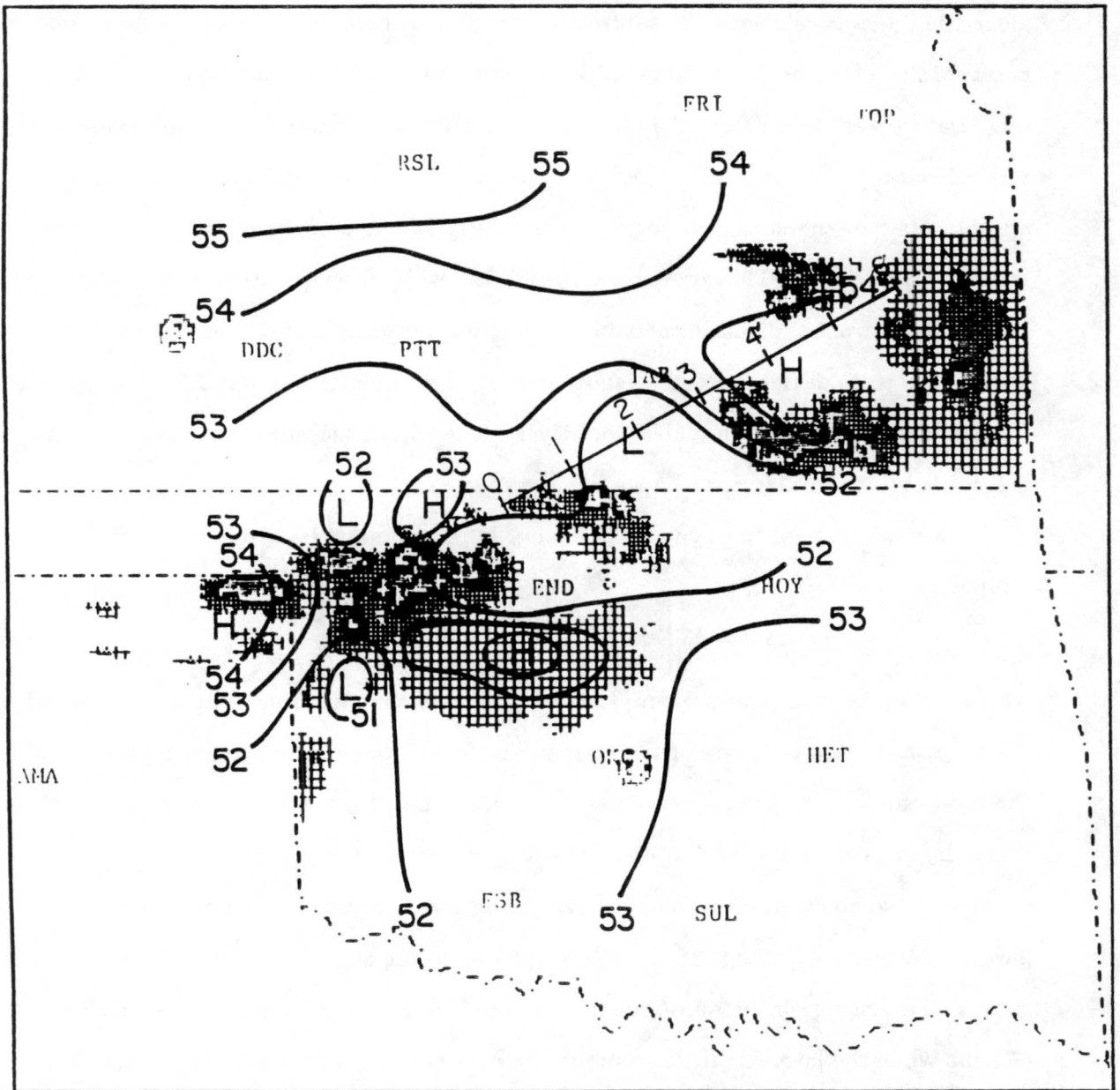


Figure 6.10: Vertical cross-section used to calculate omega and temperature deviation at 0300 UTC, 15 June 1985.

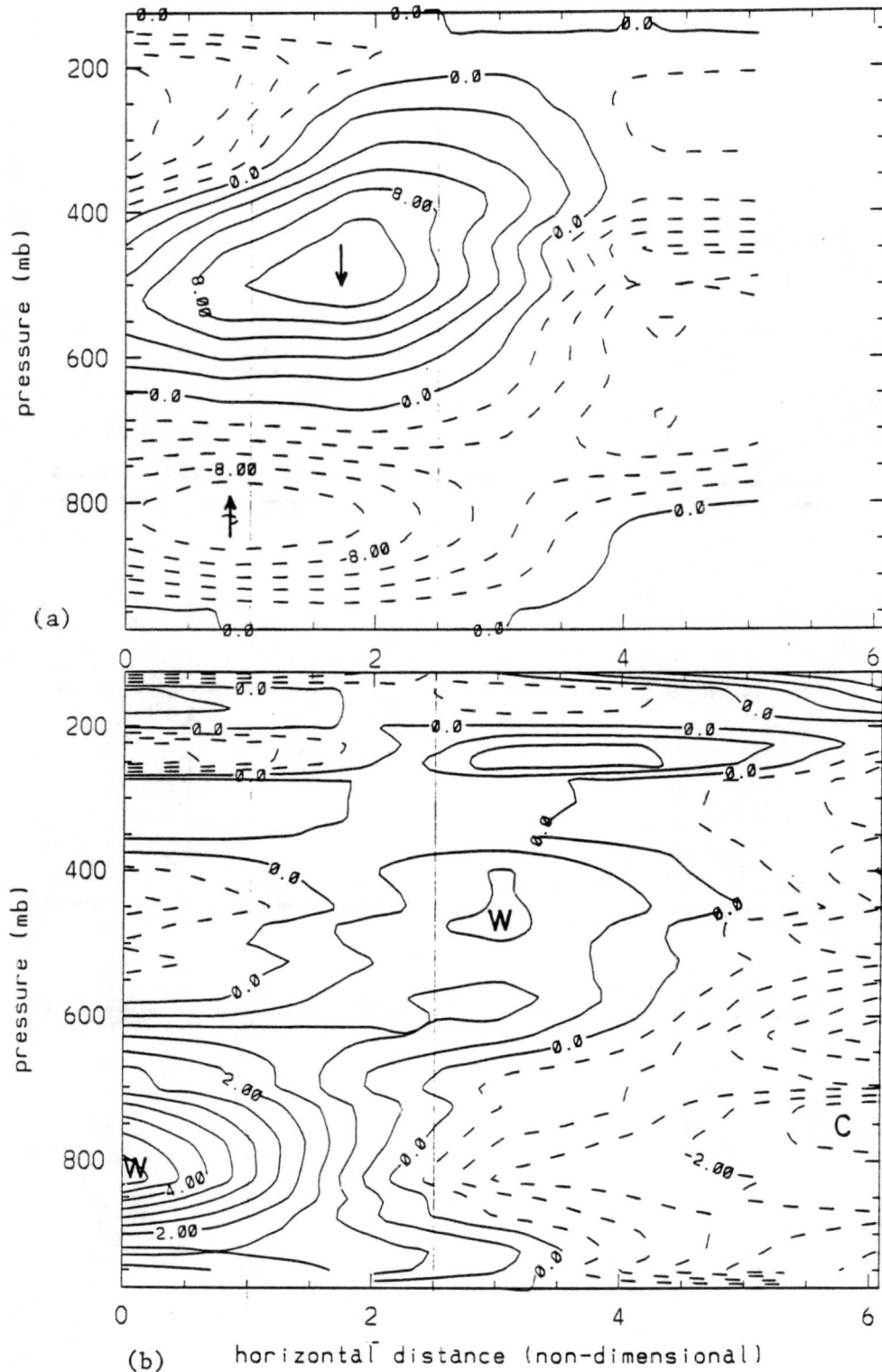


Figure 6.11: Vertical cross-sections of (a) ω ($10^{-3} \text{ mb s}^{-1}$): positive values (solid lines) indicate downward motion, negative values (dashed lines) indicate upward motion; and (b) temperature deviation ($^{\circ}\text{C}$): positive values (solid lines) indicate a warm anomaly, negative values (dashed lines) indicate a cold anomaly. Lines are drawn at increments of 2 for the ω field and at increments of 0.5 for the temperature deviation field.

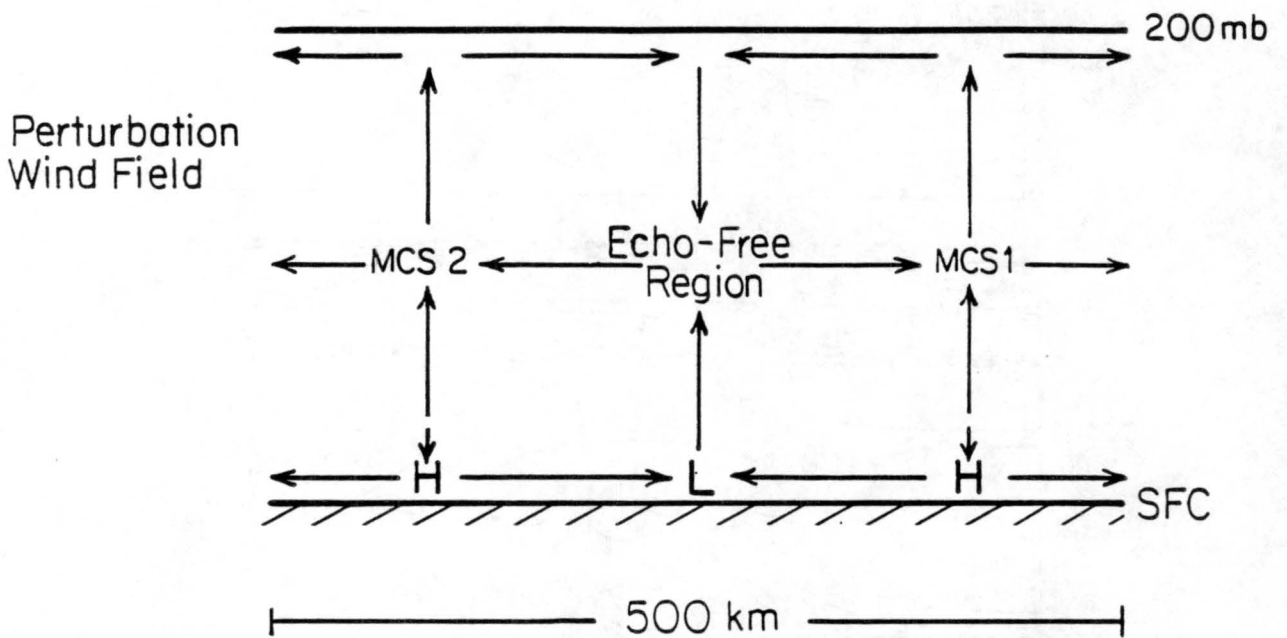


Figure 6.12: Schematic of upper level flow of 14-15 June 1985 in relation to the positions of the mesoscale convective systems, the echo-free region and the surface mesolow.

schematic shows the interactions between the two MCSs and the development of the echo-free region and surface mesolow. The results are very similar to those of Stensrud and Maddox (1988). The schematic shows the wind perturbation field as opposed to the actual wind in the horizontal in order to show the convergent and divergent flows.

Strong convergence along the front forced upward motion in the lower troposphere. Near MCS1 and MCS2 this upward motion extended into the mid- and upper levels. Downdrafts beneath the MCSs allowed some divergence at the surface and intensified convergence in the echo-free region. The upper-level outflow from the two MCSs caused convergence at upper levels and hence, mid- and upper-level subsidence between the two systems. The formation of the surface mesolow in the echo-free region can be attributed in part to the upper-level subsidence warming.

Chapter 7

SUMMARY

The purpose of this paper has been to examine and document the evolution of a broken midlatitude squall line and interactions between mesoscale convective systems (MCSs) within the line. In particular, the existence of an echo-free region or gap within the squall line between two MCSs is studied for the period 14-15 June 1985. Surface and upper air data from the PRE-STORM experiment were analyzed to determine the mesoscale circulations associated with these systems.

The analyses presented in Section 5.1 illustrated the surface pressure and precipitation structure of the systems. Two MCSs developed along a northeast-southwest cold front in Kansas and Oklahoma. As the systems progressed to the south-southeast, an echo-free region between the two persisted and a surface mesolow developed in the echo-free region.

Section 5.2 and Chapter 6 documented the vertical structure along the cold front. During the early stages, strong convergence and rising motion were found all along the front. The two MCSs developed shortly before 0000 UTC (1800 L) on the 15th and moved into the PRE-STORM network. As the MCSs matured the upper-level outflows from the two converged over the central portion of the front. This convergence resulted in subsidence and the persistence of the echo-free region from 0000 UTC until the systems began to dissipate at 0600 UTC. It was found that while there was strong surface convergence in the echo-free region it was not sufficient to overcome the upper-level subsidence. Stensrud and Maddox (1988) found similar results in their study of an echo-free region in the 23-24 June 1985 case. These results point to a difficult problem for operational forecasters since short-term forecasts are often heavily influenced by analyses of low-level forcing mechanisms such as low-level convergence.

A surface mesolow developed in the same region as the echo-free region at 0230 UTC and lasted until 0500 UTC when MCS2 began to dissipate. At 0300 UTC the mesolow was 2 mb lower than surrounding areas. Using a form of the hypsometric equation it was found that the subsidence warming above the surface mesolow could actually cause a pressure drop of .75 mb, roughly one third of the total difference. This supports the previous studies by Fankhauser (1974), Hoxit et al. (1976), and Fritsch and Chappell (1980) which attributed the development of surface mesolows ahead of and near MCSs to upper- and mid-level subsidence warming. Hence the development of both the echo-free region and the surface mesolow can be attributed to the colliding upper-level outflows from the two MCSs and the subsequent subsidence between them.

Further studies of co-existing MCSs should reveal more complex interactions between them and provide better forecasting procedures if a similar situation should occur. The National Weather Service Profiler Demonstration Network that provides high time resolution winds may allow for the realtime analyses of upper-level forcing mechanisms. In addition, more intense studies of systems with leading stratiform precipitation regions should be accomplished.

REFERENCES

- Augustine, J. A., and K. W. Howard, 1988: Mesoscale convective complexes of the United States during 1985. *Mon. Wea. Rev.*, **116**, 685-701.
- Barnes, S.L., 1964: A technique for maximizing details in numerical weather map analysis. *J. Appl. Meteor.*, **3**, 396-409.
- Bartels, D. L. and A. A. Rockwood, 1983: Internal structure and evolution of a dual mesoscale convective complex. *Preprints, 5th Conf. on Hydrometeorology*, Tulsa, Oklahoma. Amer. Meteor. Soc., 97-102.
- Bartels, D. L., J. M. Skradski and R. D. Menard, 1984: Mesoscale convective systems: A satellite-based climatology. NOAA Tech. Memo. ERL ESG 8, Dept. of Commerce, Boulder, CO, 63 pp. [NTIS PB-85-187904.]
- Bartels, D. L. and R. A. Maddox, 1991: Midlevel cyclonic vortices generated by mesoscale convective systems. *Mon. Wea. Rev.*, **119**, 104-118.
- Bluestein, H. B. and M. H. Jain, 1985: Formation of mesoscale lines of precipitation: Severe squall lines in Oklahoma during the spring. *J. Atmos. Sci.*, **42**, 1711-1732.
- Bluestein, H. B., G. T. Marx and M. H. Jain, 1987: Formation of mesoscale lines of precipitation: Non-severe squall lines in Oklahoma during the spring. *Mon. Wea. Rev.*, **115**, 2719-2727.
- Brunk, I. W., 1949: The pressure pulsation of 11 April 1944. *J. Meteor.*, **6**, 181-187.

- Byers, H. R., and R. R. Braham, 1949: The thunderstorm. Washington, D. C. U. S. Printing Office.
- Cunning, J. B., 1986: The Oklahoma-Kansas Preliminary Regional Experiment for STORM-Central. *Bull. Amer. Meteor. Soc.*, **67**, 1478-1486.
- Cunning, J. B., and M. DeMaria, 1986: An investigation of the development of cumulonimbus systems over South Florida. Part I: Boundary layer interactions. *Mon. Wea. Rev.*, **114**, 5-24.
- Cunningham, R. M., 1959: Cumulus circulation, recent advances in atmospheric electricity. Pergamon Press, 361-367.
- Fankhauser, J. C., 1974: The derivation of consistent fields of wind and geopotential height from mesoscale rawinsonde data. *J. Appl. Meteor.*, **13**, 637-646.
- Fritsch, J.M., 1975: Cumulus dynamics: Local compensating subsidence and its implications for cumulus parameterization. *Pure Appl. Geophys.*, **113**, 851-867.
- Fritsch, J. M. and C. G. Chappell, 1980: Numerical prediction of convectively driven mesoscale pressure systems. Part II: Mesoscale model. *J. Atmos. Sci.*, **37**, 1734-1762.
- Fujita, T. T., 1955: Results of detailed synoptic studies of squall lines., *Tellus*, **7**, 405-436.
- Fujita, T. T., 1959: Precipitation and cold air production in mesoscale thunderstorm systems. *J. Meteor.*, **16**, 454-466.
- Fujita, T. T., 1963: Analytical mesometeorology: A review. *Meteor. Monogr.*, **5**, No. 7, 77-125.

- Gallus, W. A., 1989: The heat, moisture, and momentum budgets of a midlatitude squall line with a trailing stratiform region. Atmospheric Science Paper No. 455, Colorado State University, Dept. of Atmos. Sci., Fort Collins, Colorado, 126 pp.
- Gamache, J. F., and R. A. Houze, Jr., 1982: Mesoscale air motions associated with a tropical squall line. *Mon. Wea. Rev.*, **110**, 118-135.
- Gamache, J. F., and R. A. Houze, Jr., 1985: Further analysis of the composite wind and thermodynamic structure of the 12 September GATE squall line. *Mon. Wea. Rev.*, **113**, 1241-1259.
- Houze, R. A., Jr. and E. N. Rappaport, 1984: Air motions and precipitation of an early summer squall line of the eastern tropical atlantic. *J. Atmos. Sci.*, **41**, 553-574.
- Houze, R. A., Jr., S. A. Rutledge, M. I. Biggerstaff and B. F. Smull, 1989: Interpretation of Doppler weather radar displays of midlatitude mesoscale convective systems. *Bull. Amer. Meteor. Soc.*, **70**, 608-619.
- Houze, R. A., Jr., B. F. Smull and P. Dodge, 1990: Mesoscale organization of springtime rainstorms in Oklahoma. *Mon. Wea. Rev.*, **118**, 613-654.
- Hoxit, L. R., C. F. Chappell, and J. M. Fritsch, 1976: Formation of mesolows or pressure troughs in advance of cumulonimbus clouds. *Mon. Wea. Rev.*, **104**, 1419-1428.
- Johnson, R. H., and M. E. Nicholls, 1983: A composite analysis of the boundary layer accompanying a tropical squall line. *Mon. Wea. Rev.*, **111**, 308-319.
- Johnson, R. H. and P. J. Hamilton, 1988: The relationship of surface pressure features to the precipitation and air flow structure of an intense midlatitude squall line. *Mon. Wea. Rev.*, **116**, 1444-1472.

- Johnson, R. H., S. Chen, and J. J. Toth, 1989: Circulations associated with a mature-to-decaying midlatitude mesoscale convective system. Part I: Surface features - Heat bursts and mesolow development. *Mon. Wea. Rev.*, **117**, 942-959.
- Johnston, E. C., 1982: Mesoscale vorticity centers induced by mesoscale convective complexes. *Preprints, Ninth Conf. on Weather Forecasting and Analysis*, Seattle, Amer. Meteor. Soc., 196-200.
- Leary, C. A. and E. N. Rappaport, 1987: The life cycle and internal structure of a mesoscale convective complex. *Mon. Wea. Rev.*, **115**, 1503-1527.
- Loehrer, S. M., 1992: The surface pressure features and precipitation structure of PRE-STORM mesoscale convective systems. Atmospheric Science Paper, No. Pending, Colorado State University, Dept. of Atmos. Sci., Fort Collins, Colorado, 297 pp.
- Maddox, R. A., 1980: Mesoscale convective complexes. *Bull. Am. Meteorol. Soc.*, **61**, 1374-1387.
- Maddox, R. A., D. M. Rodgers and K. W. Howard, 1982: Mesoscale convective complexes over the United States during 1981 - Annual Summary. *Mon. Wea. Rev.*, **110**, 1501-1514.
- Maddox, R. A., 1983: Large-scale meteorological conditions associated with midlatitude, mesoscale convective complexes. *Mon. Wea. Rev.*, **111**, 1475-1493.
- Meitín, J. G., and J. B. Cuning, 1985: The Oklahoma-Kansas Preliminary Regional Experiment for STORM-Central (OK PRE-STORM), Volume I. Daily operations summary. NOAA Tech. Memo. ERL ESG-20, Dept. of Commerce, Weather Research Program, Boulder, Colorado, 313 pp.
- Newton, C. W., 1950: Structure and mechanisms of the prefrontal squall line. *J. Meteor.*, **7**, 210-222.

- Newton, C. W., 1966: Circulations in large sheared cumulonimbus. *Tellus*, **18**, 699-712.
- O'Brien, J. J., 1970: Alternative solutions to the classical vertical velocity problem. *J. Appl. Meteor.*, **10**, 1103-1121.
- Ogura, Y., and M. T. Liou, 1980: The structure of a midlatitude squall line. A case study. *J. Atmos. Sci.*, **37**, 553-567.
- Orlanski, I., 1975: A rational subdivision of scales of atmospheric processes. *Bull. Am. Meteorol. Soc.*, **56**, 527-530.
- Purdom, J. F. W., and K. Marcus, 1982: Thunderstorm trigger mechanisms over the southeast U. S. *Preprints, 12th Conf. on Severe Local Storms*, San Antonio, Amer. Meteor. Soc. 487-488.
- Rodgers, D. M., M. J. Magnano and J. H. Arns, 1985: Mesoscale convective complexes over the United States during 1983. *Mon. Wea. Rev.*, **113**, 888-901.
- Rutledge, S. A., and R. A. Houze, Jr., 1987: A diagnostic modeling study of the trailing stratiform region of a midlatitude squall line. *J. Atmos. Sci.*, **44**, 2640-2656.
- Sanders, F., and K. A. Emanuel, 1977: The momentum budget and evolution of a mesoscale convective system. *J. Atmos. Sci.*, **34**, 322-330.
- Smull, B. F., and R. A. Houze, Jr., 1985: A midlatitude squall line with a trailing region of stratiform rain: Radar and satellite observations. *Mon. Wea. Rev.*, **113**, 117-133.
- Smull, B. F., and R. A. Houze, Jr., 1987a: Dual-Doppler radar analysis of a midlatitude squall line with a trailing region of stratiform rain. *J. Atmos. Sci.*, **44**, 2128-2148.
- Smull, B. F., and R. A. Houze, Jr., 1987b: Rear inflow in squall lines with trailing-stratiform precipitation. *Mon. Wea. Rev.*, **115**, 2869-2889.

- Srivastava, R. C., T. J. Matejka and T. J. Lorello, 1986: Doppler radar study of the trailing anvil region associated with a squall line. *J. Atmos. Sci.*, **43**, 356-377.
- Stensrud, D. J., and R. A. Maddox, 1988: Opposing mesoscale circulations: A case study. *Wea. Forecasting*, **3**, 189-204.
- Stumpf, G. J., 1988: Surface pressure features associated with a midlatitude mesoscale convective system in OK PRE-STORM. Atmospheric Science Paper No. 435, Colorado State University, Dept. of Atmos. Sci., Fort Collins, Colorado, 148 pp.
- Stumpf, G. J., R. H. Johnson and B. F. Smull, 1991: The wake low in a midlatitude mesoscale convective system having complex organization. *Mon. Wea. Rev.*, **119**, 134-158.
- Toth, J. J., 1987: Interaction of shallow cold surges with topography on scales of 100-1000 kilometers. Cooperative Institute for Research in the Atmosphere Paper, ISSN No. 0737-5352-8, Colorado State University, Ft. Collins, Colorado, 135 pp.
- Verlinde, J., and W. R. Cotton, 1990: Mesoscale vortex-couplet observed in the trailing anvil of a multicellular convective complex. *Mon. Wea. Rev.*, **118**, 993-1010.
- Watson, A. I., J. G. Meitín and J. B. Cuning, 1988: Evolution of the kinematic structure and precipitation characteristics of a mesoscale convective system on 20 May 1979. *Mon. Wea. Rev.*, **116**, 1555-1567.
- Weaver, J. F., and S. P. Nelson, 1982: Multiscale aspects of thunderstorm gust fronts and their effects on subsequent storm development. *Mon. Wea. Rev.*, **110**, 707-718.
- Wetzel, P. J., W. R. Cotton and R. L. McAnelly, 1983: A long-lived mesoscale convective complex. Part II: Evolution and structure of the mature complex. *Mon. Wea. Rev.*, **111**, 1919-1937.

- Williams, D. T., 1948: A surface micro-study of squall-line thunderstorms. *Mon. Wea. Rev.*, **76**, 239-246.
- Williams, D. T., 1953: Pressure wave observations in the Central Midwest, 1952. *Mon. Wea. Rev.*, **81**, 278-289.
- Williams, D. T., 1963: The thunderstorm wake of May 4, 1961. Nat. Severe Storms Project Rep. No. 18, U. S. Dept. of Commerce, Washington D. C., 23pp. [NTIS PB 168223].
- Wilson, J. W., and W. E. Schreiber, 1986: Initiation of convective storms at radar-observed boundary-layer convergence lines. *Mon. Wea. Rev.*, **114**, 2516-2536.

Appendix A

INSTRUMENT BIAS CORRECTIONS

As mentioned in Chapter 3, a pressure correction had to be applied to the mesonet-work surface pressures in order to obtain an accurate mesoscale analysis (within 0.5 mb). Fujita (1963) suggested the use of data from surrounding, well-calibrated stations, such as NWS stations to compare with the mesonet stations. This procedure has been used by Johnson and Toth (1986) for only the PAM stations, and by Johnson and Hamilton (1988) and Stumpf (1988) for individual PRE-STORM cases.

Loehrer (1992) calculated pressure corrections for all PAM and SAM stations for 16 PRE-STORM cases including the 14-15 June 1985 case. The pressure corrections for the 14-15 June case are found in Table A.1.

Table A.1: PAM and SAM pressure corrections for 14-15 June case.

Station	Applied pressure correction (mb)	Station	Applied pressure correction (mb)
P01	1.47	S01	0.43
P02	1.89	S02	0.39
P03	-0.03	S03	1.62
P04	-1.18	S04	1.54
P05	-0.35	S05	0.18
P06	-0.67	S06	M
P07	0.00	S07	-0.03
P08	-1.28	S08	0.23
P09	0.13	S09	M
P10	-0.83	S10	M
P11	-0.66	S11	M
P12	1.24	S12	1.79
P13	0.70	S13	1.10
P14	-1.69	S14	0.38
P15	0.05	S15	-0.13
P16	-0.82	S16	0.15
P17	-0.29	S17	0.57
P18	-0.84	S18	0.52
P19	0.77	S19	0.95
P20	-0.48	S20	1.04
P21	0.18	S21	M
P22	-0.88	S22	0.65
P23	-0.12	S23	0.64
P24	-1.23	S24	0.45
P25	0.58	S25	0.65
P26	-0.58	S26	1.38
P27	-1.12	S27	0.60
P28	-2.06	S28	0.70
P29	1.60	S29	1.29
P30	0.53	S30	-0.01
P31	1.10	S31	1.12
P32	-0.38	S32	0.44
P33	0.04	S33	-0.17
P34	0.42	S34	1.17
P35	-0.09	S35	M
P36	-0.17	S36	0.53
P37	0.61	S37	0.81
P38	0.15	S38	1.42
P39	1.70	S39	1.04
P40	0.71	S40	0.66
P41	-0.71	S41	1.90
P42	0.21	S42	0.18